Dottorato di Ricerca in Scienze della Terra

XXXth cycle – s.d. GEO/07

Melt-rock interactions in the oceanic lithosphere: microstructural and petro-geochemical constraints from ophiolites

PhD Thesis

BASCH Valentin

Supervisors

RAMPONE Elisabetta – University of Genova, Italy

CRISPINI Laura – University of Genova, Italy

GODARD Marguerite – Géosciences Montpellier, France

ILDEFONSE Benoit – Géosciences Montpellier, France

Academic years: 2014-2017

GA n°608001

Extended abstract

Melt-rock interactions have been increasingly invoked as key processes in the formation and compositional evolution of the oceanic crust, from separate lines of evidence: (1) the study of the chemical zoning and melt inclusions in lava phenocrysts (Lissenberg *et al.*, 2013; Laubier *et al.*, 2014; Coumans *et al.*, 2016), (2) peculiar compositional trends observed in mid-ocean ridge basalts (MORBs), not consistent with a process of pure fractional crystallization (Collier & Kelemen, 2010; Van den Bleeken *et al.*, 2010, 2011; Paquet *et al.*, 2016), (3) olivine-rich troctolites found enclosed in the lowermost oceanic crust, thought to represent the "hybrid" reactive product of the interaction between dunites from the crust-mantle boundary and percolating MORB melts, dissolving olivine and crystallizing interstitial plagioclase and clinopyroxene (Suhr *et al.*, 2008; Drouin *et al.*, 2010; Renna & Tribuzio, 2011; Higgie & Tommasi, 2012; Sanfilippo *et al.*, 2014; Rampone *et al.*, 2016). The latter studies thus describe melt-rock interactions as a rock-forming process, leading to the incorporation of mantle slivers into the lower oceanic crust and formation of olivine-rich lithologies after multiple episodes of melt-rock interaction (Drouin *et al.*, 2010, Sanfilippo & Tribuzio, 2012). The study presented in this thesis aims at constraining the structural and geochemical variations caused by melt-rock interaction processes acting at oceanic peridotite/gabbro transition settings, leading to the replacive formation of hybrid lithologies (plagioclase-bearing dunites, troctolites and olivine gabbros). These processes are often described in oceanic settings (Mid-Atlantic Ridge, Southwest Indian Ridge, East Pacific Rise), where clear field associations from the mantle protolith to the end-product are lacking, thus not allowing the direct observation of the evolution related to melt-rock interaction processes. The work has been developed through investigations on three ophiolitic case studies, fossil analogues of the oceanic lithosphere, preserving the primary association between mantle peridotites and gabbroic rocks: i) the Erro Tobbio peridotitic body and associated troctolites and olivine gabbros, in the Ligurian Alps (Italy), ii) the Monte Maggiore peridotites and associated dunites and troctolites, in the Alpine Corsica (France), and iii) the Maqsad massif Moho Transition Zone, in the Oman ophiolites. In all these ophiolites, previous studies documented a multi-stage melt-rock interaction history. In this study, we have used a multi-disciplinary field, structural (EBSD) and geochemical approach (mineral major and trace element analyses) to define the replacive vs magmatic origin of the gabbroic lithologies and the correlation between the structural and geochemical variations induced by melt-rock interaction processes in a field-controlled petrological setting.

In the Erro-Tobbio unit (Ligurian Alps, Italy), impregnated mantle peridotites are primarily associated to a hectometre-size mafic body composed of troctolite and plagioclase-bearing wehrlite, both crosscut by late gabbroic dykes. The troctolitic body exhibits high inner complexity, with a host troctolite (*Troctolite A*) crosscut by a second generation of troctolitic metre-size pseudo-tabular bodies (*Troctolite B*) (Borghini *et al.*, 2007; Rampone & Borghini, 2008; Rampone *et al.*, 2016). The host *Troctolite A* is characterized by two different textural types of olivine, between corroded deformed millimetre- to centimetre-size olivine and fine-grained rounded undeformed olivine, both embedded in interstitial to poikilitic plagioclase and clinopyroxene. It includes centimetre- to decimetre-size dunitic pods, surrounded by plagioclase enrichments. The *Troctolite A* shows melt-rock reaction microstructures indicative of formation after impregnation of dunites by an olivine-undersaturated melt (olivine being corroded by interstitial plagioclase). The textural evolution during impregnation is accompanied with a clear change of the olivine Crystallographic Preferred

Orientation (CPO), from dunitic aggregates bearing interstitial plagioclase preserving an axial-[100] pattern, similar to the CPO analyzed in the country peridotites, to single olivine grains embedded in poikilitic plagioclase in the most plagioclase-rich samples, showing a randoming of the olivine CPO indicative of the loss of cohesion of the solid matrix during impregnation at high melt/rock ratios (Rosenberg & Handy, 2005; Drouin *et al.*, 2010). The *Troctolite A* shows reactive mineral compositional trends of evolution, characterized by variable Anorthite contents in plagioclase at constant Forsterite content in the olivine matrix, indicative of the buffering of the melt composition by the assimilation of olivine during impregnation (modelling performed using the *pMELTS* thermodynamic software; Ghiorso *et al.*, 2002). The *Troctolite B* pseudo-tabular bodies correspond to brittle-ductile intrusions within the pre-existing *Troctolite A*, showing olivine CPO indicative of a formation by magmatic flow (shape-related orientation of the crystals; Benn & Allard, 1989; Jousselin *et al.*, 2012). They are characterized by extreme textural variations from decimetre-size dendritic to fine-grained euhedral olivines, embedded in poikilitic plagioclase. We infer that this textural variability is the result of olivine assimilation during formation of the *Troctolite A* (diffuse percolation) and intrusion of the *Troctolite B* (focused percolation), and to the related increase in the degree of undercooling of the percolating melt (increase of the melt liquidus temperature up to 65°C during olivine assimilation; Faure *et al.*, 2003, 2007; O'Driscoll *et al.*, 2007). Mineral compositions within the *Troctolite B* are similar to the ones analyzed in the *Troctolite A* and indicate that olivine-dissolving melt-rock interactions were still involved in the focused melt percolation (*pMELTS*; Ghiorso *et al.*, 2002). The gabbroic intrusions crosscutting the association between mantle peridotites and the troctolitic body show mineral compositional trends of evolution consistent with the fractional crystallization of the melts modified after the olivine-dissolving reactive melt percolation related to the formation of the *Troctolite A* and *Troctolite B* (*pMELTS*; Ghiorso *et al.*, 2002). Therefore, the Erro-Tobbio troctolitic body shows a poly-phase formation history related to the thermal evolution (Borghini *et al.*, 2007; Rampone & Borghini, 2008), from diffuse reactive percolation leading to the replacive formation of the host *Troctolite A* in ductile environments, to brittle-ductile focused reactive percolation and formation of the *Troctolite B*, to the intrusion and fractional crystallization of the modified melt and formation of the gabbroic dykes in brittle environments.

The Mt.Maggiore peridotitic body (Alpine Corsica, France) exposes a clear evolution from spinel lherzolite to plagioclase-bearing lithotypes (plagioclase peridotites, olivine-rich troctolites and troctolites) (Rampone *et al.*, 1997, 2008; Muntener & Piccardo, 2003; Piccardo & Guarnieri, 2010) during two continuous episodes of melt-rock interaction. At spinel facies, the reactive melt percolation of LREE-depleted melts, likely representing unaggregated last melt increments produced by fractional melting of underlying asthenosphere mantle, leads to the dissolution of mantle pyroxenes and the growth of olivine crystals, until the formation of replacive spinel dunites in the most reacted peridotites. As a result, metre-size dunitic pods, characterized by irregular coarse grains of olivine, are enclosed in reacted olivine-rich spinel harzburgites (Rampone *et al.*, 1997, 2008; Muntener & Piccardo, 2003; Piccardo & Guarnieri, 2010). The progressive evolution from spinel lherzolite to harzburgite to replacive dunite is accompanied by a change of olivine CPO, from axial-[100] in the lherzolite, consistent with high-temperature low-strain dislocation creep, commonly described in mantle peridotites (Tommasi *et al.*, 2000), to axial-[010] olivine CPO in the dunites, indicative of deformation in presence of melt (Holtzman *et al.*, 2003; Le Roux *et al.*, 2008). The initial percolating melt composition is consistent with single melt increments after 6% partial

melting of a depleted mantle source (Rampone *et al.*, 1997, 2008). The reactive melt percolation leads to a progressive enrichment in the melt HREE absolute concentrations, while preserving its LREE depletion (REE modelling using the Plate Model after Vernières *et al.*, 1997), consistent with the enriched analyzed HREE composition of olivine in the spinel dunite.

At shallower plagioclase facies, the melts modified after reactive melt percolation (LREE-depleted, HREE-enriched) impregnate the spinel-facies lithotypes, leading to the dissolution of olivine and crystallization of plagioclase and orthopyroxene (± clinopyroxene) in the peridotites (Rampone *et al.*, 1997, 2008; Piccardo & Guarnieri, 2010). The impregnation stage is also observed in the spinel dunites, leading to the hybrid formation of olivine-rich troctolites and troctolites, after dissolution of olivine and crystallization of interstitial plagioclase. The dissolution-precipitation reaction forming the hybrid troctolite develops progressive textural variations correlated with the modal content in olivine (decreasing during reaction). As inferred from previous studies of hybrid olivine-rich troctolites in oceanic settings (Suhr *et al.*, 2008; Drouin *et al.*, 2010), the irregular and coarse olivines from the dunite protolith are progressively corroded and disrupted by the reactive plagioclase-crystallizing melt, to form textures characterized by numerous rounded olivines embayed in poikilitic plagioclase. Therefore, during progressive impregnation, an increase in Grain Number, correlated with a decrease in grain area, aspect ratio and shape sactor of the olivine grains is observed. The textural evolution during impregnation is not accompanied by clear variations in the olivine CPO, indicative of very low instantaneous melt/rock ratios during the impregnation process. Olivine, plagioclase and clinopyroxene REE compositions analyzed in the troctolite fit a process of impregnation with a progressive closure of the porosity (at decreasing melt mass), leading to the crystallization of trapped melt and REE enrichments during the last crystallization increments (Plate Model; Vernières *et al.*, 1997). The crystallization of small trapped melt fractions is consistent with the low instantaneous melt/rock ratio suggested by the preserved olivine CPO during the impregnation process.

The Oman Moho Transition Zone (MTZ) is formed of a layering of interfingered *dunites* (sensu lato; >70 vol% modal olivine) and variably evolved *olivine gabbros* (from 10 to 70 vol% olivine; Boudier & Nicolas, 1995; Higgie & Tommasi, 2012). A recent petrological and structural study by Higgie & Tommasi (2012) demonstrated the replacive origin of the *olivine gabbro* layers, formed by a deformation-driven focused reactive percolation within the pre-existing *dunite*, corroding the olivine matrix and crystallizing interstitial clinopyroxene and plagioclase. The progressive evolution of modal compositions (decreasing modal composition of olivine) is accompanied by a change in symmetry of olivine CPO from axial-[100] patterns in the *dunite* to axial-[010] CPO in the *olivine gabbro*, observed over a range of olivine modal compositions from 60 to 40 vol%. Higgie & Tommasi (2012) interpreted this olivine CPO evolution as indicative of the higher cumulated strain and melt/rock ratio integrated over time in the *olivine gabbro* layers. The centimetre-scale at which the structural variations are observed within the *dunite* - *olivine gabbro* layering calls for a positive feedback between deformation and melt focusing in the weaker *olivine gabbro* layers, as previously described in melt-bearing simple shear experiments (Zimmerman *et al.*, 1999, Holtzman *et al.*, 2003b). Strong chemical discrepancies are observed between the *dunite* layers showing compositional trends of evolution indicative of a closed system melt impregnation, with the buffering of the melt composition by the host rock and the olivine-dissolving melt-rock interaction, and the *olivine gabbro* layers showing compositions dominated by the percolating melt composition, consistently with the open-system reactive melt percolation

previously described by Higgie & Tommasi (2012). We observed a good correlation between the transition from axial-[100] in olivine-rich samples to axial-[010] in more evolved *olivine gabbros*, and the geochemical transition from closed system (matrix-dominated) to open system (melt-dominated) mineral compositions. The clinopyroxene REE and trace elements compositions are consistent with a MORB-type melt composition, similar to the clinopyroxenes analyzed in the Oman lower crustal gabbros, indicating that melts percolating the Moho Transition Zone were then extracted and fed the oceanic crust (Kelemen *et al.*, 1997; Korenaga & Kelemen, 1997; Koga *et al.*, 2001). The *olivine gabbros* show an [olivine – clinopyroxene – plagioclase] crystallization sequence (Browning, 1984), and high-Anorthite plagioclase (An = 87-92 mol%) is associated with relatively evolved compositions of olivine (Fo = 83-84 mol%) and clinopyroxene (Mg# = 86-88 mol%). Previous studies (Kelemen *et al.*, 1997; Korenaga & Kelemen, 1997; Koga *et al.*, 2001) invoked the crystallization of hydrous melts to explain the peculiar crystallization order and mineral compositions, not consistent with the crystallization of a dry MORB-type melt at 2kbar (Koga *et al.*, 2001). However, based on the absence of any hydrous phase, the high calculated plagioclase-clinopyroxene equilibrium temperatures (REE geothermometer after Sun *et al.*, 2017), and the decoupling between Anorthite contents in plagioclase and Forsterite contents in olivine (both positively correlated with the water content in the melt), we infer that the water content of the parental melt is not the controlling factor on the composition of crystallizing minerals, rather a peculiar CaO-rich chemical signature of the primary MORB melt (high CaO/Na_2O and CaO/Al_2O_3 and fractional crystallization modelling performed using the *pMELTS* thermodynamic software; Ghiorso *et al.*, 2002), possibly formed by partial melting of a mixed pyroxenite-peridotite mantle source (e.g. Borghini *et al.*, 2017).

The results of this thesis demonstrate the possible hybrid origin of gabbroic rocks in field-controlled ophiolitic settings, and provide a textural, structural and geochemical methodology to constrain melt-rock interaction processes and the magmatic vs replacive origin of an olivine-rich gabbroic rock. The three case studies highlight a significant control of instantaneous and cumulated melt/rock ratios on both the structural and the geochemical evolution during melt-rock interaction processes. The combination of structural and geochemical analyses allows a detailed understanding of the melt-rock interaction processes from large to small scale, and the related structural and geochemical evolution of the pre-existing mantle matrix and percolating melt.

Keywords: Alpine ophiolites; Oman Moho Transition Zone; Melt-rock interaction; Reactive melt percolation; Melt impregnation; Olivine-rich troctolite; Replacive formation; Textural evolution; Crystallographic Preferred Orientation; Olivine trace elements.

Riassunto

I processi di interazione fuso-roccia rappresentano processi chiave nella formazione ed evoluzione chimica della crosta oceanica, come mostrato da diverse evidenze: (1) lo studio delle zonature chimiche e delle inclusioni fluide in fenocristalli in lave (Lissenberg *et al.*, 2013; Laubier *et al.*, 2014; Coumans *et al.*, 2016), (2) "trends" composizionali peculiari, osservati in basalti di dorsale medio-oceaniche (MORBs), non consistenti con processi di pura cristallizzazione frazionata (Collier & Kelemen, 2010; Van den Bleeken *et al.*, 2010, 2011; Paquet *et al.*, 2016), (3) troctoliti arricchite in olivina descritte nei livelli più profondi della crosta oceanica, le quali vengono ritenute rappresentare il prodotto 'ibrido' di reazione tra duniti, originariamente localizzate nel limite mantello-ctosta, e magmi MORB percolanti che dissolvono olivina e cristallizzano plagioclasio e clinopirosseno (Suhr *et al.*, 2008; Drouin *et al.*, 2010; Renna & Tribuzio, 2011; Higgie & Tommasi, 2012; Sanfilippo *et al.*, 2014; Rampone *et al.*, 2016). Gli studi sopra citati descrivono la formazione di rocce gabbriche ricche in olivina come risultato di processi multipli di interazioni fuso-roccia a spese di scaglie di peridotiti di mantello incorporate alla base della crosta oceanica (Drouin *et al.*, 2010, Sanfilippo & Tribuzio, 2012). Lo studio condotto in questa tesi ha come obiettivo quello di determinare le variazioni strutturali e geochimiche causate dai processi di interazione fuso-peridotite in ambienti di transizione mantello-crosta oceanica, processi che causano la formazione di rocce ibride (duniti a plagioclasio, troctoliti, olivin gabbri). Questi processi sono descritti negli ambienti oceanici attuali (Mid-Atlantic Ridge, Southwest Indian Ridge, East Pacific Rise) dove però sono spesso carenti le relazioni strutturali tra i diversi litotipi, dai protoliti di mantello alle rocce gabbriche "ibride", non permettendo quindi l'osservazione diretta dell'evoluzione microstrutturale e geochimica che accompagna i processi di interazione fuso-roccia. Questo lavoro di tesi e' stato sviluppato mediante lo studio di peridotiti ed associate rocce gabbriche in tre sequenze ofiolitiche che preservano le relazioni strutturali primarie tra i diversi litotipi, ed in cui studi precedenti hanno documentato processi di interazione fuso/peridotite a diversi livelli litosferici : i) l'unita' peridotitica Erro-Tobbio (Alpi Liguri; Rampone & Borghini, 2008; Rampone *et al.*, 2016), ii) le peridotiti di Mt.Maggiore (Corsica Alpina, Francia; Rampone *et al.*, 2008), e iii) la zona di transizione in Oman che presenta un layering alternato di livelli dunitici e livelli di olivin gabbri variabilmente evoluti (Koga *et al.*, 2001; Higgie & Tommasi, 2012). Lo studio è stato sviluppato seguendo un approccio multidisciplinare che combina studi di terreno, strutturali (*Electron Backscatter Diffraction, EBSD*) e di composizione chimica degli elementi maggiori ed in tracce dei minerali (*Electron Probe Micro-Analyzer* e *Laser Ablation Inductively Coupled Plasma Mass Spectrometer*) con l'obiettivo di definire l'origine ibrida o magmatica "sensu strictu" delle rocce gabbriche, e la correlazione tra cambiamenti strutturali e geochimici durante il processo di interazione tra rocce di mantello e fuso, in settings geologici vincolati da chiare evidenze di terreno.

Nell'Unità Erro-Tobbio (Alpi Liguri, Italia), le peridotiti di mantello impregnate sono primariamente associate a corpi mafici composti di troctoliti e wehrliti a plagioclasio, entrambi tagliati da dicchi di gabbro tardivi. I corpi troctolitici mostrano un'importante complessità composizionale interna: il corpo principale di troctolite (Troctolite A) è tagliato da una seconda generazione di corpi troctolitici con dimensioni metriche e forma pseudo-tabulare (Troctolite B) (Borghini *et al.*, 2007; Rampone & Borghini, 2008; Rampone *et al.*, 2016). La Troctolite A incassante è caratterizzata da due differenti occorrenze tessiturali di olivina, comprese tra olivine corrose e defornate di taglia millimetrica a centimetrica ed olivine tondeggianti, non deformate e di taglia fine; entrambe le olivine sono incluse in cristalli di plagioclasio e clinopirosseno con forma

da interstiziale a poicilitica. La troctolite A mostra inoltre aggregati dunitici di dimensioni da centimetriche a decimetriche, circondati da zone arricchite in plagioclasio. Tali caratteristiche microstrutturali indicano la formazione della troctolite incassante A per impregnazione di una dunite da parte di un fuso sottosaturo in olivina (l'olivina viene corrosa dal plagioclasio interstiziale). L'evoluzione tessiturale durante l'evento di impregnazione è accompagnata da un evidente cambio dell'orientazione preferenziale degli assi cristallografici dell'olivina (CPO), che varia dal caratteristico pattern assiale [100] degli aggregati dunitici a plagioclasio interstiziale (simile al CPO analizzato nelle peridotiti associate) ad un CPO ad orientazione "random" nei campioni arricchiti in plagioclasio dove singoli cristalli di olivina sono inclusi in plagioclasio pecilitico. Quest'ultimo indica la perdita di coesione tra i cristalli di olivina, costituenti la matrice solida, durante l'evento di impregnazione ad elevati rapporti fuso/roccia (Rosenberg & Handy, 2005; Drouin *et al.*, 2010). Le composizioni chimiche dei minerali costituenti la troctolite A mostrano trend evolutivi tipicamente di cristallizzazione "reattiva", caratterizzati da variabili contenuti in anortite nei plagioclasi a costante contenuto in forsterite nelle olivine della matrice: questo indica che la composizione del fuso viene modificata e tamponata dall'assimilazione di olivina durante il processo d'impregnazione (Borghini *et al.*, 2007; Rampone *et al.*, 2016). I corpi pseudo-tabulari di troctolite B corrispondono ad intrusioni fragile-duttili nella troctolite A pre-esistente. Il CPO dell'olivina nella troctolite B indica che la sua origine è magmatica e la sua formazione è legata ad un flusso magmatico (orientazione preferenziale della forma dei cristalli; Benn & Allard, 1989; Jousselin *et al.*, 2012). Le troctoliti B sono caratterizzate da estreme variazioni tessiturali, con olivine da dendritiche di dimensioni decimetriche a euedrali di dimensioni inferiori, entrambe incluse in plagioclasio poichilitico. Questa variazione tessiturale è il risultato dell'assimilazione di olivina durante la formazione della troctolite A (percolazione diffusa) ed intrusione della troctolite B, che causa un aumento del grado di raffreddamento del fuso percolante (aumento della temperatura di liquidus del fuso fino a 65°C durante l'assimilazione d'olivina; Faure *et al.*, 2003, 2007; O'Driscoll *et al.*, 2007). Le composizioni dei minerali costituenti la troctolite B sono simili a quelle dei minerali nella troctolite A e indicano che i processi di interazione fuso-roccia, che sono responsabili per la dissoluzione di olivina, erano continuamente attivi durante la percolazione focalizzata di fusi. I minerali nelle intrusioni gabbriche che tagliano le peridotiti di mantello ed i corpi troctolitici, mostrano variazioni composizionali consistenti con processi di cristallizzazione frazionataa partire da fusi modificati durante la percolazione reattiva che ha determinato la formazione della troctolite A e troctolite B. I corpi troctolitici dell'Erro-Tobbio registrano quindi una storia evolutiva polifasica legata all'evoluzione termica di questo settore di mantello durante la progressiva esumazione (Borghini *et al.*, 2007; Rampone & Borghini, 2008), dalla percolazione reattiva diffusa e formazione della troctolite incassante A, in aambiente duttile,alla percolazione reattiva focalizzata in ambiente fragile-duttile e formazione della troctolite B, fino alla tardiva intrusione e cristallizzazione frazionata del fuso modificato e formazione dei dicchi gabbrici in ambiente fragile più superficiale..

Le peridotiti di Monte Maggiore (Corsica Alpina, Francia) registrano una chiara storia evolutiva di progressiva esumazione litosferica, accompagnata da processi di interazione fuso-roccia, da lherzoliti e minori duniti a spinello a litotipi che presentano variabili contenuti in plagioclasio (peridotiti a plagioclasio, troctoliti ricche in olivina e troctoliti) (Rampone *et al.*, 1997, 2008; Muntener & Piccardo, 2003; Piccardo & Guarnieri, 2010).In facies a spinello, la percolazione reattiva di un fuso povero in LREE ha causato la dissoluzione di pirosseni di mantello e la crescita

di cristalli d'olivina, fino alla formazione di harzburgiti reattive, e minori corpi di duniti di sostituzione a spinello. Come risultato, aggregati dunitici di dimensioni metriche, caratterizzati da irregolari cristalli di olivina di grandi dimensioni, sono inclusi in harzburgiti a spinello reagite e ricche in olivina (Rampone *et al.*, 1997, 2008; Muntener & Piccardo, 2003; Piccardo & Guarnieri, 2010). L'evoluzione progressiva da lherzoliti a spinello, a harzburgiti fino alla formazione di duniti di sostituzione, è marcata da un cambio del CPO dell'olivina, da un pattern assiale [100] nelle lherzoliti, consistente con deformazione per dislocation creep ad alta temperatura e generalmente descritto in peridotiti di mantello (Tommasi *et al.*, 2000), al pattern assiale [010] del CPO dell'olivina nelle duniti, che tipicamente è interpretato come il risultato di deformazione in presenza di un fuso (Holtzman *et al.*, 2003; Le Roux *et al.*, 2008). La composizione iniziale del fuso di percolazione é consistente con singoli incrementi di fuso prodotti dal 6% di fusione parziale di un mantello depleto (Rampone *et al.*, 1997, 2008). La percolazione reattiva conduce al progressivo arricchimento del fuso in concentrazioni assolute di HREE, mentre preserva la concentrazione povera in LREE (Vernières *et al.*, 1997; Rampone *et al.*, 2008): queste sono consistenti con le composizioni delle olivine analizzate nelle duniti a spinello che sono arricchite in HREE.

In facies a plagioclasio, i fusi modificati durante il processo di percolazione (impoveriti in LREE, arricchiti in HREE) impregnano le peridotiti e duniti a spinello, portando alla dissoluzione di olivina e cristallizzazione di plagioclasio e ortopirosseno (+- clinopirosseno) nelle peridotiti (Rampone *et al.*, 1997, 2008; Piccardo & Guarnieri, 2010). Lo stadio di impregnazione è anche osservato nelle duniti a spinello, dove la reazione fuso-roccia porta alla formazione ibrida di troctoliti ricche in olivina e troctoliti successiva alla dissoluzione di olivina e cristallizzazione di plagioclasio interstiziale. La reazione di dissoluzione-precipitazione, che forma le troctoliti ibride, sviluppa variazioni tessiturali progressive correlate con il contenuto modale in olivina (diminuisce durante la reazione). Come dedotto da studi precedenti su troctoliti ibride ricche in olivina formatesi in ambiente oceanico (Suhr *et al.*, 2008; Drouin *et al.*, 2010), le olivine con abito irregolare e di grosse dimensioni costituenti il protolita dunitico sono corrose progressivamente e fragmentate dal fuso reattivo che cristallizza plagioclasio, per finalmente formare le tessiture caratterizzate da numerose olivine tondeggianti incluse in plagioclasio poichilitico. Durante il progressivo processo di impregnazione, si osserva l'aumento di 'grain number', il quale è correlato con la diminuzione di 'grain area', 'aspect ratio' e 'shape factor' dei cristalli di olivina. L'evoluzione tessiturale legata all'impregnazione non è accompagnata da chiare variazioni del CPO dell'olivina, quindi indicando che il processo di impregnazione è caratterizzato da bassi rapporti fuso/roccia instantanei. Le composizioni in REE di olivina, plagioclasio e clinopirosseno analizzati nelle troctoliti concordano con un processo di impregnazione associato ad una progressiva chiusura della porosità del sistema (a progressiva diminuzione della massa del fuso), la quale conduce alla cristallizzazione di fuso e, conseguentemente, all'arricchimento in REE nelle fasi cristalline durante gli ultimi incrementi di cristallizzazione (Vernières *et al.*, 1997, Rampone *et al.*, 2008). La cristallizzazione di piccole frazioni di fuso intrappolato sono consistenti con i bassi rapporti fuso/roccia instantanei suggeriti dal fatto che il CPO dell'olivina conserva caratteristiche precedenti la reazione durante il processo di impregnazione.

La zona di transizione Moho in Oman è costituita di un layering alternato di *duniti* (sensu lato; >70 vol% olivina modale) e livelli di *olivin gabbri* variabilmente evoluti (da 10 vol% a 70 vol% di olivina; Boudier & Nicolas, 1995; Higgie & Tommasi, 2012). In un recente studio

petrologico e strutturale, Higgie & Tommasi (2012) hanno dimostrato che i livelli di *olivin gabbro* sono di origine reattiva di sostituzione, formatesi durante un processo deformativo guidato dalla percolazione reattiva focalizzata in pre-esistenti *duniti*, durante il quale le olivine della matrice vengono corrose e clinopirosseno e plagioclasio cristallizzano interstiziali. La progressiva evoluzione delle composizioni modali (diminuzione della composizione modale dell'olivina) è accompagnata da un cambio della simmetria del CPO dell'olivina: da un pattern assiale [100] nelle *duniti* ad un CPO dell'olivina con pattern assiale [010] negli *olivin gabbro*, gli ultimi osservati in un range di composizione modale dell'olivina tra il 60% e 40 vol%. Higgie & Tommasi (2012) hanno interpretato quest'evoluzione del CPO dell'olivina come evidenza di un'intensa deformazione progressiva concentrata in zone ad elevato rapporto fuso/roccia nei livelli ad *olivin gabbro*. L'occorrenza di tali variazioni strutturali in scala centimetrica, che sono state osservate nel layering di *dunite-olivin gabbro*, indica una correlazione positiva tra deformazione e focalizzazione del fuso nei livelli più duttili ad *olivin gabbro*, come descritto in esperiment precedenti che riproducono deformazione per simple shear in presenza di fuso (Zimmerman *et al.*, 1999, Holtzman *et al.*, 2003b). Forti discrepanze si osservano tra le composizioni chimiche dei livelli *dunitici* e quelle dei livelli ad *olivin gabbro*: i "trends" di evoluzione composizionale delle *duniti* sono indicativi di un processo di impregnazione da fusi in un sistema chiuso, con la composizione del fuso controllata dalla roccia ospite e modificata dall'interazione fuso-roccia e dissoluzione di olivina; i livelli ad *olivin gabbro* mostrano composizioni dominate da quelle del fuso di percolazione, consistenti con un processo di percolazione reattiva in sistema aperto come descritto precedentemente da Higgie & Tommasi (2012). Abbiamo osservato una buona correlazione tra le microstrutture, che marcano una transizione da pattern assiale [100] nei campioni ricchi in olivina a pattern assiale [010] negli *olivin gabbri* più evoluti, e le composizioni geochimiche dei minerali che indicano una transizione da sistema chiuso (dominato dalla composizione della roccia) a sistema aperto (dominato dalla composizione del fuso). Le composizioni in REE ed elementi in tracce, che sono consistenti con le composizioni di fusi tipo MORB, sono simili ai clinopirosseni analizzati nei gabbri della sezione di crosta oceanica inferiore in Oman: questo suggerisce che i fusi che migrano nells zona di transizione Moho sono successivamente estratti ed alimentano la crosta oceanica (Kelemen *et al.*, 1997; Korenaga & Kelemen, 1997; Koga *et al.*, 2001). Gli olivin gabbri mostrano una sequenza di cristallizzazione [olivina-clinopirosseno-plagioclasio] (Browning, 1984), e l'elevato contenuto in anortite nel plagioclasio (An = 87-92 mol%) è associato ad una composizione relativamente evoluta di olivina (Fo = 83-84 mol%) e clinopirosseno (Mg = 86-88 mol%). Studi precedenti (Kelemen *et al.*, 1997; Korenaga & Kelemen, 1997; Koga *et al.*, 2001) hanno invocato la cristallizzazione di fusi idrati per interpretare il peculiare ordine di cristallizzazione e le composizioni chimiche dei minerali, che non sono consistenti con un fuso anidro tipo MORB a 2 kbar di pressione (Koga *et al.*, 2001). In contrasto, considerando l'assenza di fasi idrate nelle rocce investigate, le elevate temperature di equilibrio calcolate tra plagioclasio e clinopirosseno (geotermometro REE elaborato da Sun *et al.*, 2017), e la discordanza tra i contenuti in anortite nel plagioclasio ed in forsterite nell'olivina (entrambi correlati positivamente con il contenuto in acqua nel fuso), riteniamo che la composizione dei minerali che cristallizzano nelle rocce gabbriche non sia primariamente controllata dal contenuto in acqua nel magma parentale, quanto piuttosto dalla sua peculiare composizione chimica, ricca in CaO (elevati CaO/Na_2O e CaO/Al_2O_3), possibilmente acquisita per fusione parziale di una sorgente mista di mantello peridotite-pirossenite (Borghini *et al.*, 2017).

Acknowledgements - Ringraziamenti - Remerciements

Time flies … It's already been three years!
I have quite a lot of people to thank for making these three years what they were: pretty awesome!

My first many thanks go to my main supervisors in Genova: *Elisabetta Rampone*, for guidance, support, patience, and for everything you taught me! Ho l'impressione che non sapevo niente quando sono arrivato (è probabilmente vero), e hai preso del tuo tempo per aiutarmi, discuttere dati, e se ho potuto crescere cosi, e 100% grazie a te! Spero che possiamo continuare questa bella collaborazione per un bel po' di tempo, per me sarà sempre un grande piacere! Anche, grazie della tua determinazione a farmi parlare italiano! *Laura Crispini*, volevo ringraziarti due milioni di volte per il tuo aiuto sul terreno, per tutti discussioni di geologia strutturale, e sopratutto per il tuo costante buon umore e spirito positivo! Dai, una volta andiamo in Antartide insieme!

I would like to sincerely thank my co-supervisors in Montpellier, *Benoit Ildefonse* and *Marguerite Godard*, for teaching me how to use EBSD and LA-ICP-MS facilities and for fruitful discussions during my many stages in your nice city! Also, thank you *Margot* for putting together this amazing ITN ABYSS project!

I truthfully thank the external reviewers of this thesis, *Georges Ceuleneer* and *Claudio Marchesi* for accepting to take this work into their hands for review.

Many thanks to the ABYSS group! *Aurelien*, *Sofia*, *Justine*, *Zeudia*, *Barbara*, *Manuel*, *Adriana*, *Rachael*, *Karin*, *Kristina*, *Tom*, *Pavel*, *Olivier* and all senior scientists, it was **awesome** sharing all these meetings with you everywhere in Europe and beyond (science- or just life-wise)! I'll see you around! Many thanks to our two very nice project managers, *Chloé* and *Alida*, who did an amazing job! Special thanks come to *Manos* (*daddy-trainee*), for all these unforgettable moments that we shared, you're just the best! Even more super-special thanks for *Charlissima*, for all the thriving scientific brainstormings and even more non-scientific discussions! You've always been there for me, and for this, a gigantic THANK YOU! Mille baci!

Grazie a tutti a Genova! *Mattia*, *Adrian*, *Gaia*, *Nicola*, *Elisa*, *Marco*, *Donato*, *Biggie*! Per tutte le mattine, giornate, serate con voi, tutte le pizze, caffè, apperitivi ecc … Grazie! Un baccio gigante!

Grazie, *Giulio Borghini* per il tuo aiuto sul terreno e per tutti discussioni scientifiche !

For all the technical and analytical work done during these three years, I would like to thank *Paolo Campanella* and *Alessandra Gavoglio* for the very nice work they did preparing my hundreds of thin sections (also, their patience!). I would also like to thank *Christophe Nevado* and *Doriane Delmas* from Montpellier for their attention to detail on the polishing and preparation of all thin sections before EBSD analyses. Many thanks to *Laura Negretti* for assistance with the SEM analyses in Genova, *Andrea Risplendente* for assistance with the EPMA analyses in Milano, *Fabrice Barou* for assistance with the EBSD analyses in Montpellier, and *Olivier Bruguier* for assistance with the LA-ICP-MS analyses in Montpellier.

On en vient aux camarades de toujours, et d'université ! *Davidou, Marie-Eva*, *Jérémy*, *Jeanne*, *Mycki*, *Patric*, *Vincent* (super boulot sur le terrain ! Merci encore !), *Alex*, *Rodi-Roggers*, *Hugo*, *Yann*, *Allan*, *Mélissa*, *Alice*, *Auré*, *Bidoo*, *Syko*, *Jojo*, *Camilla*, *Simon*, *Thadi*, *Jean-No*, *Tim*, *Lucia, Raissa*, merci pour tout le soutien, la joie de vivre, les vacances, les apéros etc … !

ET ! Des milliards de remerciements à toi, ***Jeannou***, pour ta présence, ta patience, tes conseils savants, ton abondante joie de vivre, ta vision du monde, … Merci d'être toi, et merci de m'avoir épaulé pendant ces trois ans !

Alla grande!

TABLE OF CONTENTS

Geological context and aims of the study

At oceanic ridges, the continuous magmatic accretion and expansion of the oceanic crust is a fundamental process in the dynamic cycle of evolution of the Earth's crust (Bird, 2003). Therefore, oceanic ridges are key structures in the study of the mantle convection and decompression melting, as well as the magmatic and tectonic processes leading to the constant formation of new oceanic crust. The direct sampling of these oceanic ridges, together with the study of ophiolites as oceanic lithosphere analogues, allow to better constrain the architecture and the formation processes of the oceanic crust. Recent investigations revealed a variation of the crustal structure and composition as a function of the spreading rate (Dick *et al.*, 2006; Ildefonse *et al.*, 2014), from fast-spreading environments (>90mm/year), displaying a layered magmatic crustal sequence mainly formed by basalts and gabbros (Boudier & Nicolas, 1985), to slow-spreading ridges (<50mm/year) showing a heterogeneous structure of magmatic gabbroic lenses embedded in variably serpentinized mantle (Cannat, 1993, 1996, 1997; Dick *et al.*, 2003). These structural differences are a direct consequence of the variability of the melt budget and extension mechanisms at fast and slow spreading ridges (magmatic accretion vs tectonic extension, respectively), and highlight the complexity of the formation mechanisms of the oceanic crust.

Recent structural and geochemical studies of melt inclusions in basaltic phenocrysts (Laubier *et al.*, 2012; Coumans *et al.*, 2016), peculiar geochemical trends of evolution in mid-ocean ridge basalts, not explained by a simple process of fractional crystallization at low pressure (Lissenberg & Dick, 2008; Collier & Kelemen, 2010), geochemical zoning in the rock-forming minerals from the gabbroic lower oceanic crust (Lissenberg *et al.*, 2013, Lissenberg & MacLeod, 2017) and structural inheritance from a mantle protolith in lower crustal olivine-rich troctolites (Drouin *et al.*, 2010) and olivine gabbros from the Moho Transition Zone (Higgie & Tommasi, 2012) all called, from different lines of evidence, for the need to invoke **melt-rock interaction processes** occurring during the melt transport and crystallization processes of the oceanic crust. These dissolution-precipitation reactions can lead to strong geochemical variations in the percolating melt and host rock, and to the replacive formation of hybrid rocks, constituted of a matrix of relict mantle minerals embedded in magmatic interstitial minerals. Such hybrid lithologies form part of the lower oceanic crust at fast (Higgie & Tommasi, 2012) and slow spreading ridges (Suhr *et al.*, 2008; Drouin *et al.*, 2010; Sanfilippo *et al.*, 2014), implying the incorporation of mantle slivers into the oceanic crust by the described melt-rock interaction processes.

The study presented in this thesis aims at **constraining the structural and geochemical variations** caused by **melt-rock interaction processes** acting at **oceanic peridotite/gabbro transition settings,** leading to the **replacive formation of hybrid lithologies (melt-impregnated dunites, troctolites and olivine gabbros)**. These processes are often described in oceanic settings (Mid-Atlantic Ridge, Southwest Indian Ridge, East Pacific Rise), where clear field associations from the mantle protolith to the end-product are lacking, thus not allowing the direct observation of the evolution related to melt-rock interaction processes.

The work has been developed through investigations on three ophiolitic case studies, fossil analogues of the oceanic lithosphere, preserving the primary association between mantle peridotites and gabbroic rocks: i) the **Erro Tobbio peridotitic body** and associated troctolites and olivine

gabbros, in the Ligurian Alps (Italy), ii) the **Monte Maggiore peridotites** and associated dunites and troctolites, in the Alpine Corsica (France), and iii) the **Maqsad massif Moho Transition Zone**, in the Oman ophiolites. In all these ophiolites, previous studies documented a multi-stage melt-rock interaction history.

In this study, we have used a multi-disciplinary field, structural (EBSD) and geochemical approach (mineral major and trace element analyses) to define the **replacive vs magmatic origin of the gabbroic lithologies** and the correlation between the structural and geochemical variations induced by melt-rock interaction processes in a **field-controlled** petrological setting.

The working methodology is common to the three case studies (see Chapter 2 for detailed field and analytical methods):

Field work and *detailed petrographic observations* (optical microscope) were used to define the field associations, mantle and magmatic structures and the different melt-rock interactions stages characterizing each lithotype. When possible, we sampled detailed transects across the lithological variations.

Electron Backscatter Diffraction analyses (EBSD) were performed on a representative set of thin sections, in order to quantify the modal compositions, the textural heterogeneities, the deformation and the Crystallographic Preferred Orientation (CPO) of the rock-forming minerals, and to investigate the structural evolution between the various lithotypes and textures in a field-controlled geological setting.

Electron Probe Micro-Analyser (EPMA) and *Laser Ablation Inductively Coupled Plasma Mass Spectrometer* (LA-ICP-MS) were used to analyse mineral major and trace elements in the rock-forming minerals (olivine, clinopyroxene, orthopyroxene, plagioclase, spinel). The previous structural analyses allowed to investigate the correlation between textural variability (euhedral vs anhedral, undeformed vs deformed crystals, core vs rim vs interstitial vs vermicular) and chemical major and trace elements compositions. We also investigated the chemical major and trace elements zoning within the rock-forming minerals by analysing major and trace elements profiles. (closed vs open-system melt percolation).

In the Erro Tobbio troctolitic body, *Scanning Electron Microscope* (SEM) and *Field Emission Scanning Electron Microscope* (FE-SEM) analyses were used to investigate 10-μm size inclusions and related trace elements enrichments in corroded olivines (see Chapter 3).

Structure of the thesis

This thesis comprises six chapters, organized as the following:

The *first chapter* is a review of the present-day knowledge of the structural variability of the lithosphere, between fast- and slow-spreading ridges, and the processes of formation of the oceanic crust. We also present the results of recent experimental crystallization studies on the controlling factors impacting the composition of crystallized minerals, a review of the melt transport mechanisms and the related melt-rock interaction processes occurring in both the mantle and in the oceanic crust. We conclude this introduction chapter with a detailed review of the structural and geochemical properties of the olivine crystal, since it is the main studied mineral in this thesis.

The *second chapter* is a description of the field and analytical methods used in this study, namely detailed petrography, EBSD structural analyses, EPMA mineral major elements analyses, LA-ICP-MS mineral trace elements analyses, and SEM-FESEM inclusion analyses.

The *third chapter* presents the results from the first case study, the Erro Tobbio troctolitic body (Ligurian Alps), in which we investigated the inner structural and geochemical complexity and the possible hybrid origin of the olivine-rich troctolites. Using EBSD analyses combined to mineral geochemical analyses, we demonstrated the complex evolution of this troctolitic body associated with mantle peridotites, linking the replacive formation of the host olivine-rich troctolite by diffuse reactive porous flow, to the intrusion of a second generation of troctolite during brittle-ductile focussed reactive porous flow, to the emplacement of olivine gabbros along fractures in brittle environments.

The *fourth chapter* is acceptable for publication after minor revisions in the Lithos Special Issue "*Reactive Geological Systems from the Mantle to abyssal sub-seafloor*". It is entitled **"***From mantle peridotites to hybrid troctolites: textural and chemical evolution during melt-rock interaction history (Mt.Maggiore peridotites, Corsica, France)*", and presents the results from the second case study addressed in this thesis, using the same combined structural-geochemical approach. We quantified the textural evolution of the olivine matrix during field-controlled evolution from spinel lherzolites to spinel dunites to hybrid troctolites, and investigated the geochemical variations induced by the multi-stage melt-rock interaction processes.

The *fifth chapter* presents the results from the third case study: The Oman Moho Transition Zone, characterized by a centimetre-scale layering between dunites (100% modal olivine) and olivine gabbros (10% olivine). The previous structural investigation by Higgie & Tommasi (2012) demonstrated the replacive formation of the olivine gabbro layers, after a deformation-driven focussed melt flow in the gabbroic layers. We used the same set of samples to investigate the geochemical variability induced by this extensive melt-rock interaction process.

The *sixth and final chapter* is a general discussion of the results obtained from the three investigated case studies. We draw general considerations on melt-rock interactions and their structural and geochemical implications in the percolated rock and percolating melt.

The research conducted in this thesis has received funding from the Initial Training Network (ITN) ABYSS, an FP7-funded Marie Curie Action under grant agreement GA n°608001.

Chapter 1: Introduction

1.1 Structural variability of the oceanic lithosphere

Oceanic ridges run continuously on more than fifty thousand kilometres all around the Earth. They are located at the limit between two divergent lithospheric plates, where oceanic spreading occurs by accretion of newly formed mafic crust (Bird, 2003). They are key structures in the study of the mantle convection and decompression melting, as well as the magmatic and tectonic processes leading to the constant formation of new oceanic crust. Geophysical and geological oceanographic campaigns, together with oceanic dragging and drilling since 1968 (DSDP, ODP and IODP), allow the direct study of the structure and composition of the oceanic crust.

Different spreading rates among the various oceanic ridges around the Earth lead to important differences in morphology between slow- to ultra-slow- (<50 mm/year, e.g., Mid-Atlantic Ridge), intermediate (50-90mm/year, e.g., Juan de Fuca Ridge) and fast-spreading environments (>90mm/year, e.g., East Pacific Ridge). The ridge in the slow-accreting oceanic lithosphere is characterized by an axial valley up to 30-kilometre wide and one kilometre in depth (Fig. 1.1, Elthon *et al.*, 1982; Sinton & Detrick, 1992; Cannat *et al.*, 1993; Canales *et al.*, 2000; Buck *et al.*, 2005). By contrast, fast-spreading ridges are narrow, and show a flat topography that slopes away from the ridge (Fig. 1.1; Buck *et al.*, 2005).

The morphology of the ridges is also characterized by an offset of its axis through a dismembering into segments of varying dimension, tens to thousands of kilometres in length (Fig. 1.2, Schouten *et al.*, 1985; MacDonald *et al.*, 1988). This segmentation is observed at different scales, the main permanent transform faults separating hundred to thousand kilometres-long sections. These first order structures are parallel to spreading direction and stable in time. A second order segmentation delimitates smaller segments from ten to hundred kilometres long, stable only from 3 to 9 Ma (Sempéré *et al.*, 1990, 1993; Fox *et al.*, 1991; Grindley *et al.*, 1992; Gente *et al.*, 1995; Gràcia *et al.*, 2000). These smaller segments are delimited by both transform and non-transform discontinuities (Fig. 1.2).

The lithological structure of the oceanic crust was first studied through geophysical profiles, seismic velocities allowing inferences on its compositional variability. The first model of the structure of the oceanic crust was provided by Raitt in 1963 (Juteau & Maury, 1997). It corresponds to a model of a layered oceanic crust, defining 3 layers of variable seismic velocity. Later, using ophiolites as an analogue of the oceanic crust, these 3 layers were interpreted as three distinct lithological units (Anonymous, 1972). The seismic Layer 1 (Vp < 3km/s) was assigned to the sedimentary cover, Layer 2 (3-5 < Vp < 6-7 km/s) to basalts and pillow lavas, and Layer 3 (6.7 < Vp < 7.7 km/s) to gabbros.

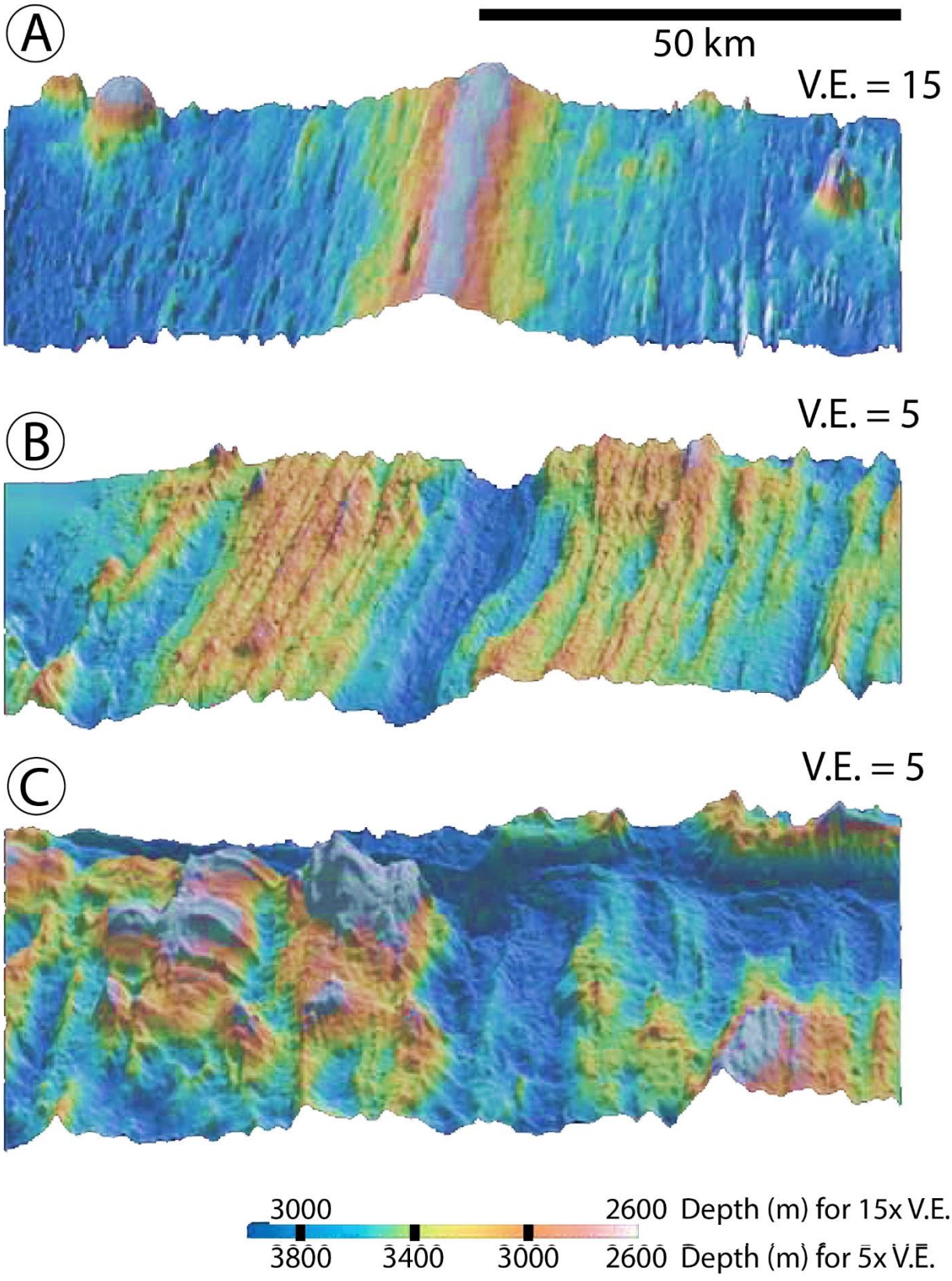

***Figure 1.1**: Bathymetric maps showing variations in axial morphology related to accretion rate (after Buck et al., 2005): (a) fast-spreading (East-Pacific Ridge 9°37'N), (b) Intermediate spreading rate (South-East Indian Ridge 115°E), and (c) slow spreading rate (Mid-Atlantic Ridge 23°25'N). Vertical exaggeration (V.E.) is three times greater in the top image than for the two others.*

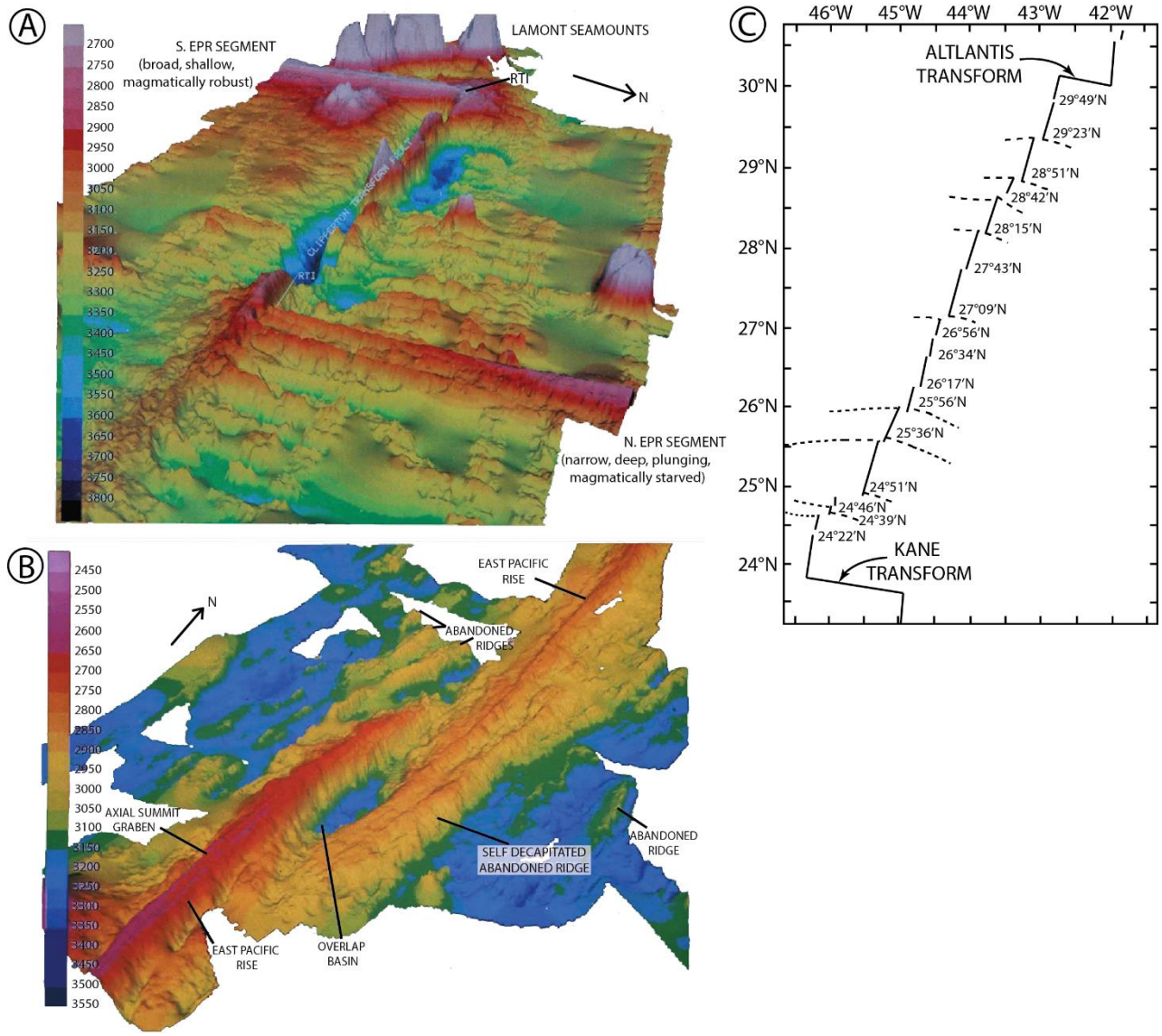

***Figure 1.2**: Bathymetric maps of East Pacific Ridge. A: transform first-order discontinuity; B: non-transform second order discontinuity (after Macdonald et al., 1988). Vertical exaggeration is 10; C: Non-transform discontinuities of the axial ridge (thick black line, second order discontinuities) between the Kane and Atlantis Transforms (first order discontinuities) (Sempéré et al., 1993).*

1.1.1. Fast-spreading ridges – Layered oceanic crust

This layered model of oceanic crust was refined later with sub-layers (sub-layers 2A, 2B, 2C, Houtz & Ewing, 1976; sub-layer 3A and 3B, Maynard, 1970; Sutton *et al.*, 1971). The sub-layer 2A ($3 < Vp < 4$ km/s) corresponds to the most superficial layer of the oceanic crust, formed at the axial ridge. It corresponds to basalts, highly porous and fractured after hydrothermal alteration. Sublayer 2B, characterized by higher seismic velocities ($4.8 < Vp < 5.5$ km/s) was described as massive and metamorphosed basalts. The sub-layer 2C ($5.8 < Vp < 6.2$ km/s) corresponds to the sheeted dike complex. The sublayers 3A and 3B form the lower oceanic crust, they are assigned to the isotropic gabbros ($Vp = 6.8$ km/s) and the more primitive layered gabbros ($7 < Vp < 7.7$ km/s), respectively.

After the detailed study of seismic profiles of oceanic lithosphere, along with the description of the main ophiolites worldwide (i.e. Cyprus and Oman), the “Penrose” Conference set a general model of a layered oceanic crust (Anonymous, 1972), which structure (Fig. 1.3) from top to bottom is the following:

A low density **Volcanic Complex** composed of basaltic “pillow” lavas, 0.5 to 1 kilometre in thickness (sub-layers 2A and 2B).

A **Sheeted Dike Complex** made of basaltic intrusions vertically intruded, up to 1-1.5-kilometre-thick (sub-layer 2C).

A high-density **Gabbroic Complex** composed of slowly cooled isotropic to layered gabbros, associated to ultramafic rocks. It is the thickest part of the oceanic crust, up to 6-7 kilometres in thickness (sub-layer 3A and 3B). The base of the thick gabbroic complex is defined by the petrologic Moho (Fig. 1.3).

An **Ultramafic Complex (Mantle)** composed of dunites and spinel to plagioclase lherzolites and harzburgites, in variable proportions. There is a high change of seismic velocity between the Gabbroic complex and the Ultramafic complex (Seismic Moho).

This layered structure of the oceanic lithosphere has later been recognized as viable for intermediate (50-90 mm/year, e.g., Juan de Fuca Ridge) to fast-spreading ridges (<90 mm/year, e.g., East Pacific Rise) mostly, where permanent and continuous magmatic chambers and thus important magmatic supply enable to build the layered oceanic crust.

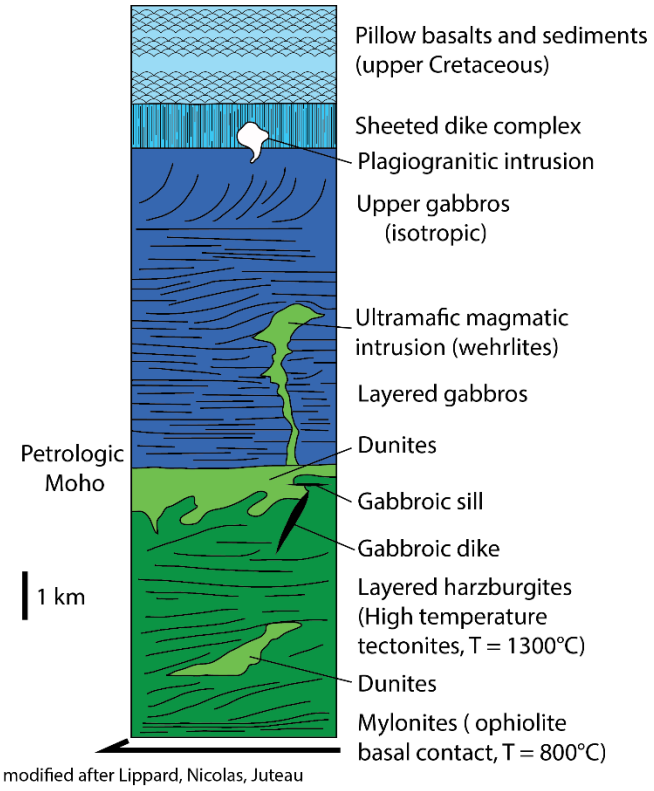

***Figure 1.3**: Structural and petrologic architecture of the Oman oceanic lithosphere. Redrawn after Browning (1982) and Boudier and Nicolas (1985).*

1.1.2. Slow- to ultra-slow-spreading ridges

Long before the Penrose Conference and the establishment of a reference stratigraphic column of the oceanic crust (Anonymous, 1972), Hess (1962) and Dietz (1963) proposed a model where the seismic Moho observed at the base of the sub-layer 3B corresponded to the transition between serpentinized peridotites and the underlying fresh peridotites. More and more data of dragging at slow-spreading ridges reported exposures of ultramafic and oceanic lower crustal gabbros at the seafloor, and the Penrose model increasingly appeared inappropriate to describe the structure of the oceanic lithosphere at ultra-slow to slow-spreading environments (Fox & Heezen, 1965; Van Andel & Bowin, 1968, Bonatti *et al.*, 1971). In the 1980-1990s, drilling and more samples from dragging allowed to understand that the basaltic cover is thin and that ultramafic rocks are exposed outside fracture zones, directly at the seafloor (Karson *et al.*, 1987; Lagabrielle & Cannat, 1990; Juteau *et al.*, 1990; Cannat, 1993, 1996; Cannat *et al.*, 1995). These observations led to modern models of a discontinuous stratigraphy of the oceanic lithosphere at slow-spreading ridges (Figs. 1.4, 1.5).

Observations along the Mid-Atlantic Ridge evidenced a morphological, petrological and geophysical variability along a single segment of the ridge (Fig. 1.4). Geophysical gravimetric and seismic refraction analyses both showed that there is a varying crustal thickness along the ridge (Tolstoy *et al.*, 1993), from centres of the segments to the edges. The thickening can be as important as 4 kilometres, from a thick crust (6km) in the centre to a thin crust (lower than 3km thick) at the end of the segments (Lin *et al.*, 1990; Madge *et al.*, 1997; Canales *et al.*, 2000; Hooft *et al.*, 2000). These observations have recently been confirmed by the discovery of a magmatic chamber under the Mid-Atlantic slow-spreading ridge at 37°18'N, allowing this central part of the segment to show a structure analogue to a fast-spreading environment (Singh *et al.*, 2006).

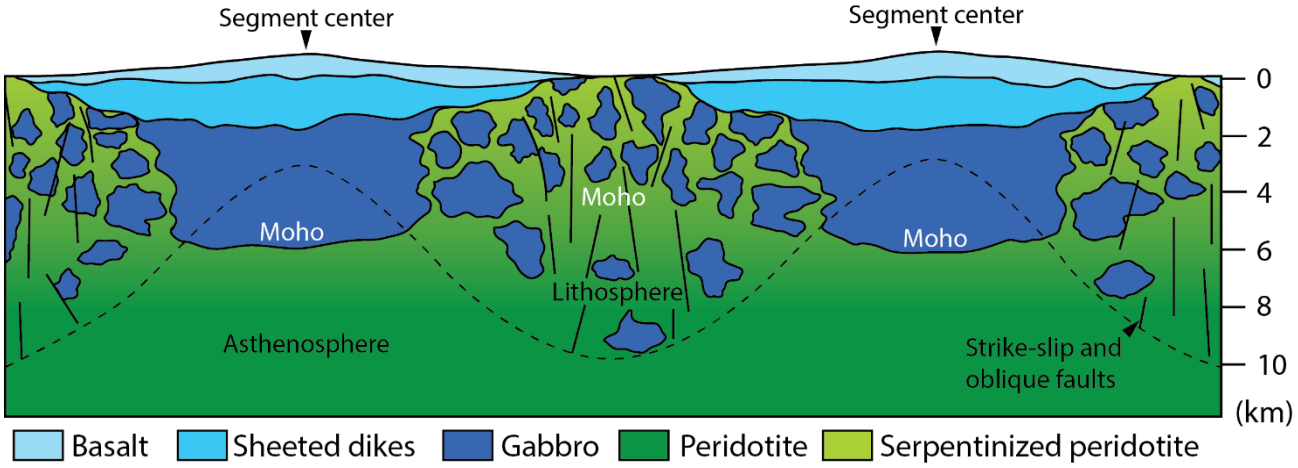

***Figure 1.4**: Along-axis lithological and crustal thickness variability. The shallower Moho beneath segment ends reflects seismic observations along the northern Mid-Atlantic Ridge (Canales et al., 2000). The black dashed line corresponds to the 1100°C isotherm. From Cannat et al. (1995); redrawn after Ildefonse et al. (2007).*

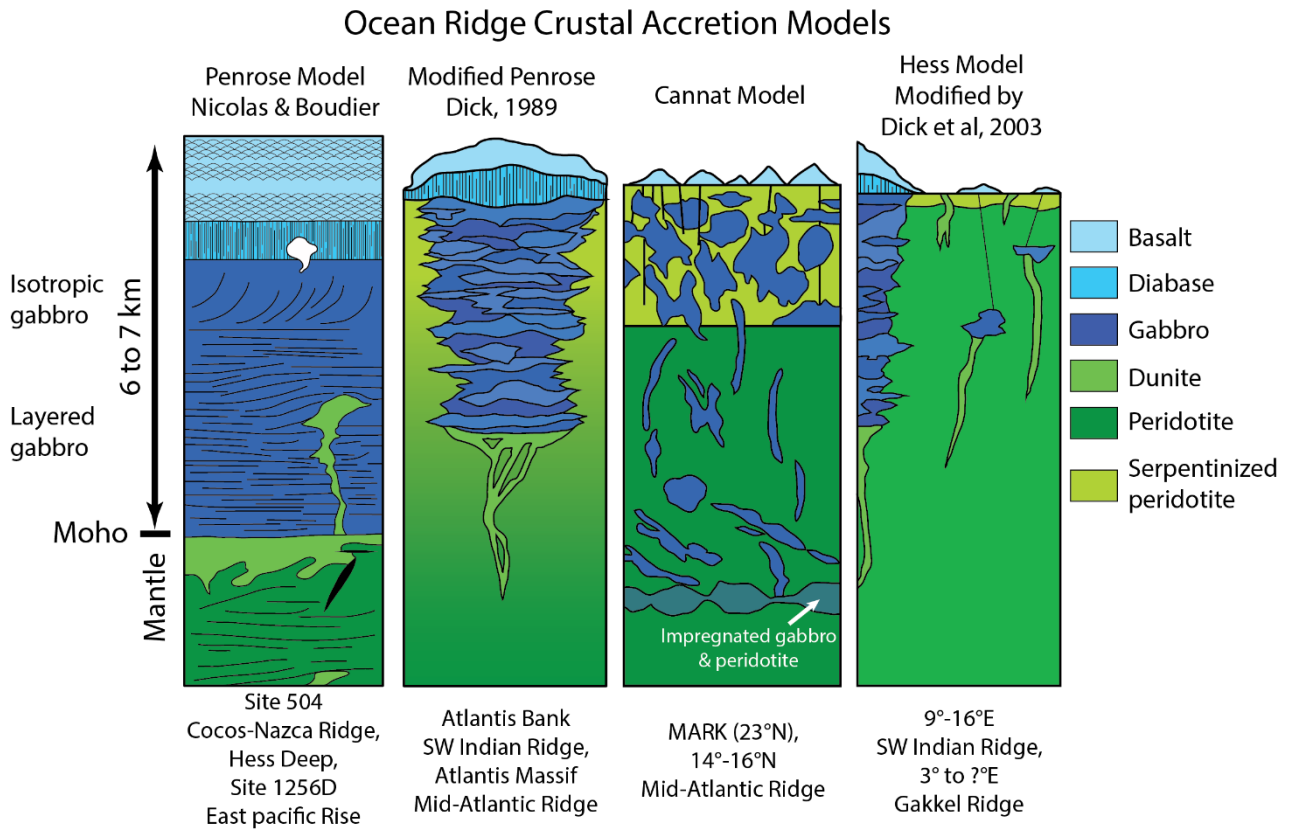

Figure 1.5: *Various architecture of oceanic crust, after Dick et al. (2006). A: Penrose model of oceanic crust as modified by Boudier & Nicolas (1985), as described from Site 504 Cocos-Nazca Ridge, Hess Deep, Site 1256D East Pacific Rise; B: Modified Penrose model after Dick (1989) as described from Atlantis Bank SW Indian Ridge, Atlantis Massif Mid-Atlantic Ridge; C: Cannat (1996, 1997) model as described from MARK (23°N), 14-16° Mid-Atlantic Ridge; Hess model, modified by Dick et al. (2003), as described from 9-16°E SW Indian Ridge, 3°E Gakkel Ridge (Michael et al., 2003).*

Morphological variations with spreading rate observed in various ridges around the world (Mid-Atlantic Ridge, South-West Indian Ridge, Gakkel Ridge) led to various models of oceanic crust formation at slow-spreading environments (Fig. 1.5), far from the Penrose reference model. They describe variable amounts of gabbroic lenses intruded in mantle peridotites, and the occurrence of a discontinuous and thinner basaltic cover. Peridotites can be extensively exposed at the ocean floor, and their serpentinization decreases with depth, which leads to a continuous variation in the seismic velocity, unlike the fast-spreading layered oceanic crust (Fig. 1.6).

No permanent and continuous magmatic chamber is feeding the oceanic crust at slow-spreading ridges. The recently discovered magmatic chamber feeding the oceanic crust under the Lucky Strike segment of the Mid-Atlantic Ridge (Singh *et al.*, 2006) is only 7 kilometres long and not continuous along the ridge axis as observed in fast-spreading ridges (East Pacific Ridge; Lissenberg *et al.*, 2013). Therefore, the evolved compositions of some of the sampled abyssal gabbros point to the need of small magmatic chambers where melts fractionate, even if not continuous in time (Sinton & Detrick, 1992). These variably evolved gabbros are found exposed on the seafloor (Fig. 1.4), and thus a process exhuming lower crustal rocks must also be invoked.

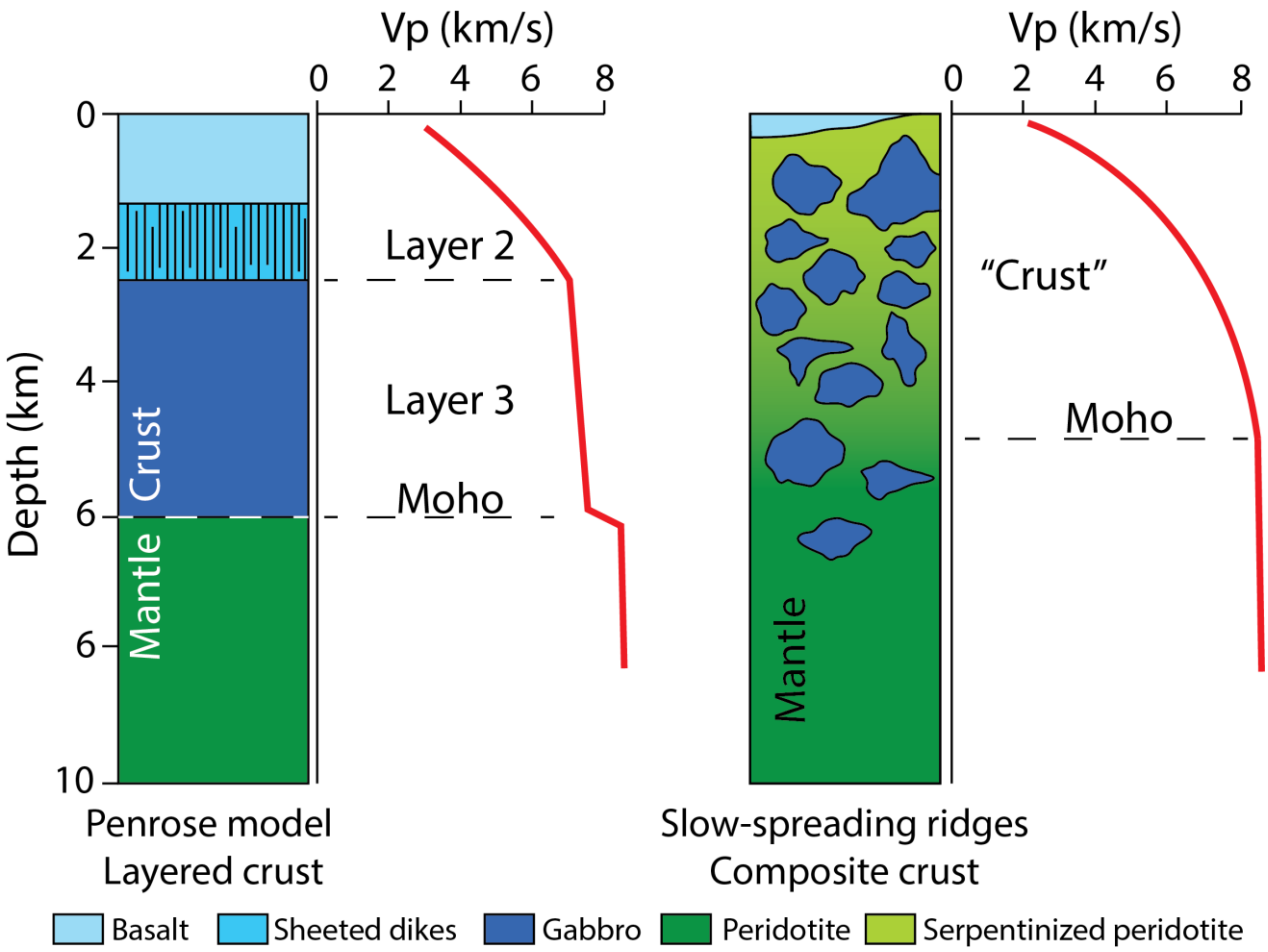

***Figure 1.6**: Seismic velocity profiles of the oceanic crust two end member models, after Mével (2003). Left: Penrose model of a layered magmatic crust; Right: Composite crust model, few magmatic intrusions into variably serpentinized peridotites.*

A low magmatic activity means that the related accretion of oceanic crust is not extensive enough to account for the observed full spreading rate (Mid-Atlantic Ridge: 4-5 centimetres/year full spreading rate; Dick *et al.*, 2003), and thus volcano-tectonic cycles (magmatic and amagmatic alternation) of a duration of about 2 million years have been proposed (Lagabrielle *et al.*, 1998; Tucholke *et al.*, 1998) to form the oceanic seafloor. During periods when magmatic activity predominates, the main spreading is done via crustal accretion from magmatic chambers similar to the one imaged at the Lucky Strike segment (Singh *et al.*, 2006). When magmatic activity decreases, the tectonic activity predominates, and detachment faults lead to the exhumation of the oceanic lithosphere, unroofing gabbroic lenses and serpentinized mantle peridotites (Fig. 1.7) (Cannat *et al.*, 1992; Cannat, 1993; Smith & Cann, 1993; Thatcher & Hill, 1995; Karson, 1999; Escartin *et al.*, 2003; Buck *et al.*, 2005; Ildefonse *et al.*, 2007; Tucholke *et al.*, 2008). The accretion-related crustal spreading forms symmetrically the seafloor from the crystallization of the upwelling magmas, whereas the tectonic exhumation of lower crustal rocks results in an asymmetry of the oceanic lithosphere, with the exhumation of the footwall of the detachment fault (Fig. 1.7) (Escartin *et al.*, 2008).

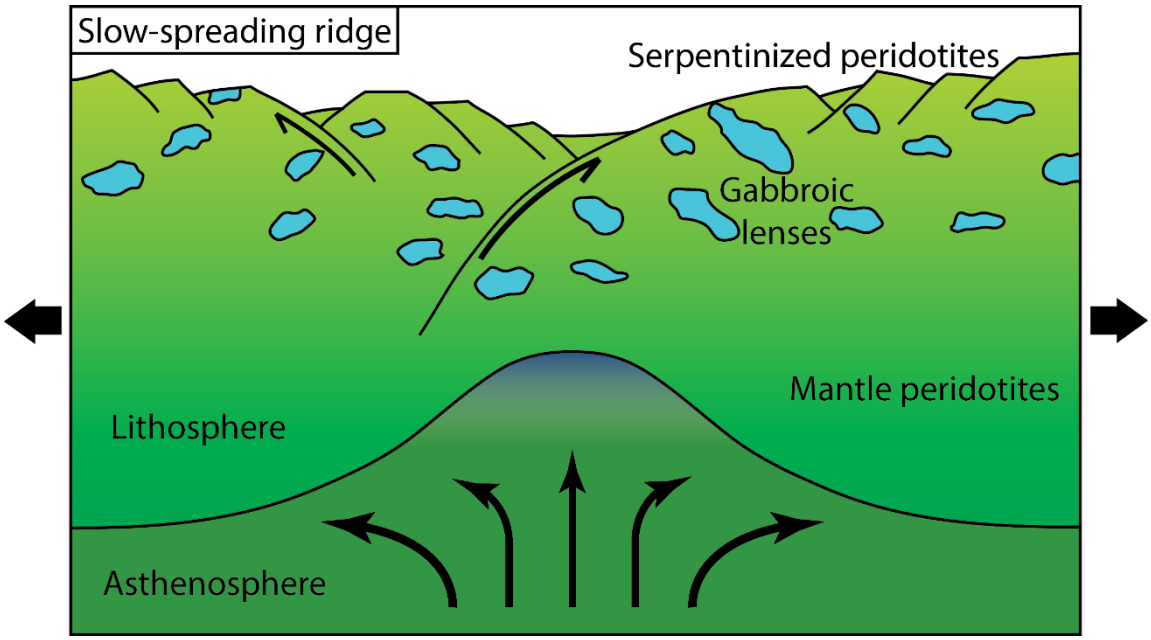

Figure 1.7: *Schematic representation of the tectonic-extension stages accommodated by detachment faults exhuming deeper levels of the oceanic crust. The detachment faults lead to the exhumation of gabbroic bodies formed at various depths.*

1.1.3. Passive margins – Ocean Continent Transition

In slow-spreading environments, the continental break-up and onset of seafloor spreading is closely related to asymmetric tectonic exhumation of sub-continental and oceanic mantle peridotitic rocks (Cannat *et al.*, 1992; Escartin *et al.*, 2008; Manatschal & Müntener, 2009). Therefore, in such environments it is difficult to pinpoint the limit between continental crust and oceanic crust. The present-day Iberia-Newfoundland magma-poor rifted margins exhibit an Ocean Continent Transition (OCT) characterized by a gradual transition of crustal seismic velocities ranging from 4 to 8 km/s within the uppermost 6 kilometres of basement (Péron-Pinvidic *et al.*, 2007, Robertson, 2007; Tucholke & Sibuet, 2007). At the OCT, tectono-sedimentary breccias are progressively grading to compositions free of continental clasts towards the ocean. The discovery of an extensional allochthon formed by continental crust in the Iberia OCT (Fig. 1.8, Péron-Pindivic *et al.*, 2007) indicates that mantle exhumation through tectonic detachment occurs before break-up of the continental crust, and thus cannot be only attributed to oceanic processes (Manatschal & Müntener, 2009). Both drill hole and geophysical data indicate that there is no sharp limit between OCT and the first oceanic crust, but rather a transitional evolution towards oceanic spreading processes (Fig. 1.8). The structures described at Iberia-Newfoundland rifted margins, namely the primary contact between subcontinental mantle and marginal sequences, the occurrence of heterogeneous breccias (both continental and ultramafic clasts) overlying exhumed mantle, have been found in some Alpine-Apennine ophiolites, suggesting that at least some of these ophiolites are not representative of oceanic spreading but are rather derived from ancient Ocean Continent Transitions (Trommsdorff *et al.*, 1993; Florineth & Froitzheim, 1994; Hermann & Muntener, 1996; Manatschal & Nievergelt, 1997; Marroni & Pandolfi, 2007).

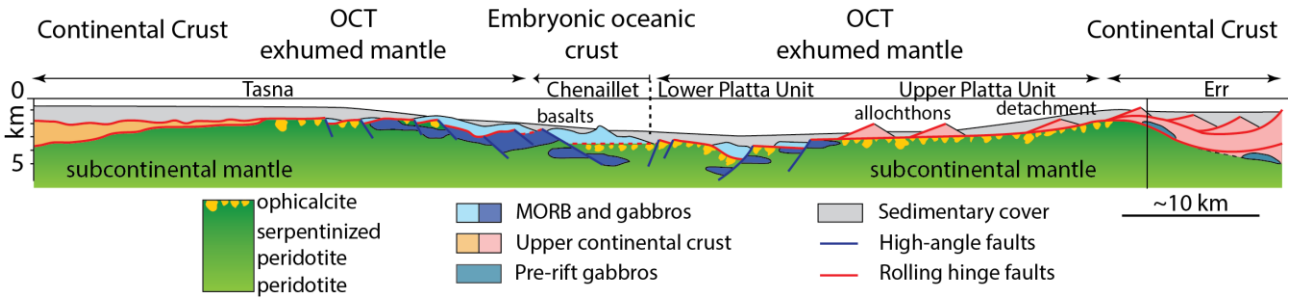

***Figure 1.8**: Reconstructed cross-section of the continental break-up and architecture of OCTs, after Manatschal and Müntener, 2009.*

1.1.4. Oman ophiolites: a fast-spreading analogue

Ophiolites are characterized by tectonically emplaced mafic-ultramafic rock associations found in orogenic belts. They represent fragments of oceanic lithosphere obducted on continental or oceanic crust (Bodinier & Godard, 2003). One of the case study presented in this thesis is the Maqsad massif Moho Transition Zone, located in the Oman ophiolites (see Chapter 5; Fig. 1.9), defined as an analogue of present-day fast spreading oceanic lithosphere. The Oman ophiolite displays the complete stratigraphic sequence from ultramafic lithologies to mafic gabbros to the volcano-sedimentary cover and has been used as a reference to develop the Penrose model of a layered oceanic crust (Fig. 1.5; Boudier & Nicolas, 1985). It is made up of several large massifs exposing a more or less complete ophiolitic sequence. Two main magmatic sequences can be distinguished in the extrusive section of the Oman ophiolites (Pearce *et al.*, 1981; Alabaster *et al.*, 1982; Lippard *et al.*, 1986; Beurrier, 1987; Ernewein *et al.*, 1988; Einaudi *et al.*, 2003; Godard *et al.*, 2003). The lower V1 Geotimes extrusive sequence (Pearce *et al.*, 1981; Lippard *et al.*, 1986; Beurrier, 1987; Ernewein *et al.*, 1988; Nicolas *et al.*, 2000; Einaudi *et al.*, 2003; Godard *et al.*, 2003) is exposed along all ophiolitic massifs (Fig. 1.9), and shows compositions consistent with mid-ocean-ridge basalts (Alabaster *et al.*, 1982; Ernewein *et al.*, 1988; Einaudi *et al.*, 2000), which formation is associated with the accretion of the Oman paleo-ridge (94-95 My; Hacker *et al.*, 1996). The upper V2 sequence is mainly exposed in the northern part of the ophiolite (Fig. 1.9) (Pearce *et al.*, 1981; Alabaster *et al.*, 1982; Lippard *et al.*, 1986; Beurrier, 1987; Ernewein *et al.*, 1988; Einaudi *et al.*, 2003; Godard *et al.*, 2003) and is characterized by low-Ti and incompatible trace elements tholeiitic melts, interpreted either as the first stages of island arc volcanism in an immature arc environment (Pearce *et al.*, 1981; Beurrier *et al.*, 1989; Godard *et al.*, 2003), either as the product of the fluid-enhanced melting of the over-ridden lithosphere during intra-oceanic thrusting of the Oman paleo-ridge (Boudier *et al.*, 1988; Ernewein *et al.*, 1988). Therefore, the spatial organisation of the Oman extrusives indicates an increased “arc signature” in the northern V2 lavas, whereas the southern ophiolitic massifs represent the MORB-type crustal accretion at the Oman paleo-ridge (Fig. 1.9; Godard *et al.*, 2003).

The extensive mapping of mantle flow patterns (Rabinowicz *et al.*, 1987; Ceuleneer *et al.*, 1988, 1996; Ceuleneer, 1991; Ceuleneer & Rabinowicz, 1992; Ildefonse *et al.*, 1995; Jousselin *et al.*, 1998; Godard *et al.*, 2000; Nicolas *et al.*, 2000) along the Oman ophiolites evidenced that crustal accretion is related to mantle diapiric structures representing zones of focussed melt flow and mantle upwelling (Godard *et al.*, 2000). The mantle diapirs are concentric structures from which foliations radiate and progressively flatten away from the diapir (Rabinowicz *et al.*, 1987; Ceuleneer *et al.*, 1988, 1996; Ceuleneer, 1991; Ceuleneer & Rabinowicz, 1992; Ildefonse *et al.*, 1995; Jousselin *et al.*, 1998). The Maqsad diapir is the best exposed example of such a mantle diapir (Fig. 1.10), showing

radiating peridotite lineations and kilometre-scale continuous flow structures (Ceuleneer, 1991; Ceuleneer & Rabinowicz, 1992; Ildefonse *et al.*, 1993; Nicolas & Boudier, 1995; Ceuleneer *et al.*, 1996; Boudier *et al.*, 1997; Jousselin *et al.*, 1998; Godard *et al.*, 2000) and interpreted as the spreading centre of at least part of the Sumail massif (Fig. 1.10). The geochemical investigation of the harzburgites and dunites from the Maqsad area by Godard *et al.* (2000) demonstrated that the diapirs represent instabilities triggered by partial melt upwelling and high melt flows. The mantle diapir is topped by a layer of replacive dunites indicative of the accumulation of large quantities of melt at the mantle-crust transition (Nicolas & Prinzhofer, 1982; Boudier & Nicolas, 1995; Godard *et al.*, 2000; Jousselin & Nicolas, 2000; Koga *et al.*, 2001; Higgie *et al.*, 2012; Abily & Ceuleneer, 2013).

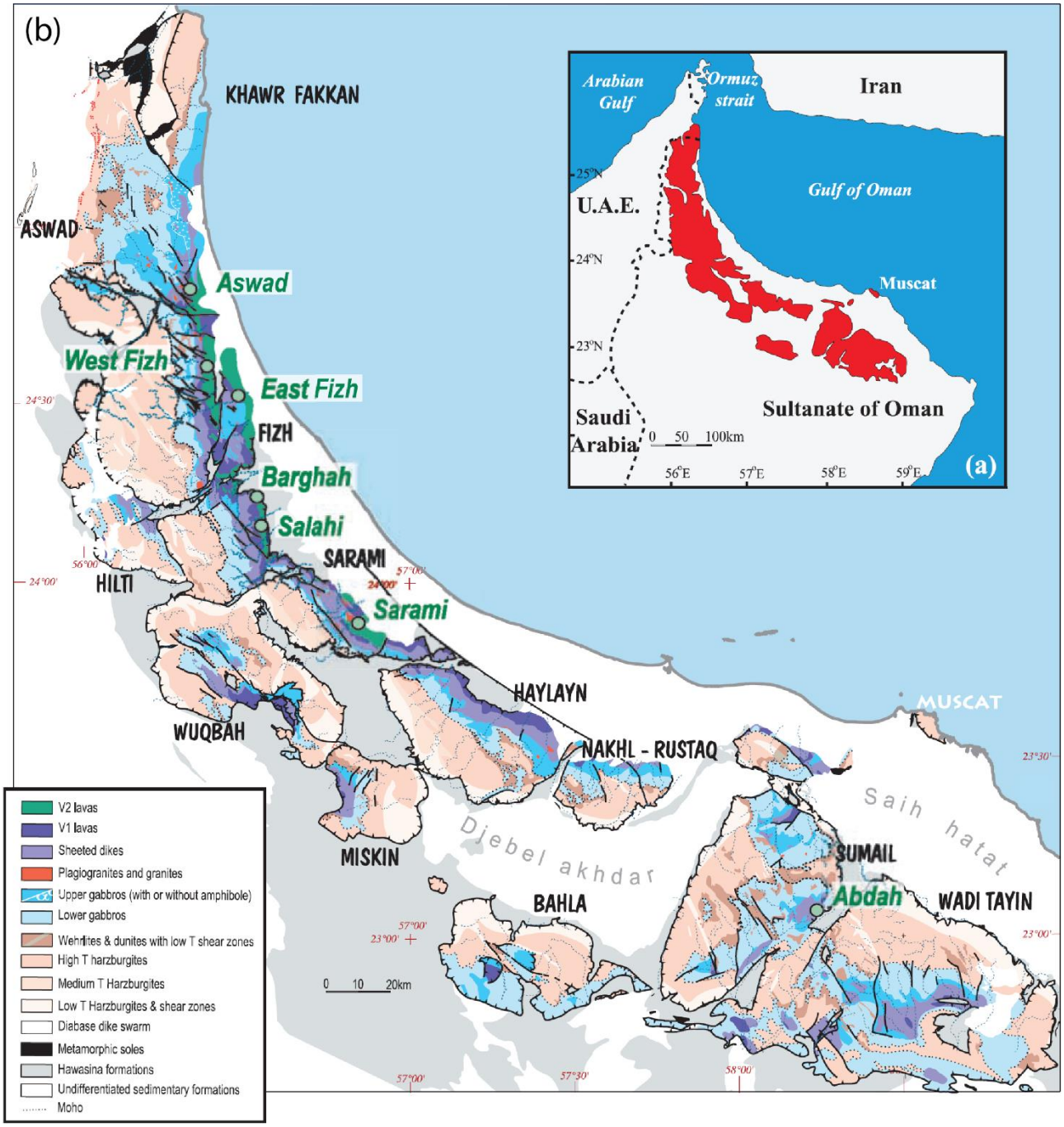

***Figure 1.9**: A: Location of the Oman ophiolite, NE of the Arabian Plate; B: 12 principal structural massifs (names indicated in black upper case) and constituting lithotypes, after Godard et al. (2003).*

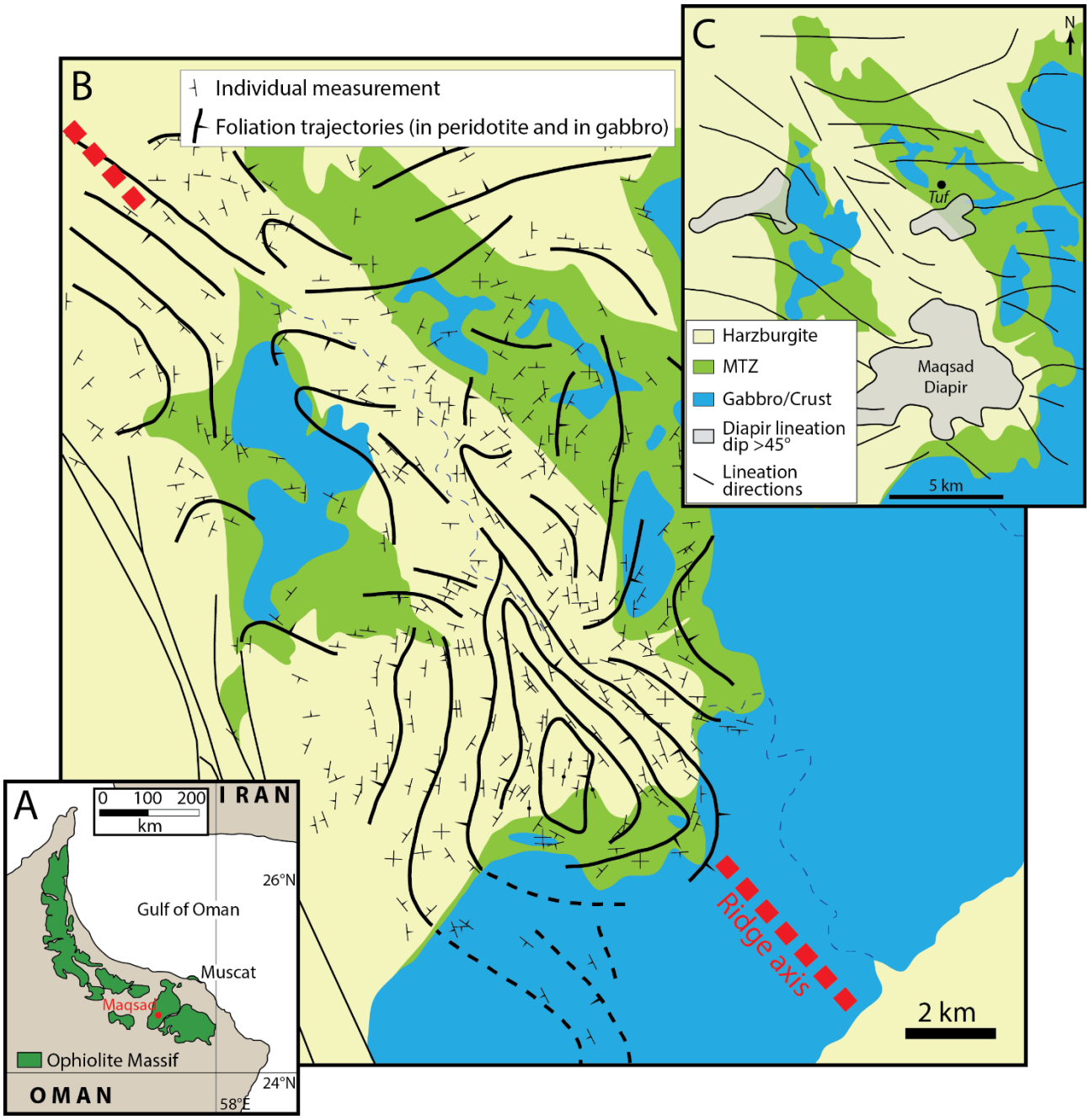

***Figure 1.10**: Mapping of the foliation planes in the harzburgites, Moho Transition Zone, and gabbros, after Jousselin et al. (1998). A: Location of the diapiric structure in the Oman ophiolite; B: Mapping of the planar structures including individual measurements, and the proposed position of the paleo-ridge axis; C: Mapping of lineation directions and location of the Maqsad Diapir, after Nicolas et al. (2000), Jousselin et al. (2012) and Higgie & Tommasi (2012).*

The Moho Transition Zone (Fig. 1.10), the focus of the Oman case study presented in this thesis, represents the transition between mantle harzburgites and the gabbroic lower crust, and is characterized by a layering of interfingered dunites and variably evolved olivine gabbros (Boudier & Nicolas, 1995; Kelemen *et al.*, 1997; Korenaga & Kelemen, 1997; Koga *et al.*, 2001; Higgie *et al.*, 2012). This layering was long considered to be formed either by intrusion and fractional crystallization in horizontal fractures associated with a reorientation of the stress field (Ildefonse *et al.*, 1993; Boudier *et al.*, 1996) or by melt accumulation during porous flow in a media with variable porosity (Rabinowicz *et al.*, 1987; Boudier & Nicolas, 1995; Kelemen *et al.*, 1997; Korenaga &

Kelemen, 1997). Rather, the recent structural study by Higgie & Tommasi (2012) demonstrated the replacive origin of the olivine gabbro layers after open system reactive porous flow in the dunite and progressive dissolution of olivine and crystallization of plagioclase and clinopyroxene. The layering formed by a positive feedback between the focused deformation in weak layers and the melt focused flow in deformed permeable layers (Higgie & Tommasi, 2012).

1.1.5. The Alpine-Apennine ophiolites: an ultra-slow spreading analogue vs OCT

The two other case studies presented in this thesis are part of the Alpine-Apennine ophiolites (Erro-Tobbio ultramafic body, see Chapter 3; Monte Maggiore peridotitic body, see Chapter 4). The Alpine-Apennine ophiolites were formed during passive extension of the Europe-Adria continental lithosphere and opening of the Jurassic Ligurian Tethys (or Alpine Tethys) ocean, a small slow-spreading oceanic basin with maximum estimated width of 800 kilometres, an overall length of 1000 kilometres, and spreading rate of 2 cm/year (see Rampone *et al.*, 2014; and references therein).

Salient feature of the Alpine-Apennine ophiolites is the predominant association of old (pre-Jurassic) lithospheric mantle that was exposed at the sea floor and largely subordinate younger (Jurassic) oceanic crustal rocks (gabbroic intrusions and discontinuous basaltic cover). Accordingly, they were defined as "passive margin ophiolites", sharing great similarities with modern non-volcanic passive continental margins (Iberia-Newfoundland Ocean Continent Transition; Péron-Pindivic *et al.*, 2007) and ultra-slow spreading ridges (Rampone & Piccardo, 2000; Piccardo *et al.*, 2002; Marroni & Pandolfi, 2007; Manatschal & Müntener, 2009; Piccardo, 2009; Mohn *et al.*, 2010; Piccardo & Guarnieri, 2010). This was already described in pioneering studies (Elter, 1972; Lemoine *et al.*, 1987) inferring mantle exhumation as a key process in the oceanic evolution of these ophiolites.

The ophiolitic units cropping along the Alpine-Apennine belt have been assigned to different (pericontinental vs. intraoceanic; Fig. 1.10) settings within the Jurassic Ligurian Tethys ocean (Manatschal & Müntener, 2009; Marroni & Pandolfi, 2007; Mohn *et al.*, 2010, Picazo *et al.*, 2014) (Fig. 1.11). Recent structural and petrologic studies on the Central and Western Alps ophiolites (Müntener & Piccardo, 2003; Manatschal & Müntener, 2009; Picazo *et al.*, 2014) provided a paleogeographic reconstruction of the Alpine Tethys oceanic lithosphere, with distinct mantle domains (from marginal to more intra-oceanic), corresponding to different deformation and melt-related processes recorded in the exhumed mantle (Fig. 1.12): i) old "inherited" subcontinental lithospheric mantle (primarily associated to continental crust) which was tectonically exhumed and did not experience melting and/or melt migration events during Jurassic, ii) more internal, "infiltrated" lithospheric mantle (Fig. 1.12) which was affected by multiple melt-rock interaction stages during exhumation and, eventually, partial melting to produce the Jurassic crust. The External Liguride (Northern Apennines), Lanzo North (Western Alps) and Malenco, Upper Platta, Totalp (Eastern Central Alps) peridotites are mostly reconcilable to subcontinental mantle domains (Figs. 1.11, 1.12), whereas the Erro-Tobbio (Ligurian Alps), Lanzo South, Mt.Maggiore (Alpine Corsica), Internal Liguride (Northern Apennines) peridotites largely represent mantle domains affected by melt infiltration events (Figs. 1.11, 1.12). Although being a simplified scheme, because interference and transition from "inherited" to "infiltrated" mantle domains are visible in a specific mantle unit at the outcrop scale, it is anyhow useful to introduce the different, partly overprinted, melt-rock reaction stages that these peridotites experienced during their long-lived mantle evolution.

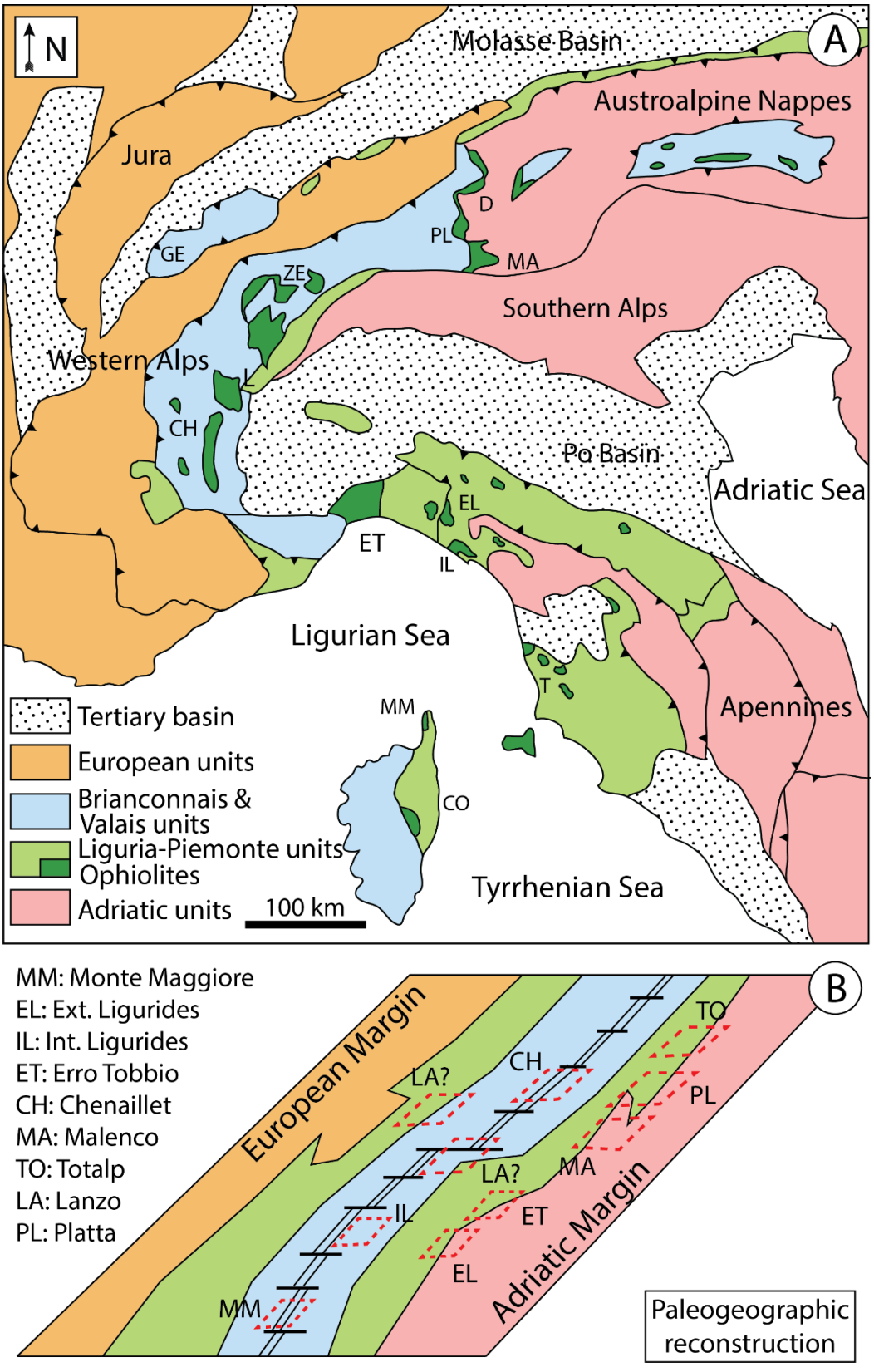

***Figure 1.11**: A: Tectonic map showing the location of the major Alpine units, and major ophiolite massifs in the Central-Western-Ligurian Alps, Northern Apennines, and Alpine Corsica. B: Paleogeographic reconstruction of the Piemont-Ligurian ocean during Late Jurassic, with proposed location of the major ophiolitic units. Redrawn after Manatschal & Müntener (2009) and Rampone & Hofmann (2012).*

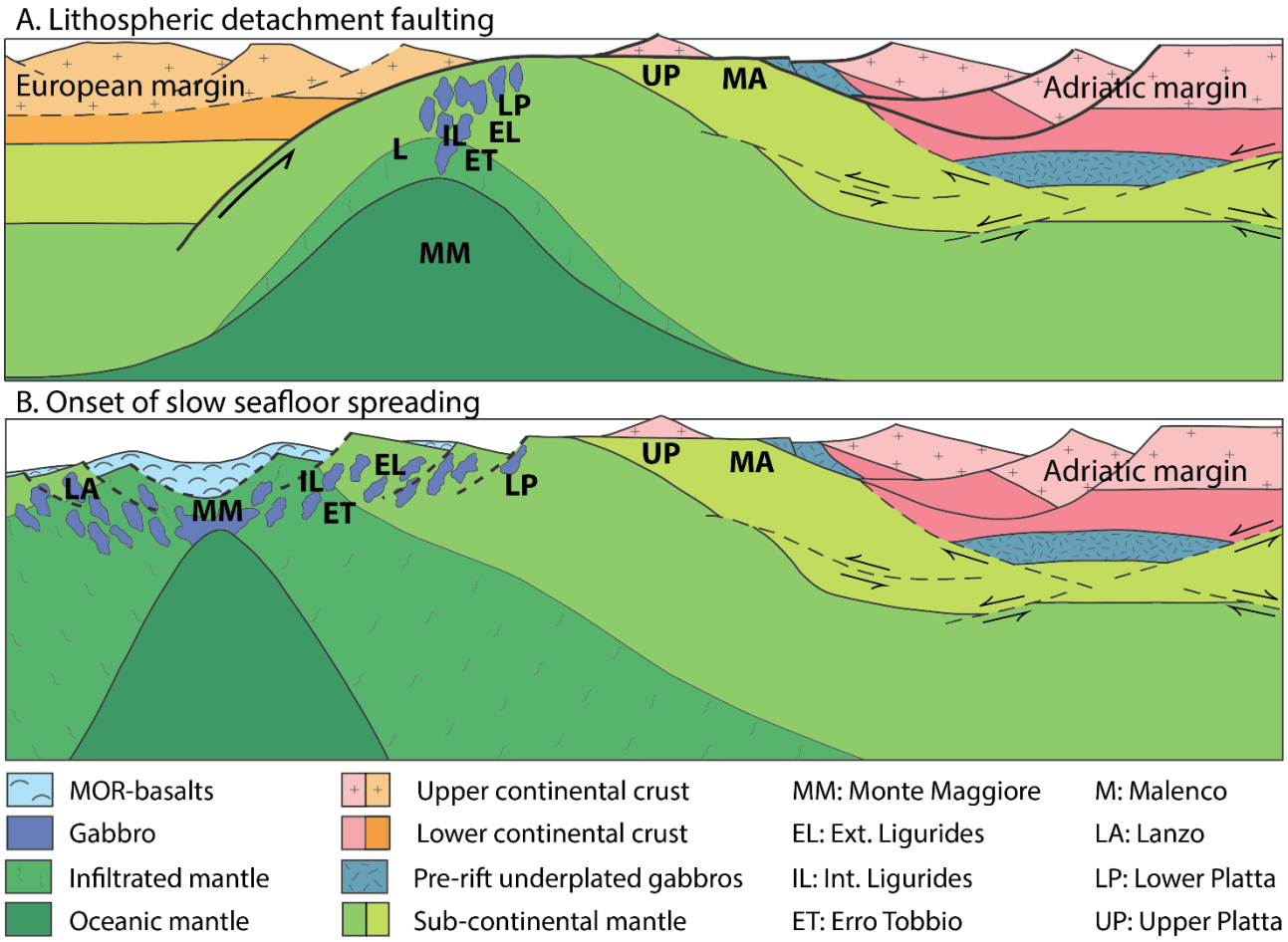

***Figure 1.12**: Tectonic sketch of evolution of the Piemont-Ligurian basin during opening. A: Lithospheric detachment faulting and exhumation of sub-continental mantle at the seafloor. B: Complete break-up and onset of slow seafloor spreading by formation of oceanic crust and exhumation of oceanic asthenospheric mantle. Redrawn after Müntener & Piccardo (2003).*

1.2 Formation of the oceanic crust

1.2.1. Formation of MORB-type melts during mantle decompression

Tholeiitic melts are formed during decompression partial melting of the upwelling asthenospheric mantle, under the oceanic ridge axis (Green & Ringwood, 1967; Green *et al.*, 1979; Warren, 2016). Numerous dredging of abyssal peridotites confirmed the variably depleted composition of the lithospheric mantle rocks underlying the oceanic crust, consistent with their residual character after variable melting degrees (Johnson *et al.*, 1990; Salters & Stracke, 2004; Workman & Hart, 2005; Warren, 2016). MORB-type melts, although showing strong compositional variabilities (Collier & Kelemen, 2010; Gale *et al.*, 2013; Paquet *et al.*, 2016), have been described as aggregates of single melt increments of mantle partial melting, produced over a great range of depths in a mantle column, starting in the garnet stability field (Johnson *et al.*, 1990; Sobolev & Shimizu, 1993; McDonough & Sun, 1995; Workman & Hart, 2005; Gale *et al.*, 2013, 2014) (Fig. 1.13). The composition of the melt produced by decompression melting varies with the amount of melting, from LREE-enriched melts at low degrees of melting to LREE-depleted melts at higher degrees of melting (Fig. 1.13), consistent with the higher incompatibility of the Light Rare Earth Elements. Therefore, an aggregated normal MORB (N-MORB) is characterized by a relatively flat REE pattern, from 15 to 20 times C1 chondrite compositions (Fig. 1.13; Gale et al., 2013).

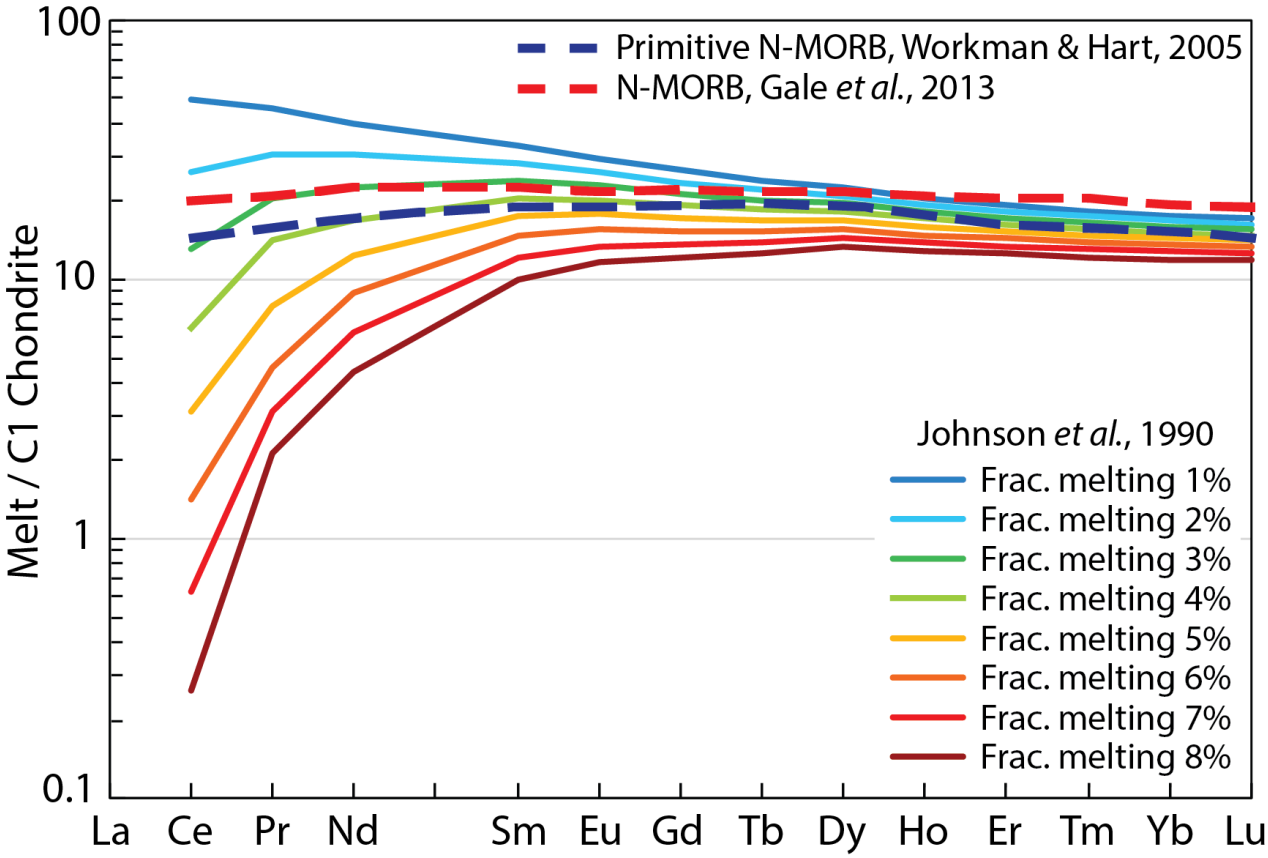

Figure 1.13: *Modelled single melt increments compositions produced by partial melting of a depleted MORB mantle (Workman & Hart, 2005), following the equation of Johnson et al., 1990. The red and blue dashed lines correspond to N-MORB and primitive N-MORB, after Workman & Hart (2005) and Gale et al. (2013) respectively.*

The MORB melts produced by the aggregation of these single melt increments show primitive compositions (Mg# = 70-71), therefore in equilibrium with the rock-forming minerals of the residual mantle peridotite (Olivine Forsterite = 90) (Kinzler & Grove, 1993). However, most basaltic rocks sampled along mid-ocean ridges show more evolved compositions (Mg#<68; Green & Falloon, 2005; Gale *et al.*, 2013), suggesting that primary magmas must undergo differentiation processes during upward migration within the oceanic crust (Grove *et al.*, 1992; O'Hara & Herzberg, 2002; Herzberg, 2004; Herzberg *et al.*, 2007; Laubier *et al.*, 2012; Gale *et al.*, 2013; Coogan & O'Hara, 2015).

1.2.2. The lower oceanic crust: two end-member models of formation

The oceanic crust is formed by the accumulation and the crystallization of ascending tholeiitic MORB melts. Models of formation of the lower oceanic crust (Sublayer 3A and 3B) imply the accumulation of melts in magmatic chambers and the formation of cumulate gabbros. The number of magmatic chambers needed in the process of formation of accretion is still a matter of debate. Two end-member models have been defined: The "Gabbro Glacier model" (Henstock *et al.*, 1993; Phipps Morgan & Chen 1993; Quick & Denlinger; 1993) and the "Sheeted Sills model" (Bédard *et al.*, 1988; Kelemen *et al.*, 1997; Korenaga & Kelemen, 1997; MacLeod & Yoauancq, 2000) (Fig. 1.14). The "Gabbro Glacier model" infers that all the lower oceanic gabbros are formed mainly from a shallow and a deep sill and then subside downwards and away from the ridge, whereas the "Sheeted Sills model" is based on numerous sills throughout the lower crust, that crystallize the gabbroic cumulates in situ, without any downward movement. The melt extraction from a sill to upper levels of the lower oceanic crust is done through periodic hydrofracturing of the formed cumulates (Fig. 1.14).

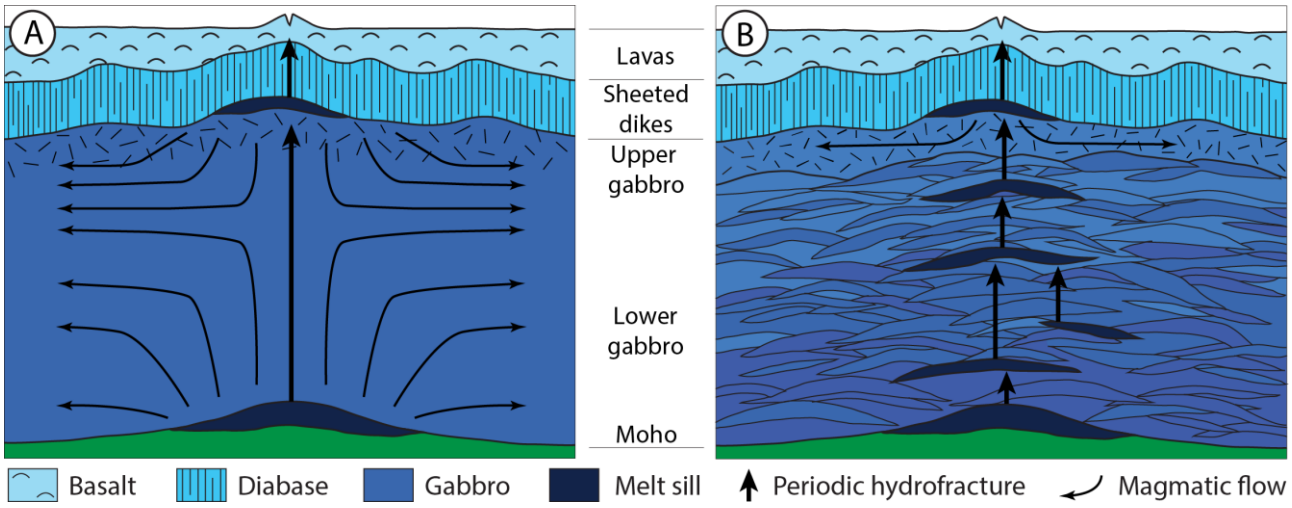

***Figure 1.14**: Schematic illustrations of the two end-member models of formation of the lower oceanic crust. Redrawn after Kelemen et al. (1997). A: Lower crustal gabbros mostly crystallized in two major sills, one near the Moho Transition Zone, and a second just below the base of the sheeted dikes. Flow of the gabbroic crystalline mush from the two sills progressively forms the lower oceanic crust. The melt is extracted from the lower sill by a periodic hydrofracturing. The composition of the gabbros is expected to be uniform with depth in this scenario. B: The lower gabbros form in "sheeted sills" that crystallize the crust in situ. In this model, there will be an irregular chemical variation of the gabbros with depth, trending towards more evolved compositions at shallower depths.*

Both end-member models of formation of the lower oceanic crust have further implications. In terms of cooling rates, a mainly conductive cooling of the crust is possible in the case of the "Gabbro Glacier model", but a convective cooling of the crust is needed for the "Sheeted Sills model", with deep hydrothermal fluids extracting the heat from the lowest part of the oceanic crust. The "Gabbro Glacier model" would form a gabbroic lower oceanic crust with relatively constant bulk chemical compositions, all formed from the same melt lense, whereas the "Sheeted Sills model" would lead to chemical variations with depth, with melts trending towards more evolved compositions at shallower depths, after fractional crystallization in the deepest parts. Available data do not allow to clearly define the dominating model of formation of the crust (Kelemen *et al.*, 1997; Korenaga & Kelemen, 1997).

The IODP oceanic drillings directly sample the present-day oceanic crust, and the bulk chemical analyses in a gabbroic section of the Southwest Indian Ridge (Leg 176) reported by Dick *et al.* (2000) reveals a vertical stacking of magmatic sequences showing an evolution of the composition up-section, corresponding to cumulate crystallization from several sills or magmatic chambers (Fig. 1.15) within the crust, therefore supporting the Sheeted Sills model.

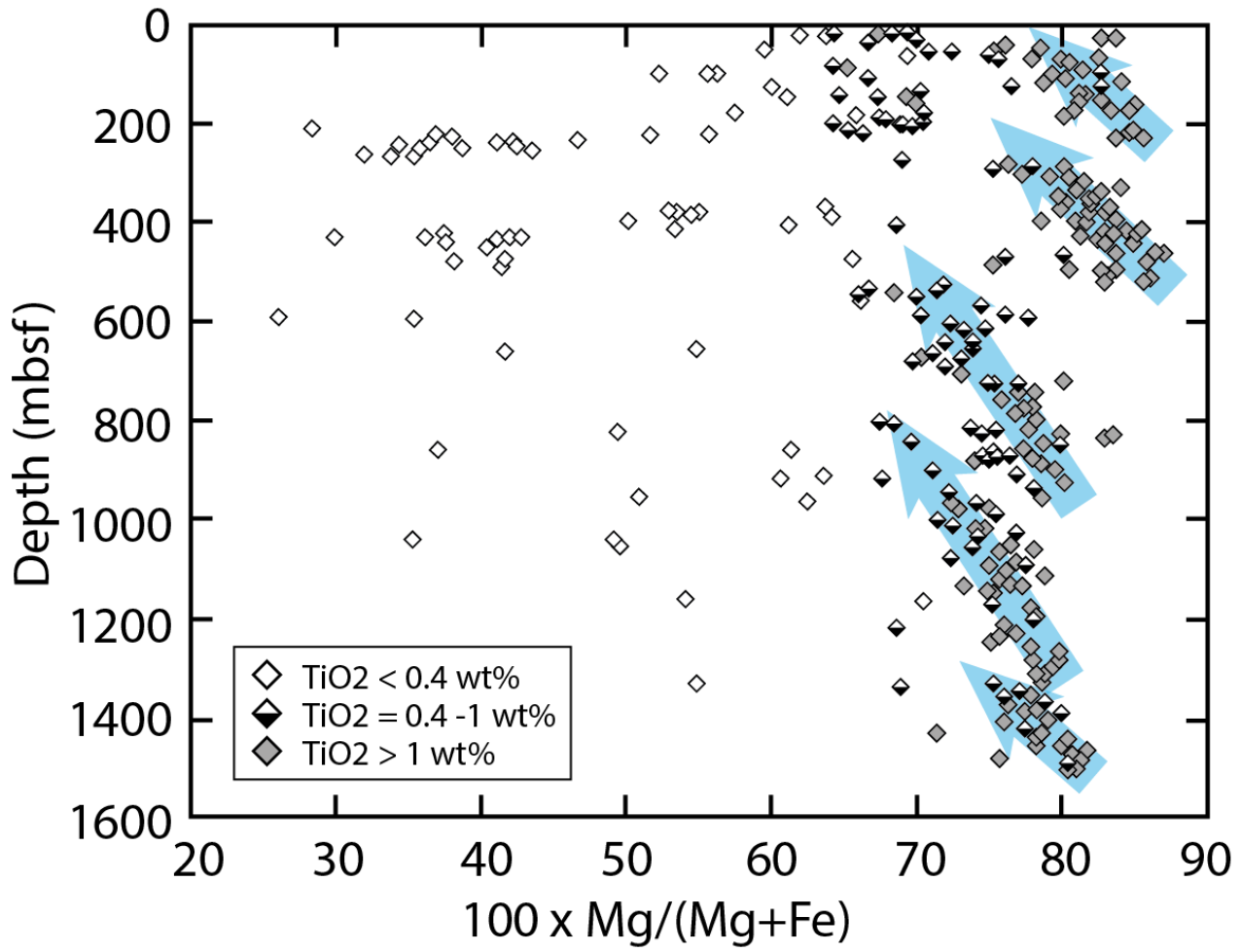

***Figure 1.15**: Southwest Indian Ridge (Leg 176) magmatic evolution of the compositions with fractionation in several magmatic sequences, redrawn after Dick et al. (2000). Shipboard X-Ray Fluorescence (XRF) bulk-rock molecular $Mg/(Mg+Fe^{2+})$ against sample depth. $FeO = 0.85 \times Fe_2O_3$ (Dick et al., 1991, 1999). Arrows in the background indicate each evolution trend within the gabbroic section.*

1.2.3. Fractional vs Equilibrium crystallization

Both end-member models of formation of the lower oceanic crust infer the crystallization of the lower crustal gabbros as cumulates in sills. Within the gabbros, the occurrence of textural features typical of solid-liquid separation processes (i.e. modal and grain-size layering, cumulate texture varying from ad- to orthocumulate) indicates that fractional crystallization of the melt within the sills is the dominant process in the formation of the lower oceanic crust (Villiger *et al.*, 2004; 2007a). The fractional crystallization is defined by the removal of the crystallized phases during the differentiation process. This does not enable any reaction between the crystallized phases and the remaining melt fraction, thus corresponding to an open system crystallization of the melt. Equilibrium crystallization processes, on the other hand, characterize a closed system crystallization of the melt, where the remaining melt can interact with the solid phases formed.

Numerous experiments have been performed using various melt compositions at variable conditions of Temperature, Pressure, Oxygen fugacity and Water content to understand the phase equilibria of basaltic magmas at the Earth's surface and in shallow-level magma chambers (e.g. Bowen, 1914, 1928; Andersen, 1915; Yoder & Tilley, 1962; Green & Ringwood, 1967; O'Hara, 1968; Thompson, 1975; Bender *et al.*, 1978; Grove & Bryan, 1983; Nielson & Dungan, 1983; Baker & Eggler, 1987; Grove & Juster, 1989; Longhi, 1991; Grove *et al.*, 1992; Yang *et al.*, 1996; Villiger *et al.*, 2004, 2007a, 2007b; Feig *et al.*, 2006, 2010; Gillis *et al.*, 2014). Although most of the experimental studies use an equilibrium crystallization method, Villiger *et al.* (2004, 2007a, 2007b) compared the results of the equilibrium crystallization of a basaltic glass (i.e. closed system crystallization of the melt during cooling) to the fractional crystallization process, using a series of experiments where the remaining glass after each step of crystallization at a given temperature is used as a starting material for the following 30°C cooler experiment. This enables to remove the crystallized phases after each step of 30°C cooling and continue the crystallization experiment from the remaining melt fraction. They compared the difference between the two processes of crystallization and observed a faster evolution of the melt composition when no reaction is possible between the remaining melt and the crystallized phases (i.e. for fractional crystallization) (Fig. 1.16). An important difference is observed in the crystallized mass at a given temperature between the fractional and equilibrium crystallization, respectively 93% and 69% crystallized at 1090°C (Fig. 1.16c,d). The phase saturation and the order in which the different phases crystallize (olivine, spinel, plagioclase, clinopyroxene, orthopyroxene, quartz and ilmenite) does not change from one end-member crystallization process to the other. Though, the temperature at which these phases appear varies, leading to changes in the composition of the remaining melt fraction (Fig. 1.16a,b). Fig. 1.16 b shows clearly that the liquid line of descent of Al_2O_3 (weight% in the melt) drastically changes with the saturation and crystallization of plagioclase. The fractional crystallization process leads to a faster evolution of the melt composition (Villiger *et al.*, 2004, 2007a, 2007b) and reaches saturation of Quartz at 1090°C, whereas the equilibrium crystallization reaches saturation of plagioclase only at 1120°C (Fig. 1.16).

1.2.4. Controlling factors on MORB crystallization

Very few experiments of fractional crystallization have been performed (Villiger *et al.*, 2004, 2007a, 2007b), hence we will here consider the results of the Equilibrium Crystallization experiments. The chemical evolution of the melt during progressive crystallization is related to the fractionated phases (Fig. 1.16), thus is similar for most primitive MORB melts, which are characterized by the low-pressure crystallization sequence: [Olivine + Liquid] – [Olivine + Plagioclase + Liquid] – [Olivine + Plagioclase + Clinopyroxene ± Orthopyroxene + Liquid] (Grove & Ringwood, 1967; Grove & Bryan, 1983; Tormey *et al.*, 1987; Juster *et al.*, 1989; Grove *et al.*, 1992; Herzberg, 2004; Villiger *et al.*, 2004).

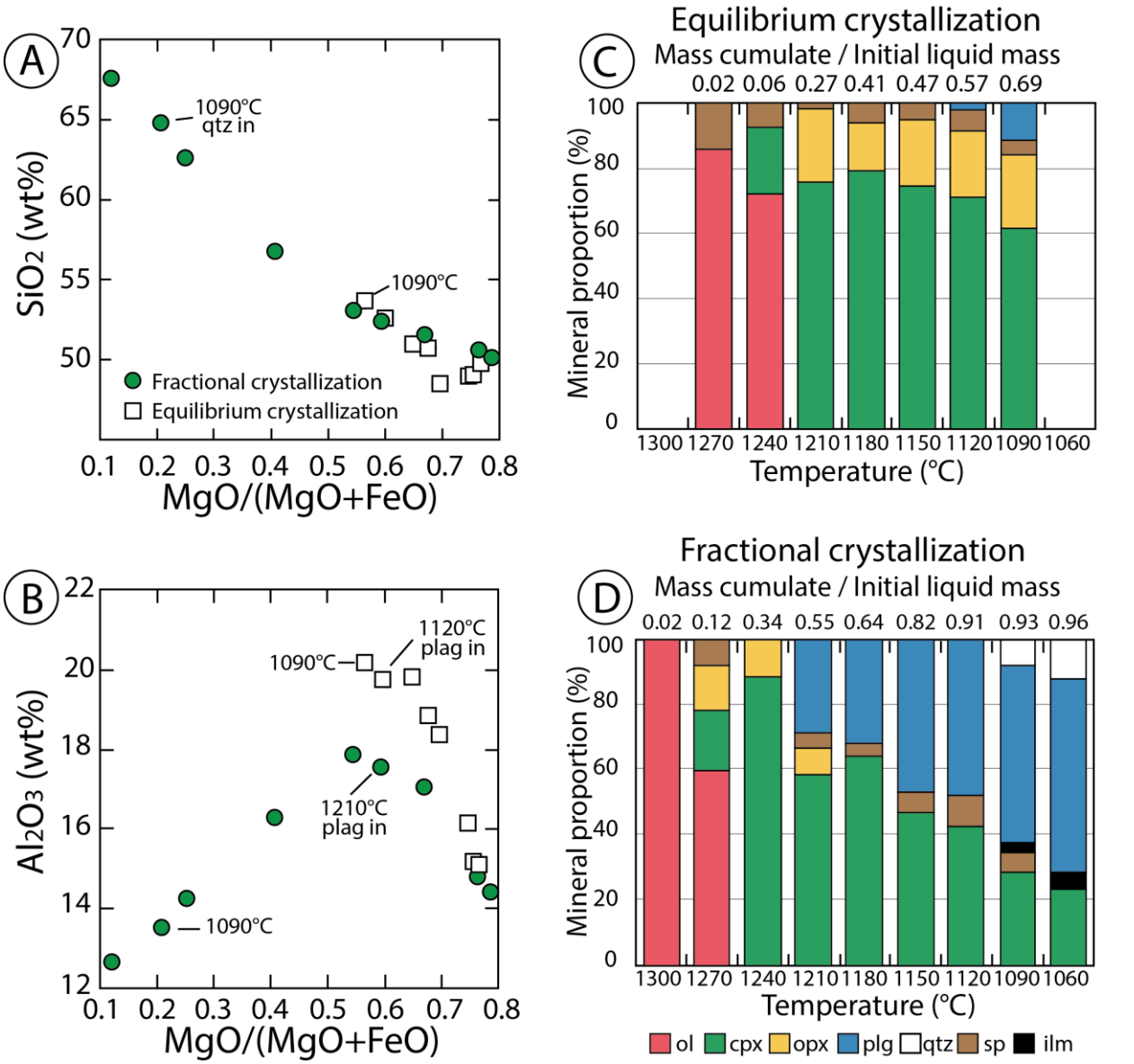

***Figure 1.16**: Equilibrium vs Fractional crystallization of a basaltic melt, after Villiger et al. (2004). A: Glass MgO/(MgO+FeO) against SiO_2 (wt%), empty squares represent the Equilibrium crystallization, whereas the green circles are Fractional crystallization; B: Glass MgO/(MgO+FeO) against Al_2O_3 (wt%); C: Evolution of the cumulate mass and modal composition during equilibrium crystallization of the melt; D: Evolution of the cumulate mass and modal composition during fractional crystallization of the melt.*

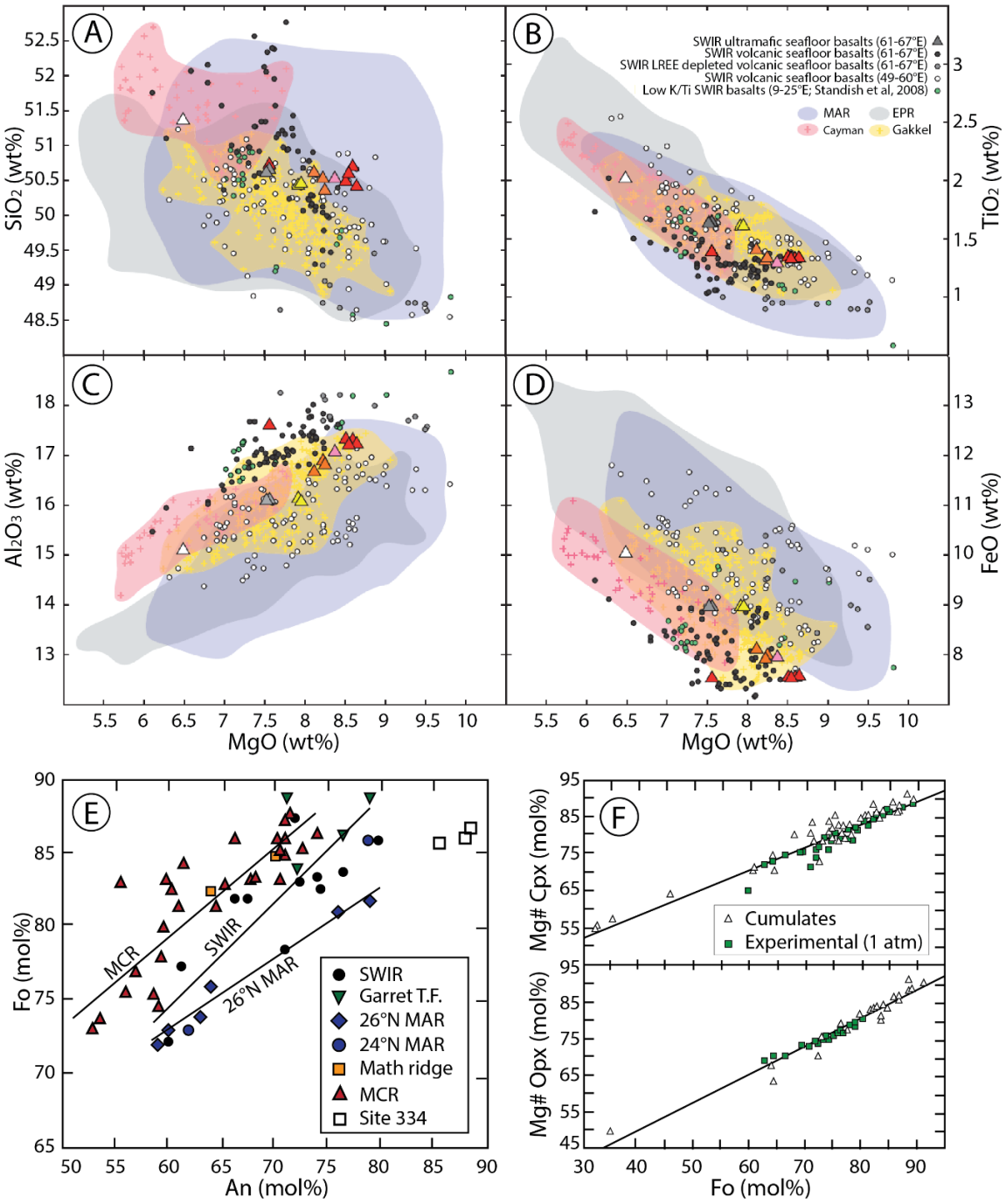

***Figure 1.17**: A-D: Major elements chemical compositions of basaltic glasses, after Paquet et al. (2016). MgO (wt%) against A: SiO_2 (wt%); B: TiO_2 (wt%); C: Al_2O_3 (wt%); D: FeO (wt%). Reference data from PetDB dataset (Lehnert et al., 2000; Meyzen et al., 2003; Standish et al., 2008; Gale et al., 2014); E: Forsterite vs Anorthite covariation in oceanic gabbroic suites. Approximate trends of variation for South-West Indian Ridge, Mid-Atlantic Ridge, and Mid-Caiman Ridge are given by the black lines. Data are after Meyer et al. (1989) for SWIR, Hebert et al. (1983) for Garret Transform, Tiezzi & Scott (1980) and Miyashiro & Shido (1980) for MAR, Vanko & Batiza (1982) for the Mathematician Ridge, Elthon (1987) for the MCR, and Hodges & Papike (1976) and Clarke & Loubat (1977) for DSDP site 334; F: Forsterite vs Mg-number in clinopyroxene and orthopyroxene after Elthon et al. (1992). The data for cumulates are from Hodges & Papike (1976), Tiezzi & Scott (1980), Elthon (1987), Bloomer et al. (1989), Meyer et al. (1989) and Hebert et al. (1991). Experimental data are from Grove & Bryan (1983), Tormey et al. (1987) and Grove & Juster (1989).*

This crystallization sequence gives rise to ubiquitous chemical covariations between the rock-forming minerals and chemical trends of variation of the remaining melt fraction over gabbroic suites worldwide (Fig. 1.17a,b,c,d) (Elthon *et al.*, 1992; Paquet *et al.*, 2016). Fig. 1.17 shows that from a primitive MORB melt to a more evolved melt (i.e. at decreasing MgO content), a trend of increase in SiO_2, TiO_2 and FeO, and decrease in Al_2O_3 is observed in basaltic glasses from both slow- and fast-spreading environments (East Pacific Rise, Mid-Atlantic Ridge, Cayman Ridge, Gakkel Ridge, Paquet *et al.*, 2016). The crystallized phases define positive correlations of Forsterite in olivine, Anorthite in plagioclase and Mg# in both ortho- and clinopyroxene (Fig. 1.17e,f) (Bender *et al.*, 1978; Elthon *et al.*, 1992; Grove *et al.*, 1992; Herzberg, 2004). In natural gabbroic suites, the Forsterite value in olivine generally ranges from 90 to 60 mol%, the Anorthite value in plagioclase ranges from to 90 to 50 mol% (Fig. 1.17e), and the Mg# (MgO/FeO+MgO) in ortho- and clinopyroxene ranges from 90 to 60 mol% (Fig. 1.17f). They all decrease with evolving compositions of the melt (i.e. at decreasing melt fraction).

Figure 1.17 also evidences that, in spite of similar covariation trends, different MORB series exhibit large chemical heterogeneity, at a given MgO. Similarly, different gabbroic suites define distinct, although roughly parallel Forsterite-Anorthite trends (Fig. 1.17e). Experimental studies on the crystallization of basaltic melts showed that the phase saturation and the chemical composition of minerals can vary as a function of some parameters, such as the melt composition, water content and crystallization pressure. The major control on phase saturation and order of crystallization is given by the composition of the melt. In Fig. 1.18, three different starting melt compositions are presented (Husen, 2014; Husen *et al.*, 2016), namely the relatively primitive melt AH-6 (8.6 wt% MgO), an intermediate melt AH-3 (8.0 wt% MgO), and the more evolved AH-5 (6.4 wt% MgO). The crystallization of Olivine is strongly suppressed in more evolved melts (AH-5, Fig. 1.18 C), while the crystallization of Clinopyroxene is favoured, becoming the liquidus phase. Primitive melts are also characterized by higher temperatures of crystallization, with up to 50°C difference between the liquidus temperature of AH-6 (8.6 wt% MgO, 1200°C at 1 atm) and AH-5 (6.4 wt% MgO, 1150°C at 1 atm).

Pressure has long been considered to have a minor effect on the results of crystallization experiments (Walker *et al.*, 1979), which is the reason why many studies have been conducted at atmospheric pressures (Grove & Bryan, 1983; Grove & Baker, 1984; Juster *et al.*, 1989; Sano *et al.*, 2001; Thy *et al.*, 1998, 1999). However, the crystallization of MORB melts occurs mainly in the oceanic crust (1 to 6 km depth, corresponding to approximatively 30 to 200MPa), and only few studies performed their experiments at pressures relevant for crustal levels (Feig *et al.*, 2006, 2010; Husen, 2014; Husen *et al.*, 2016). Bender *et al.* (1978) showed that the stability field of clinopyroxene is strongly influenced by the pressure, with an earlier crystallization (at higher temperature) at higher pressures. As a result, we observe a change in the order of crystallization of a primitive melt (AH6 and AH3) from the classical [olivine – plagioclase – clinopyroxene] to [clinopyroxene – plagioclase – olivine] (Fig. 1.18). An increase in the pressure leads to an increase in the liquidus temperature of a melt (Husen, 2014; Husen *et al.*, 2016), thus an earlier crystallization of the first mineral phases (the liquidus phase being clinopyroxene at high pressures). A correlation between pressure and the chemical composition of the crystallized phases has also been observed (Fig. 1.19a), with an increase of Al_2O_3, Na_2O and TiO_2 abundances in clinopyroxene (Putirka *et al.*, 1996, 2003), and a decrease in Anorthite content at increasing pressures (at a given temperature).

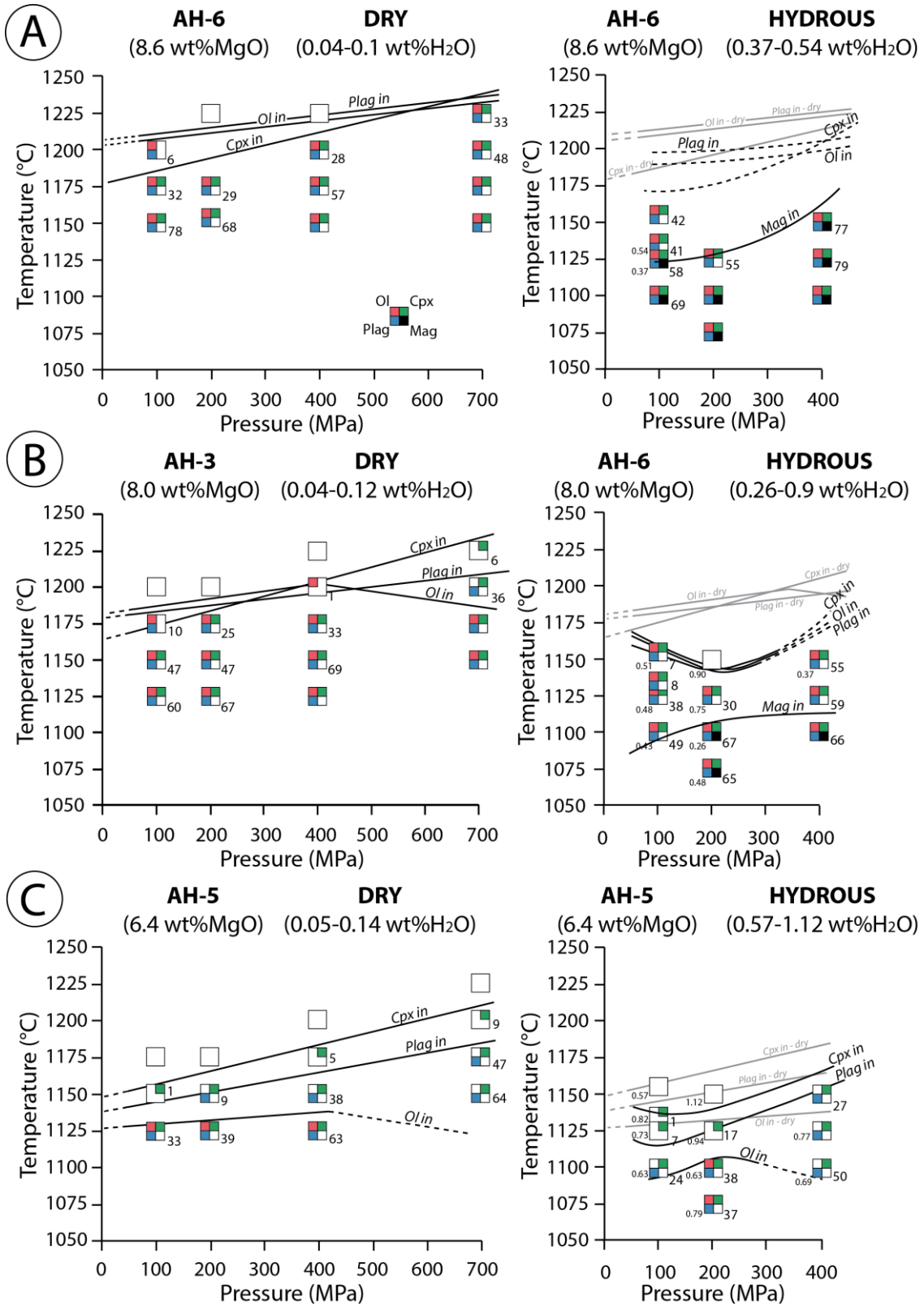

Figure 1.18: *Stability of the mineral phases as a function of pressure and temperature for three different starting material, after Husen et al. (2016). The initial MgO content decreases from top to bottom (AH6: 8.6%, AH3: 8%, AH5: 6.4%). The filled corners of the squares represent the presence of the corresponding phase (Top left: Olivine, top right: Clinopyroxene, bottom left: Plagioclase, bottom right: Magnetite. Numbers next to the squares indicate the crystallized portion, and the stability field are indicated by the solid lines. For each initial composition, dry (left column) and hydrous (right column) experiments have been performed.*

Addition of water in a dry system has been shown to decrease drastically the liquidus temperature of a melt. This in turn increases the amount of melt at a given temperature and has a significant effect on MORB petrogenesis (Danyushevsky, 2001; Asimow & Langmuir, 2003; Feig *et al.*, 2006, 2010). High water contents can invert the crystallization order of a tholeiitic melt at low pressure, causing a decrease in the stability field of plagioclase. The observed order of crystallization at high water contents thus becomes [Olivine – Clinopyroxene – Plagioclase] (Gaetani *et al.*, 1993, 1994). The presence of water also favours the formation of hydrous minerals, such as amphibole and biotite. Aside the effects on the mineral stability fields at higher water contents, changes in mineral composition have been observed (Fig. 1.19c,d), such as a significant increase in the Forsterite content in olivine (up to 12 mol% at constant temperature; Toplis & Carroll, 1995; Berndt *et al.*, 2005; Feig *et al.*, 2006, 2010), Anorthite content in plagioclase (up to 25 mol% increase at a constant temperature from a moderate bulk water to a water-saturated run; Koepke *et al.*, 2004; Berndt *et al.*, 2005; Feig *et al.*, 2006), and Mg-number in clinopyroxene (MgO/[FeO+MgO])(Fig. 1.19b,c).

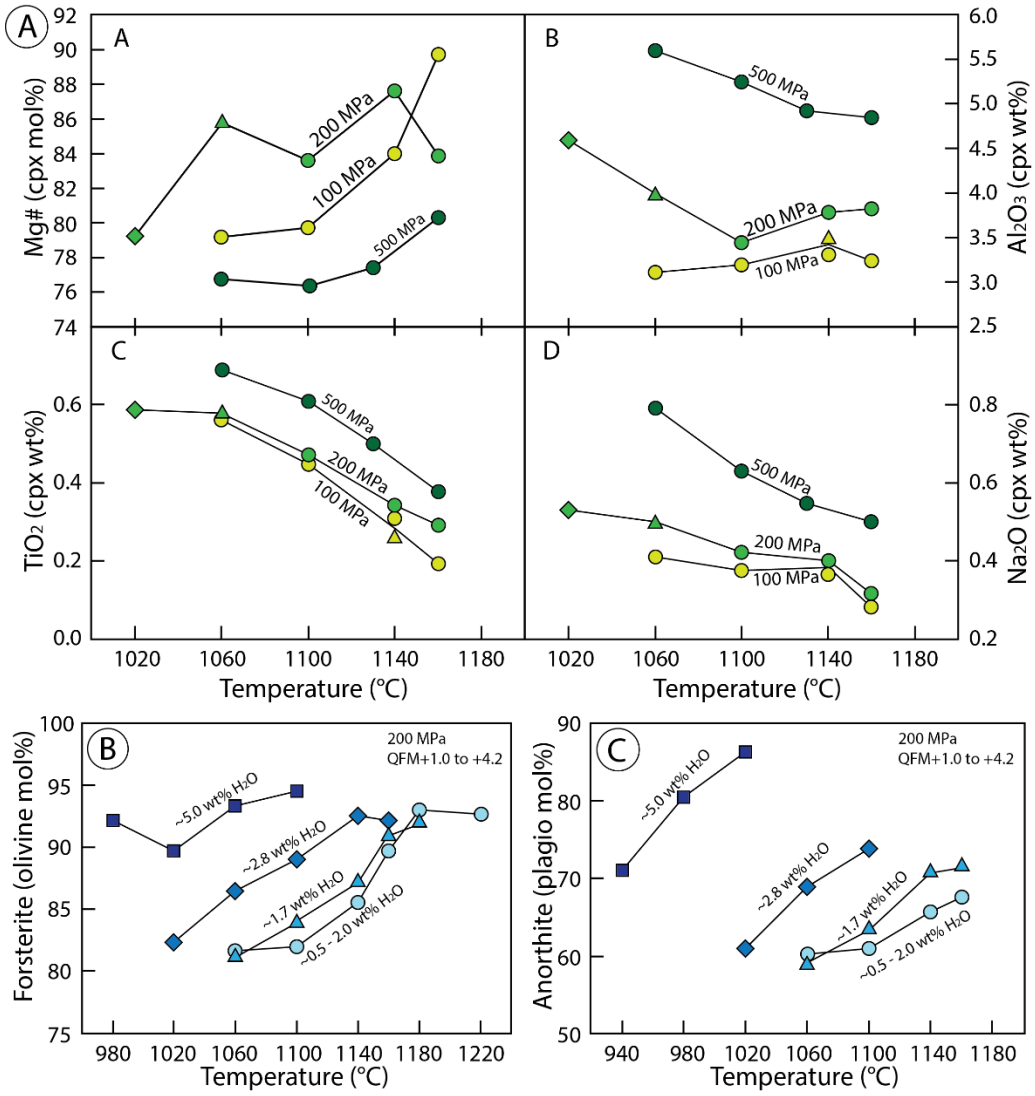

Figure 1.19: *Experimental results of the evolution of mineral compositions with pressure and water content in a tholeiitic melt, after Feig et al. (2006). A: Composition of Mg# (MgO/[MgO+FeO]), Al_2O_3 (wt%), TiO_2 (wt%), Na_2O (wt%) in the clinopyroxenes crystallized at different temperatures and pressures (100, 200 and 500MPa); B: Forsterite content in olivines crystallized at different temperatures and water contents in the melt; C: Anorthite content in plagioclase crystallized at varying temperatures and water contents in the melt.*

1.3 Melt-rock interaction processes

1.3.1. Melt transport

Melts formed in the upwelling mantle need to be transported to shallower levels through the mantle, in order to crystallize and generate the oceanic crust. Within the ductile mantle, the dominating transport mechanism is porous flow (percolation of the melt through the peridotitic matrix, Stevenson, 1989; Daines & Kohlstedt, 1994; Spiegelman *et al.*, 2001; Miller *et al.*, 2014; Pec *et al.*, 2015). The organization of the melts at grain scale within a partially molten peridotite is a critical parameter for the transport of the melt (Goetze, 1977, Kohlstedt, 1992). Melt migration by porous flow is faster if melt-filled intergranular space is well interconnected and slower if melt remains trapped in isolated pockets (Fig. 1.20a,b,c, Faul, 1997; Cmiral *et al.*, 1998; De Kloe *et al.*, 2000; De Kloe, 2001; Miller *et al.*, 2014). Theoretically, at chemical equilibrium, the textural reorganization of the peridotite-melt system is driven by the minimisation of total surface free energy γ, the extra free energy of atoms at interfaces between phases and at the boundary between grains of the same phase. Surface energy minimisation results in the interdependent processes of continuous grain growth and redistribution of liquid into lower energy configurations (Cmiral *et al.*, 1998; De Kloe *et al.*, 2000; De Kloe, 2001). In a polycrystalline aggregate, the criterion for disappearance of a solid-solid grain boundary by wetting is: $\gamma_{gb} > 2\ \gamma_{sl}$, where γ_{gb} is the grain boundary energy and γ_{sl} is the solid-liquid interfacial energy. The surface energy can be expressed as a function of the dihedral angle θ, defined at the contact between the solid-solid grain boundary and the liquid (Fig. 1.20d,f). For $\gamma_{gb} > 2\ \gamma_{sl}$, $\theta = 0°$, the grain boundaries are not stable, and the grain surfaces are completely wetted (Smith, 1964; Cmiral *et al.*, 1998, De Kloe *et al.*, 2000). When the dihedral angle at the triple grain junctions is less than 60°, a network of connected grain edge tubes is formed (Fig. 1.20d,e,f; Smith, 1964; Bulau *et al.*, 1979; Waff & Bulau, 1982; Toramaru & Fujii, 1986; Riley & Kohlstedt, 1991; Beeman & Kohlstedt, 1993; Hirth & Kohlstedt, 1995, De Kloe *et al.*, 2000). For an olivine-basalt system, dihedral angles between 20 and 50° have been reported (Fig. 1.20f), and thus the formation of an interconnected melt network is possible at melt fractions lower than 1% (Waff & Bulau, 1979; McKenzie, 1984; Von Bargen & Waff, 1986; Daines & Richter, 1988; Riley *et al.*, 1990; Bussod & Christie, 1991; Riley & Kohlstedt, 1991, Cmiral *et al.*, 1998; De Kloe *et al.*, 2000).

The distribution of the melt in the solid matrix is modified when the host rock is under stress and being deformed. At differential stresses exceeding 10MPa, interface energies are replaced by the applied differential stress as the main driving force for grain boundary diffusion (Visser, 1999). In the experimental studies of Jin *et al.* (1994) and Bai *et al.* (1997), this change in driving force results in the formation of melt layers at differential stresses between 10 and 40MPa. The melt that resided in the melt tubes at static conditions spreads out along grains interfaces under differential stress, indicative of a dihedral angle of the olivine-basalt system of 0°. In these conditions, the solid-solid and solid-liquid interface energies no longer determine the melt distribution.

This melt organization is also observed at larger scale with development of high permeability, melt-enriched channels. Several processes have been investigated to account for their formation. The first process invoked, that will be discussed later (see 1.3.2. Melt rock interactions in the mantle), inferred melt channelling by reactive infiltration instability mechanism. It infers that during adiabatic ascent, the melt becomes undersaturated in pyroxene and that this instability leads to a positive feedback that amplifies the local perturbations in melt distribution and thus in permeability (Ortoleva *et al.*, 1987; Daines & Kohlstedt, 1994; Aharonov *et al.*, 1995, 1997).

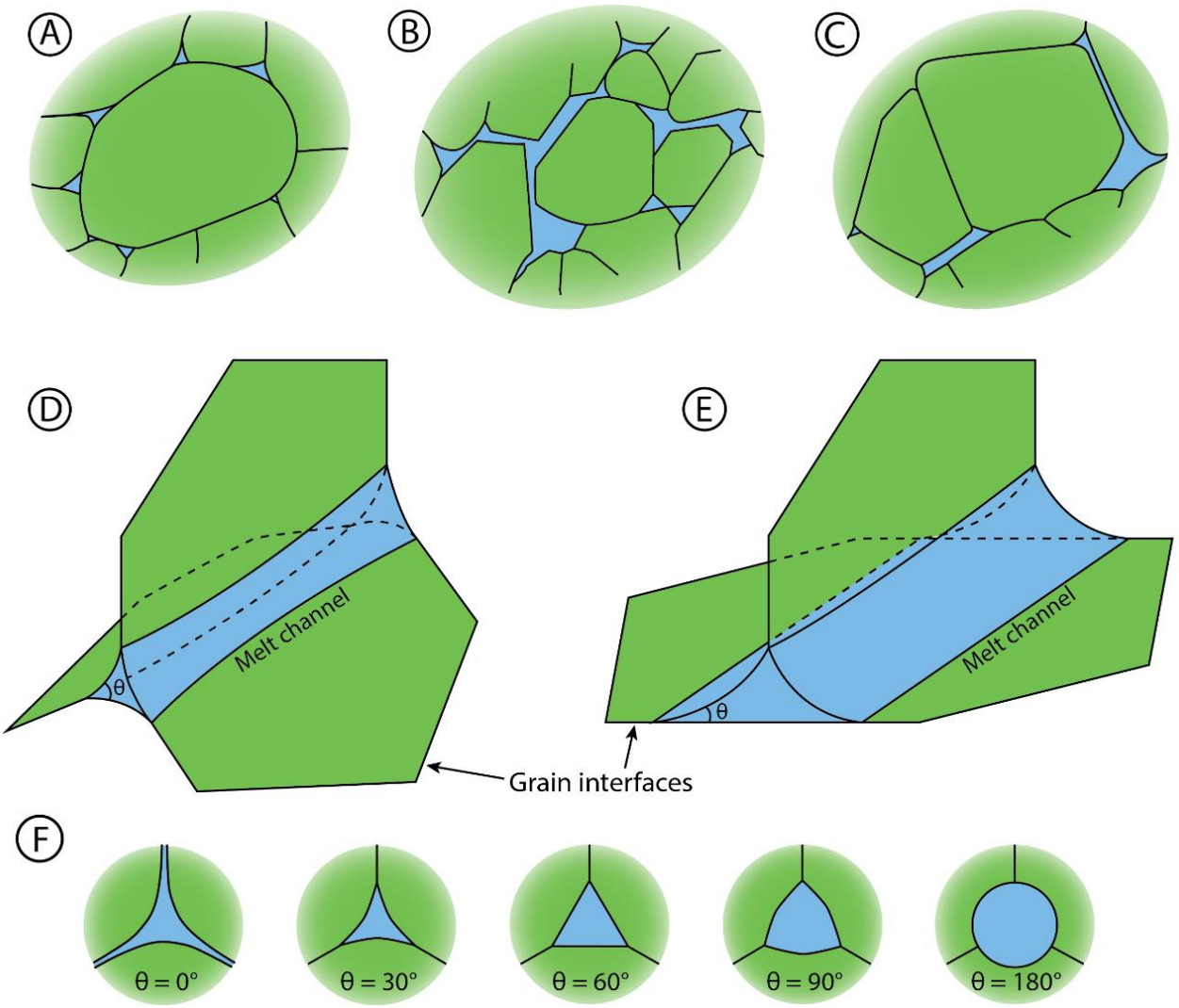

***Figure 1.20**: A-C: Different types of melt occurrence in a partially molten peridotite, after De Kloe et al., (2000) and De Kloe (2001). A: The melt concentrates in grain edge tubes, forming triangular shaped triple junctions; B: Higher melt/rock ratio, the melt connectivity extends along several grains; C: Continuous melt layers along grain interfaces. Nanometre-scale melt films may occur along all grain interfaces indicated by solid lines; D-F: Schematic representation of melt tubes along three-grain intersections, after De Kloe (2001). D: Symmetrical grain edge tube; E: Flattened melt tube along a crystallographic flat face, characterized by lower dihedral angles at the contact between the flat face and the melt phase. Note the larger cross-sectional area of the melt tube; F: Schematic geometry of the grain edge melt tube for increasing dihedral angles at triple grain junctions. Connectivity of melt-filled grain edge melt tubes is established at dihedral angles below 60°.*

The second process of channel formation is stress-driven melt segregation (Fig. 1.21; Stevenson, 1989; Kelemen & Dick, 1995; Holtzman *et al.*, 2003a,b, Kohlstedt & Holtzman, 2009). Holtzman & Kohlstedt (2007) infer that the melt is locally focussed into the weaker zones, thus into the permeable deformed zones enriched in melt (Stevenson, 1989), and creates a positive feedback leading to melt segregation and channel growth. Both mechanisms lead to the formation of high-permeability channels that isolate the melt phase from the solid host rock (Fig. 1.21), thus causing a chemical disequilibrium between the ascending magmas and the host rock (Kelemen *et al.*, 1997a).

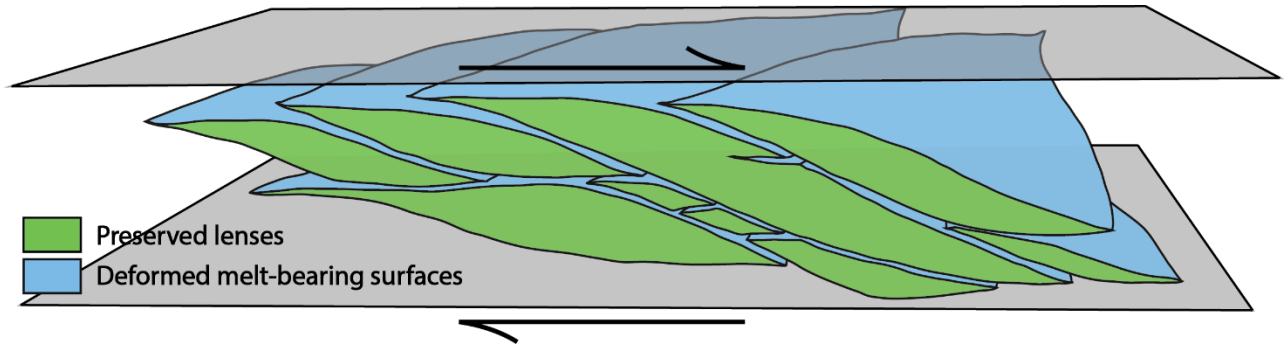

***Figure 1.21**: Experimental deformation-induced focussed flow after Holtzman & Kohlstedt (2007). The two planes are undeformable and melt-rich bands are transparent. The positive feedback between the weakening of melt-rich layers and the preferential input of melt into weak layers leads to the formation of deforming high porosity channels.*

Temperature-pressure conditions also play a role on the large-scale organization of the migrating melt. At lower temperatures, in the Thermal Boundary Layer (TBL), the initiation of crystallization of plagioclase and clinopyroxene fills the pore space and therefore decreases the permeability of the host rock. The formation of a permeability barrier is therefore possible when the melt reaches multiple saturation and increased crystallization rate of [plagioclase + clinopyroxene] (Sparks & Parmentier, 1991; Spiegelman, 1993; Korenaga & Kelemen, 1997; Hebert & Montési, 2010). The formation of this permeability barrier is related to the multiple saturation of the melt, thus depending on the thermal regime at the ridge axis (Hebert & Montési, 2010). It deepens away from the ridge following isotherms (Fig. 1.22). This impermeable layer is inferred to be a barrier for melt migration, leading the melt focussing in the highest temperature zones towards the ridge axis (Fig. 1.22).

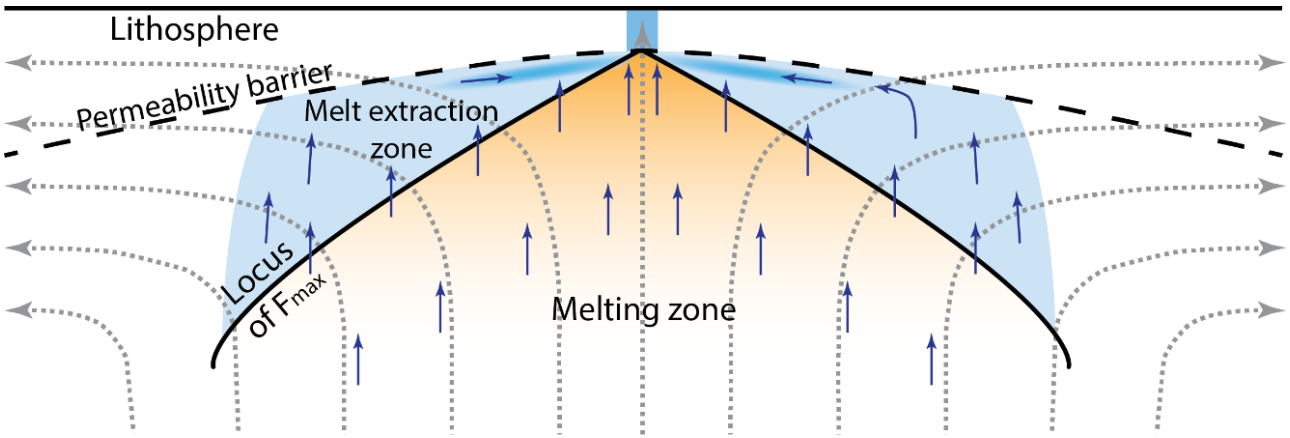

***Figure 1.22**: Schematic representation of melt organization and focussing at spreading ridges, after Hebert & Montési (2010). Permeability barrier is marked by the black dashed line. Blue arrows represent melt flux.*

1.3.2. Melt-rock interactions in the mantle

The percolation of melts by porous flow into mantle peridotites is accompanied by melt-rock interactions, whose effects are dominated by the melt composition, and physical parameters (temperature, pressure). The most ubiquitously described dissolution-precipitation reactions are: (1) open system reactive porous flow occurring at spinel facies conditions; (2) melt impregnation occurring at plagioclase facies conditions (e.g., Rampone & Borghini, 2008; Rampone *et al.*, 2018).

(1) During ascent from the melting region in the asthenosphere to the thermal boundary layer and lithospheric mantle, melts become progressively undersaturated in pyroxenes and oversaturated in olivine (Kelemen, 1990; Kelemen *et al.*, 1990, 1995a,b, 1997a, 2000). At spinel facies conditions, the disequilibrium between mantle peridotites and the percolating melt leads to a reactive porous flow characterized by dissolution of mantle pyroxenes and crystallization of olivine. Field evidence, such as the dissolution of primary pyroxenite layers and increasing modal composition of olivine in peridotites, as well as microstructural features (e.g. embayments of olivine on exsolved and deformed mantle pyroxenes) have been extensively described in ophiolites worldwide and interpreted as the result of this olivine-saturated reactive melt percolation at spinel facies depths (Ronda peridotites: Soustelle *et al.*, 2009; Trinity ophiolite: Dygert *et al.*, 2016; Lanzo peridotites: Bodinier, 1988; Piccardo *et al.*, 2004, 2005, 2007a; Erro Tobbio peridotites: Rampone *et al.*, 2004; Borghini *et al.*, 2007; Piccardo & Vissers, 2007; Rampone & Borghini, 2008; Monte Maggiore peridotites: Müntener & Piccardo, 2003; Piccardo, 2003, 2007; Rampone *et al.*, 2008; Piccardo & Guarnieri, 2010; Oman ophiolite: Nicolas & Prinzhofer, 1982; Boudier & Nicolas, 1995; Kelemen *et al.*, 1995; Godard *et al.*, 2000; Hanghoj *et al.*, 2010; Higgie & Tommasi, 2012; Abily & Ceuleneer, 2013). This dissolution-precipitation reaction can lead to changes in the major and trace elements composition of the melt. Several studies showed that the reaction between the percolating melts and the host harzburgitic wall-rock, dissolving pyroxenes and crystallizing olivine, will rapidly drive the melt to orthopyroxene-saturation (Kelemen *et al.*, 1995b; Dijkstra *et al.*, 2003; Rampone *et al.*, 2008; Van den Bleeken *et al.*, 2011), and Rampone *et al.* (2008) modelled changes in the melt REE composition related to the reactive melt percolation at spinel facies, namely an M-HREE-enrichment at constant LREE fractionation.

The increasing porosity resulting from the dissolution-precipitation reaction creates a positive feedback, i.e. melt input will continuously focus in the weaker melt-bearing zones, characterized by higher dihedral angles, and ultimately lead to the formation of high-permeability dunite channels (Fig. 1.23; Kelemen, 1990; Kelemen *et al.*, 1990, 1995a, b, 1997a, 2000; Suhr, 1999; Suhr *et al.*, 2008; Higgie *et al.*, 2012). The formation of these high-permeability dunitic channels has strong implications for melt extraction processes and geochemical evolution of the percolating melts (Kelemen *et al.*, 1995a). Numerical models have been developed on the possible fractal distribution of these dunite channels (Hart, 1993; Aharonov, 1995; Kelemen *et al.*, 1995b, 2000; Spiegelman *et al.*, 2000). Hebert & Montesi (2010) infer that a network of porous dunite channels anastomose upward, such that the melts formed in a hundred-kilometre-wide region of partial melting in the mantle coalesce at shallow levels (following the permeability barrier), in a five-kilometre-wide melt-rich zone, under oceanic spreading ridges (Figs. 1.22, 1.23; Hopson *et al.*, 1981; Bishimetal Exploration, 1987; Kelemen *et al.*, 1995b, 2000, 2007; Hebert & Montesi, 2010). Based on field observations in the mantle section of the Oman ophiolites (Kelemen *et al.*, 1995a, b, 1997a, 2000, 2007), the theoretical organisation of the melt evolved from a "tree-like" network, in which dunite channels anastomose at depth, forming a "trunk" channel (Fig. 1.23a,b; Kelemen *et al.*, 1995a), to a

"bush-like" network, in which individual dunite channels directly feed the melt lense located at the base of the oceanic crust at fast-spreading environments (Fig. 1.23c,d; Kelemen *et al.*, 2007). The focussed percolation of melts in the high-porosity dunitic channels allows an efficient extraction from mantle depths where melts are formed to crustal levels where they crystallize and form the oceanic crust (Kelemen *et al.*, 1995a, 1995b, 2000, 2007). Dunite channels are reequilibrated with the high melt/rock ratios flowing through them (Kelemen *et al.*, 1995a; Godard *et al.*, 2000; Sanfilippo *et al.*, 2017), and therefore, during extraction by focussed percolation, the melts do not react with the surrounding peridotite and do not change composition. The melts extracted from depths within the dunite high-porosity channels are not in equilibrium with the shallow mantle peridotites; they do not show saturation in orthopyroxene, although it is a major phase in the shallow peridotites (harzburgite and lherzolite) (Bodinier & Godard, 2014).

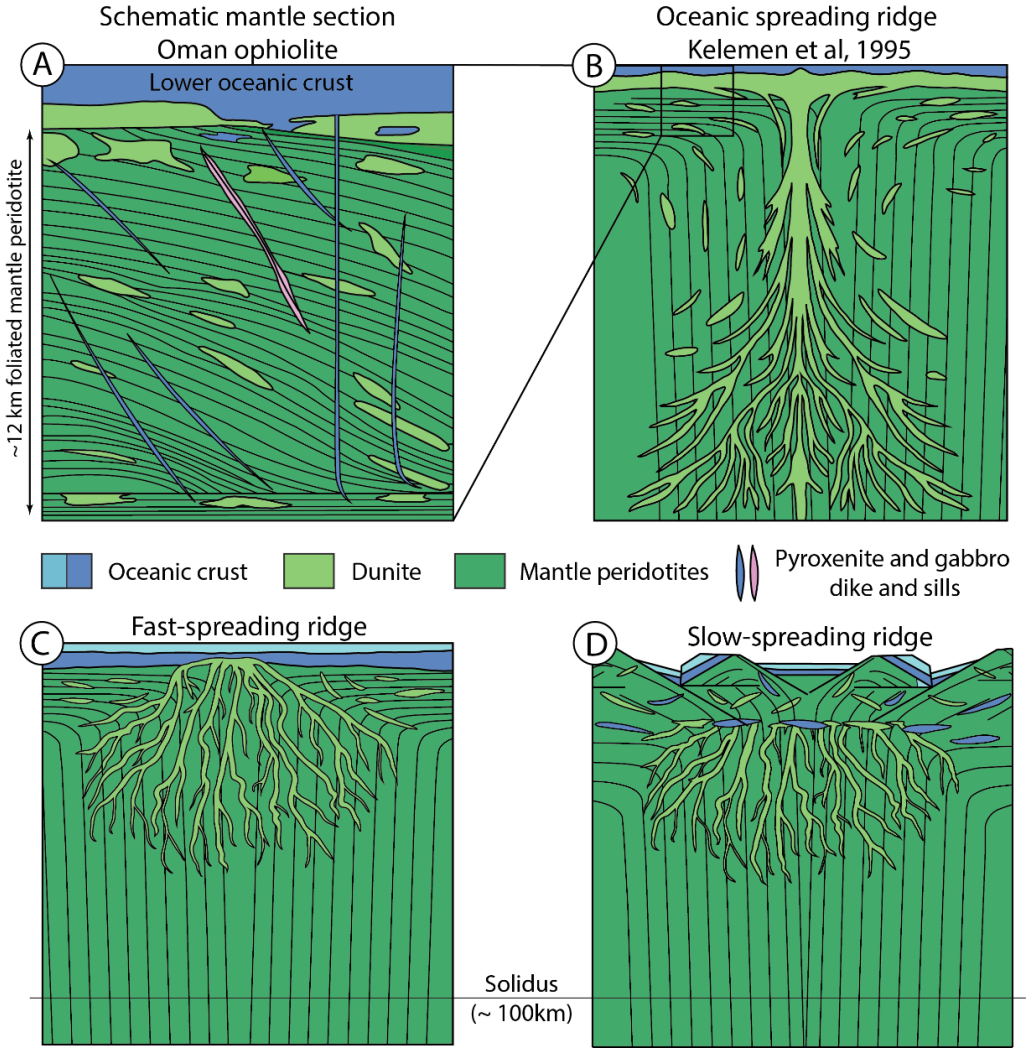

***Figure 1.23**: A: Schematic cross-section of the Oman ophiolite after Kelemen et al. (1995) and Kelemen et al. (2000); Black lines are foliation orientations within the mantle peridotites; B: Schematic representation of the possible ridge axis geometry of residual harzburgite, dunite conduits for melt flow and oceanic lower crust. C: Refined model of organization of coalescent dunite channels, applied to fast spreading ridge, after Kelemen et al. (2007). Note that the dunite channels directly feed the melt lense located at the base of the oceanic crust; D: Refined model of organization of coalescent dunite channels, applied to slow spreading ridge, after Kelemen et al. (2007). Note that the impregnated peridotites and gabbroic lenses form at the base of the conductive layer, >15 km below the seafloor, because of the cooler thermal regime at slow-spreading ridges.*

(2) At shallower plagioclase facies mantle depths, variably reacted spinel peridotites are affected by melt impregnation, which leads to the reactive formation of plagioclase-rich peridotites. This is a ubiquitous process in modern oceanic mantle, as it has been widely documented in peridotites from various geodynamic settings (ocean-continent transition, fast- vs. slow- vs. ultraslow-spreading ridges; e.g. Seyler & Bonatti, 1997; Tartarotti *et al.*, 2002; Chazot *et al.*, 2005; Dick *et al.*, 2010; Laukert *et al.*, 2014; Harigane *et al.*, 2016).

In the Alpine-Apennine peridotite massifs (e.g. Erro-Tobbio, Mt.Maggiore, Lanzo South, Platta), the spinel peridotites grade to plagioclase-bearing peridotites, which show clear impregnation textures, i.e. diffuse and heterogeneous plagioclase enrichment, plagioclase-rich gabbroic and gabbronoritic veinlets with irregular contact against the host peridotites, indicating local coalescence of impregnating melts. Melt impregnation in the peridotites is testified by the ubiquitous development of peculiar microstructures (Fig. 1.24; Rampone *et al.*, 2008; Rampone & Borghini 2007): i) partial dissolution and replacement of deformed mantle clinopyroxene by plagioclase and orthopyroxene intergrowths, ii) large poikilitic orthopyroxene grains replacing deformed mantle olivines, iii) plagioclase crystallizing as anhedral interstitial crystals between olivine grains or crosscutting large olivines. In the gabbronoritic veinlets, orthopyroxene and clinopyroxene occurs as idiomorphic to subidiomorphic crystals, whereas plagioclase is interstitial.

The crystallization of plagioclase (± pyroxenes) in spinel peridotites cause a re-enrichment in fusible components, marked by an increase in Al_2O_3 and CaO contents. The plagioclase peridotites, relative to the spinel-facies protoliths, are systematically shifted at lower MgO and higher Al_2O_3/CaO ratios. The role of such refertilization and melt focussing in the deformation and weakening of the extending lithosphere has been nicely shown in a detailed study of a high-temperature mylonitic shear zone in the Lanzo plagioclase-rich peridotites (Kaczmarek & Müntener, 2008, 2010). In these works, the authors performed bulk compositional profiles from porphyroclastic to mylonitic peridotites and documented progressive chemical homogenization (in terms of Al and Ca contents) in the mylonites, indicative of melt accumulation in the shear zone. They thus claimed that melt migration and high-temperature deformation were juxtaposed in time and space, and that deforming peridotites may act as important areas of melt focusing in the upper mantle.

The plagioclase-facies melt impregnation leads to significant chemical variations in mantle minerals, mostly marked by i) higher Cr-number and TiO_2 abundances in spinel, ii) Al decrease coupled to REE, Ti, Zr, Y increase in clinopyroxene and orthopyroxene (Rampone *et al.*, 1997, 2008; Rampone & Borghini 2008; Piccardo *et al.*, 2007; Sanfilippo & Tribuzio, 2011; Kaczmarek & Müntener, 2008; Müntener *et al.*, 2009). Figure 1.25a shows the REE composition of "reacted" clinopyroxenes in plagioclase peridotites (i.e. the clinopyroxene relics, partly substituted by plagioclase ± orthopyroxene intergrowths), compared with the REE compositions of clinopyroxenes in the spinel peridotites, free of plagioclase, in the Erro-Tobbio (Rampone *et al.*, 2005; Borghini *et al.*, 2007) and Mt.Maggiore peridotites (Rampone *et al.*, 2008). Despite an overall increase of the REE abundances, coupled to development of negative Eu_N anomalies, reacted clinopyroxene in Erro-Tobbio and Mt.Maggiore plagioclase peridotites preserve strong LREE depletion (Fig. 1.25 a).

The olivine-dissolving reactive percolation associated to the melt impregnation also leads to chemical changes in the percolating melt composition. Figure 1.25b shows the Forsterite-Anorthite compositional trends of olivine-plagioclase couples in olivine gabbros from oceanic (Elthon, 1987; Casey, 1997; Dick *et al.*, 2002) and ophiolitic settings (Browning, 1982; Kelemen *et al.*, 1997; Koga *et al.*, 2001), compared to the compositional trends of olivine-plagioclase couples in plagioclase peridotites (Tartarotti *et al.*, 2002; Bodinier & Godard, 2003; Niu, 2004; Kelemen *et al.*, 2007).

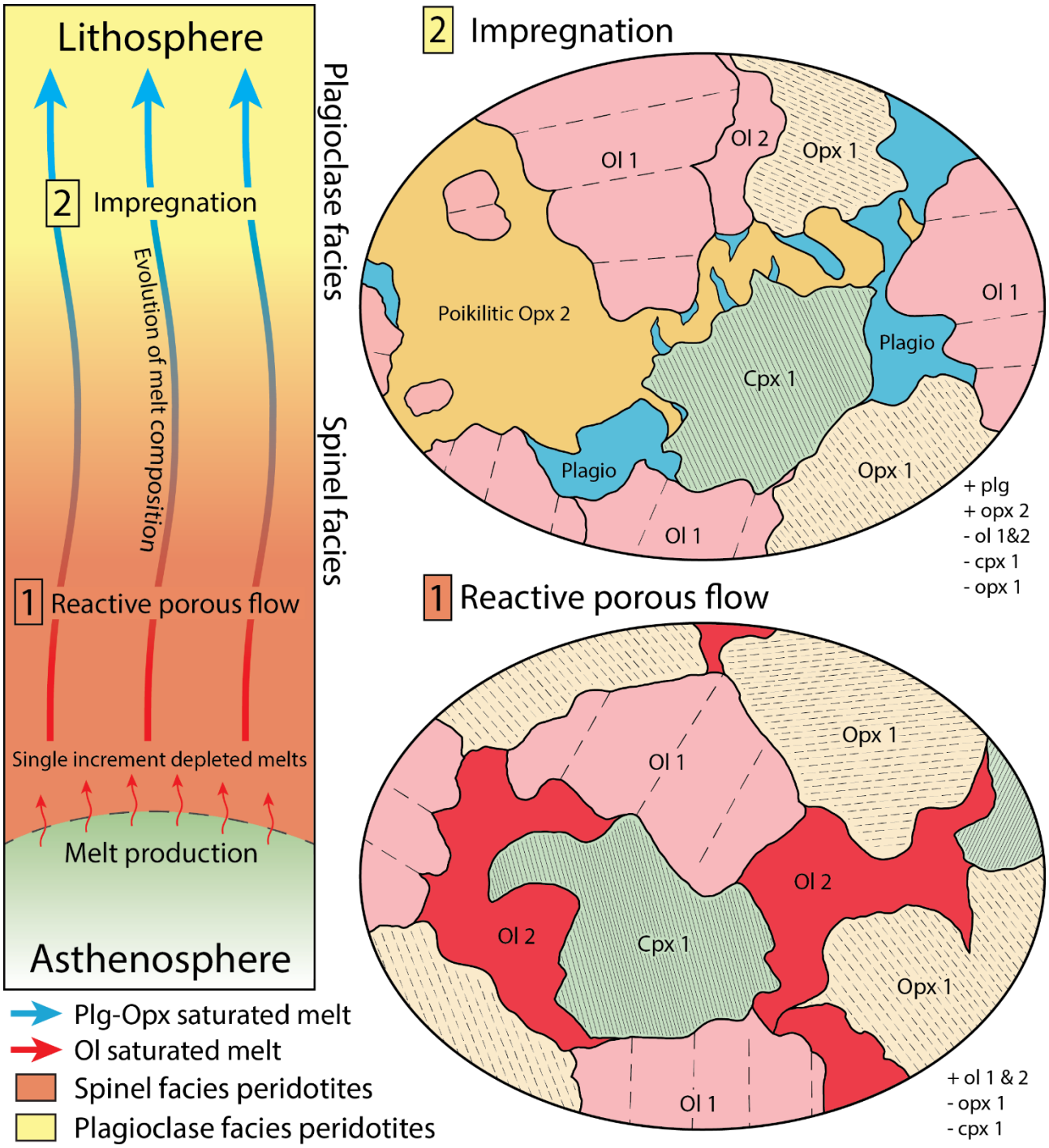

***Figure 1.24**: Progressive evolution of the microstructures in mantle peridotites during extension-related upwelling and associated melt-rock interaction history from spinel-facies depths to shallower plagioclase-facies levels, after Rampone et al., in prep. Left: composition of the percolating melt, progressively modified from olivine-saturation to orthopyroxene and plagioclase-saturation by the reactive porous flow occurring at spinel facies in a mantle column. 1. Representative microstructures characterizing the spinel-facies reactive porous flow, corrosion of exsolved clinopyroxene$_1$ and orthopyroxene$_1$, and crystallization of interstitial olivine$_2$; 2. Representative microstructures characterizing the plagioclase-facies melt impregnation, corrosion of pre-existing olivine$_{1-2}$, exsolved clinopyroxene$_1$ and orthopyroxene$_1$, and crystallization of interstitial to poikilitic orthopyroxene and plagioclase intergrowths. It is noteworthy that in places the microstructures indicative of the reactive porous flow occurring at spinel facies (olivine$_2$ corroding mantle clinopyroxene and orthopyroxene) are still observed in the impregnated plagioclase peridotite.*

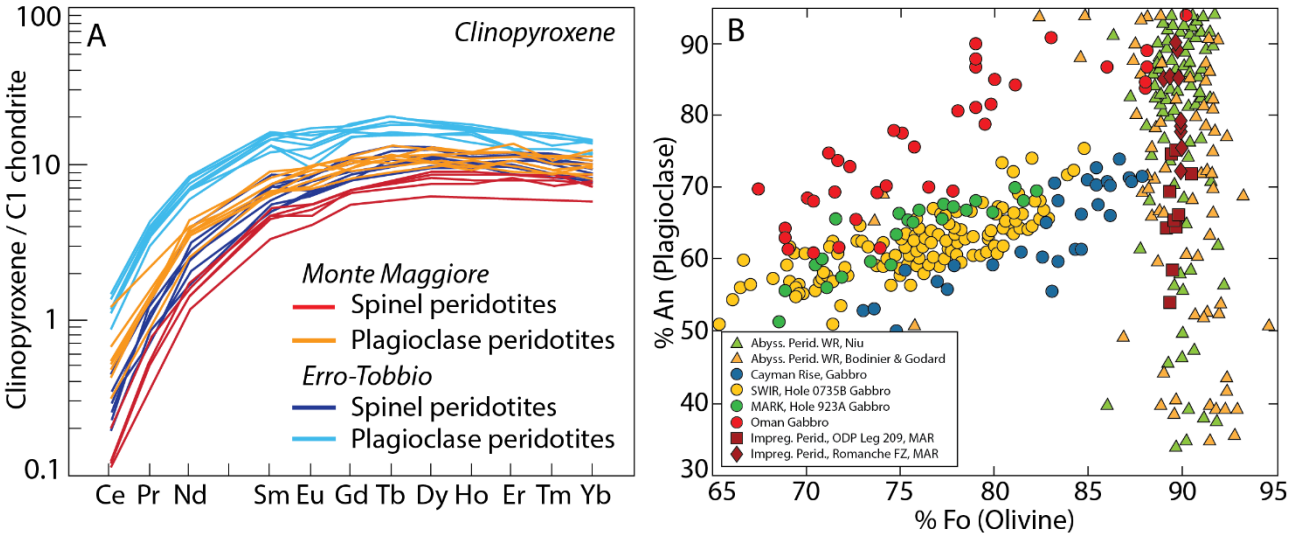

***Figure 1.25**: Chemical variations related to melt-rock interactions in the host rock and percolating melt. A: Clinopyroxene REE compositions in spinel and plagioclase peridotites from the Erro Tobbio (Rampone et al., 2005; Borghini et al., 2007) and Monte Maggiore peridotites (Rampone et al., 2008); B: Diagram of correlation between Fo (olivine) and An (plagioclase) in impregnated peridotites and gabbroic sequences from slow-(MAR) and ultraslow-(SWIR) spreading ridges. Redrawn after Collier & Kelemen, 2010. Data are from Browning (1982), Elthon (1987), Casey (1997), Kelemen et al. (1997), Koga et al. (2001), Dick et al. (2002), Tartarotti et al. (2002), Bodinier & Godard (2003), Niu (2004), Kelemen et al. (2007).*

Oceanic and ophiolitic olivine gabbros define trends of *fractional crystallization*, showing a positive correlation between the Forsterite contents in olivine and the Anorthite contents in plagioclase (Fig. 1.25b; Browning, 1982; Elthon, 1987; Casey, 1997; Kelemen *et al.*, 1997; Koga *et al.*, 2001; Dick *et al.*, 2002). In the impregnated plagioclase peridotites, strong variations of Anorthite contents in plagioclase (An = 35-92 mol%) are observed at constant high Forsterite contents in olivine (Fo = 87-92 mol%) (Tartarotti *et al.*, 2002; Bodinier & Godard, 2003; Niu, 2004; Kelemen *et al.*, 2007), indicative of the buffering of the melt Mg-value and the free evolution of the plagioclase composition during olivine-consuming *reactive crystallization* ($Mg\#_{melt} \approx 70$, in equilibrium with olivine Fo_{90}; Fig 1.25b; Collier & Kelemen, 2010). Reactive crystallization trends of evolution are indicative of a melt composition dominated by the melt-rock interaction occurring during the melt transport and by the percolated host rock.

1.3.3. Melt-rock interactions in the oceanic crust

Melt-rock interaction have recently been invoked in the lower oceanic crust. These reactions are thought to modify the chemical composition of the pre-existing gabbroic matrix (e.g., Meyer *et al.*, 1989; Bedard *et al.*, 2000; Dick *et al.*, 2002; Lissenberg & Dick, 2008; Lissenberg *et al.*, 2013), as well as the percolating MORB melts (e.g., Kvassnes & Grove, 2008; Lissenberg & Dick, 2008; Lissenberg *et al.*, 2013). Lower crustal oceanic gabbros often display microstructures related to melt-rock interactions, such as compositional zoning indicative of corrosion surfaces followed by crystal growth (Fig. 1.26a) and corroded olivine and plagioclase crystals included in poikilitic clinopyroxene (Fig. 1.26b). These textures are indicative of reactive porous flow of MORB-type melts leading to crystallization of interstitial to poikilitic clinopyroxene at the expense of a pre-existing [olivine + plagioclase] troctolitic gabbro (Fig. 1.26; Lissenberg & Dick, 2008; Lissenberg *et al.*, 2013; Lissenberg & MacLeod, 2017).

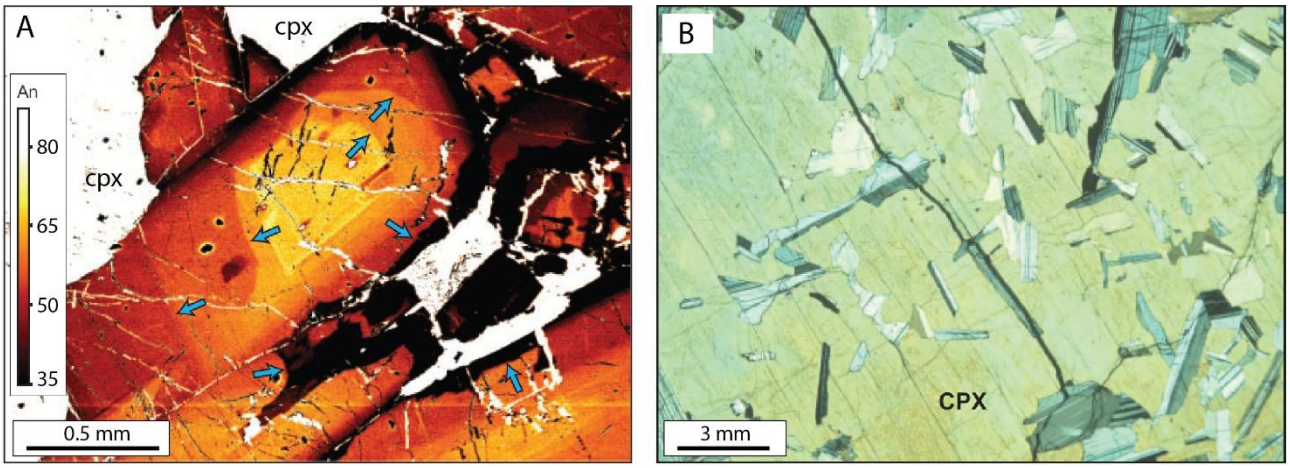

***Figure 1.26**: Melt-rock interaction microstructures, after Lissenberg & MacLeod (2017); A: Anorthite chemical zoning in a plagioclase crystal, dissolution boundaries are evidenced by blue arrows; B: Poikilitic clinopyroxene including corroded plagioclase crystals.*

High Mg and Cr contents in the melt crystallizing the clinopyroxene are thought to be acquired during olivine- and spinel-dissolving melt-rock interaction. Trace elements enrichments from core to rim of clinopyroxene crystals have been considered as indicative of the progressive enrichment of the most incompatible elements in the melt during ongoing melt-rock interaction (Lissenberg & MacLeod, 2017). Reactive porous flow appears to be a common, if not ubiquitous, process in oceanic magma chambers, leading to modifications in the modal and geochemical composition of the pre-existing crystal mush, and the geochemical composition of the percolating melt (Meyer *et al.*, 1989; Dick *et al.*, 2002; Lissenberg *et al.*, 2013; Lissenberg & MacLeod, 2017). Evidence of melt-rock interactions in the lower oceanic crust has also been documented from the study of mid-ocean ridge basalts formed by extraction and eruption of the percolating melts.

1.3.4. Melt-rock interactions recorded in Mid-Ocean Ridge Basalts

The eruption of the percolating tholeiitic melts leads to the formation of MORBs at the seafloor. Recent studies investigated melt inclusions in olivine and plagioclase phenocrysts in MORBs (Fig. 1.27), thought to be entrapped during magma pooling at the base of the lower oceanic crust (Laubier *et al.*, 2012; Coumans *et al.*, 2016). These melt inclusions display peculiar major and trace elements compositions (i.e. high Al, low Si, positive Sr and Eu anomalies and negative Zr, Nb anomalies) that have been inferred to result from assimilation of a plagioclase-rich cumulate by the percolating melts at the base of the lower oceanic crust (Lissenberg *et al.*, 2008; Laubier *et al.*, 2012; Coumans *et al.*, 2016). These studies further support the inference that melt-rock interaction occurring in primitive (troctolitic) oceanic gabbros is an important process in the construction of the oceanic crust (Lissenberg & Dick, 2008; Lissenberg *et al.*, 2013; Lissenberg & MacLeod, 2017).

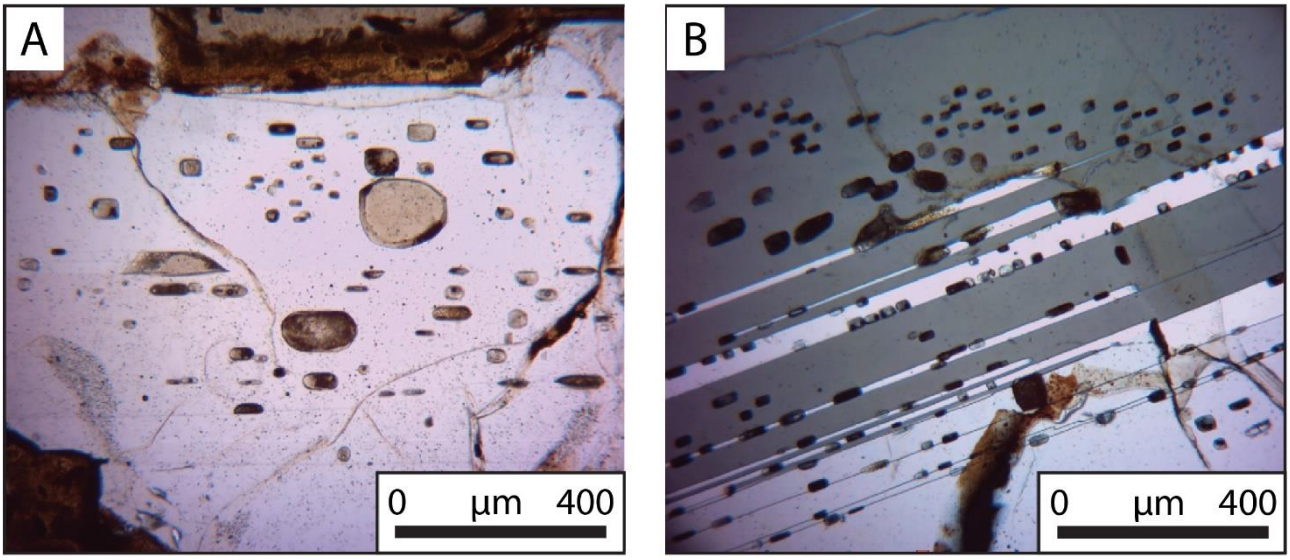

***Figure 1.27**: Transmitted light photomicrographs of melt inclusions in plagioclase crystals, after Coumans et al. (2016). A: Rounded melt inclusions ranging in size from <10 µm to >100 µm; B: Melt inclusion bands following the growth faces of plagioclase phenocryst.*

The large variations in the MORB field of compositions (e.g. CaO variations at constant MgO; Fig. 1.28; Lissenberg & Dick, 2008; Collier & Kelemen, 2010) have long been described as the result of fractional crystallization processes occurring at variable pressures, from low atmospheric pressures to 8kbar, at which the increasing stability field of clinopyroxene with increasing pressure leads to a change in the MORB-type melt crystallization order from [olivine – plagioclase – clinopyroxene] to [olivine – clinopyroxene – plagioclase], and therefore leads to a stronger decrease in CaO at constant MgO (Fig. 1.28). Several recent studies investigated the effect of melt-rock interactions on the melt composition during melt transport in the uppermost mantle and in the lower crust.

Collier & Kelemen (2010) performed a modelling of the liquid lines of descent of two melt compositions (produced by melting of a hot and cold mantle, yellow and blue star in Fig. 1.28a, respectively) during reactive fractional crystallization involving the dissolution of varying amounts (0 to 3g/°C of cooling) of "*average abyssal peridotite*" (Dick, 1989) (Fig. 1.28a), using the *pMELTS* thermodynamic software (Ghiorso *et al.*, 2002). Collier & Kelemen (2010) demonstrated that the wide MORB field of composition could be covered by low pressure crystallization, assuming a reactive crystallization of the melts during their transport in the upper mantle. The assimilation of the *average abyssal peridotite* drastically decreases the CaO content of the melt, at constant MgO content (Fig. 1.28a).

Lissenberg & Dick (2008) performed a modelling of the liquid lines of descent of a MORB-type melt during low-pressure reactive crystallization involving the assimilation of a lower crustal troctolitic component (olivine + plagioclase) and demonstrated that this process could account for the wide MORB MgO-CaO compositional field (Fig. 1.28b). The assimilation of various plagioclase:olivine ratios (from 6:1 to 2:1) all show a decreasing CaO at increasing MgO in the melt (Lissenberg & Dick, 2008), mimicking high pressure compositions of the melt (calculated after Herzberg, 2004). Therefore, the low-pressure reactive crystallization trends involving assimilation of lower crustal troctolites cover the MORB compositional range of variation previously interpreted as high-pressure crystallization products (Grove *et al.*, 1992; Danyushevsky, 2001; Herzberg, 2004; Villiger *et al.*, 2007).

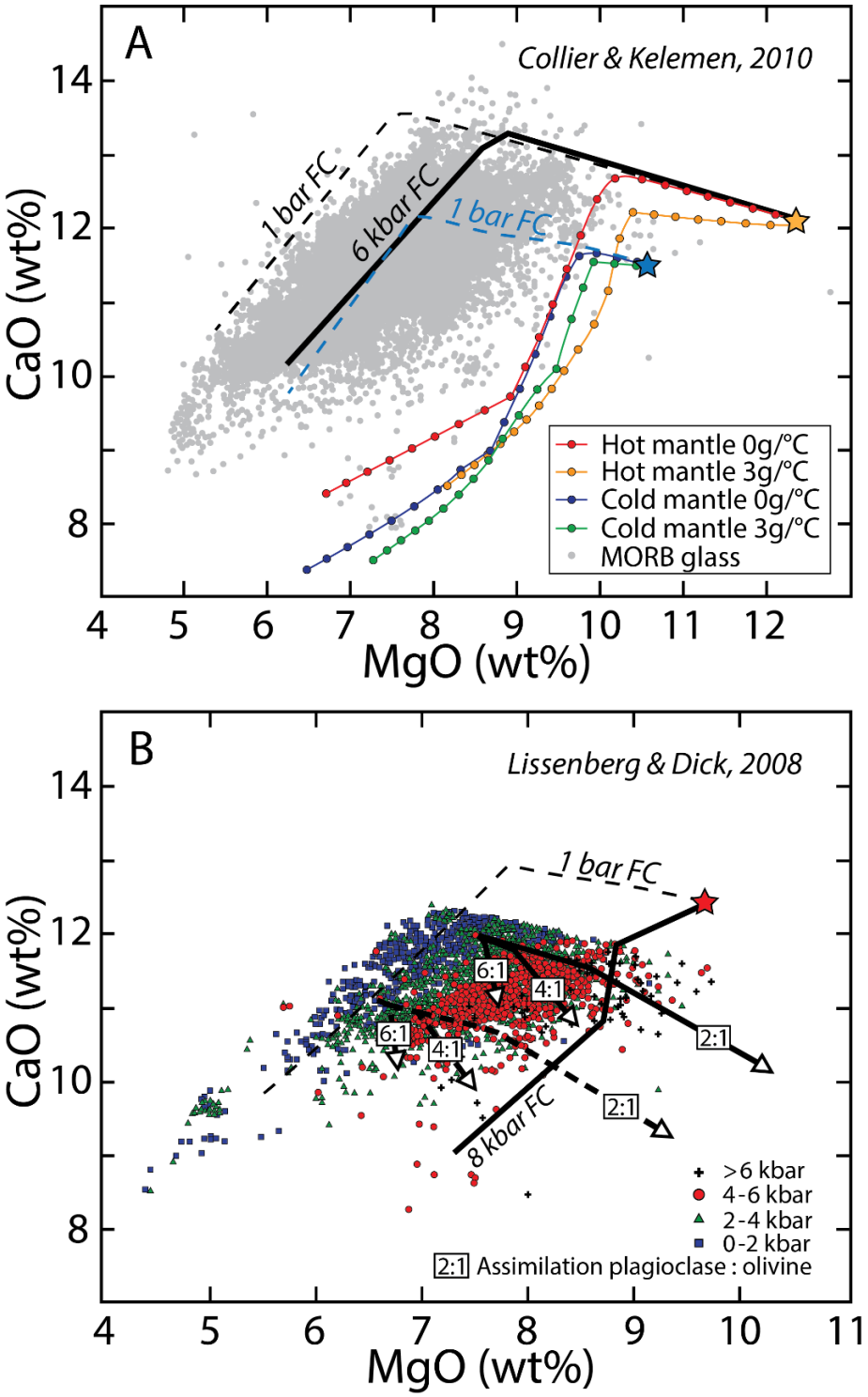

***Figure 1.28**: MgO vs CaO (wt%) compositions in MORB glasses, compared to liquid lines of descent during fractional crystallization at varying pressures, and during reactive crystallization processes. A: Redrawn after Collier & Kelemen (2010). Dashed and solid black and blue lines represent the fractional crystallization of two melt compositions formed by melting of a high and low potential temperature mantle (yellow and blue stars) at 1 bar and 6 kbar, respectively (Weaver & Langmuir, 1990). The solid coloured lines represent the melts liquid lines of descent during reactive crystallization and assimilation of various amounts of "average abyssal peridotite" (Dick, 1989); B: Redrawn after Lissenberg & Dick (2008). Calculated 1 bar and 8 kbar fractional crystallization MORB liquid lines of descent (Danyushevsky, 2001) compared with two different reactive crystallization liquid lines of descent involving the assimilation of lower crustal troctolite (labels on the thick solid and dashed arrows indicate the ratio of plagioclase:olivine assimilation). MORB glasses from the PetDB database, colour coded according to their calculated pressures (Herzberg, 2004).*

In summary, separate lines of evidence found the need to invoke melt-rock interaction processes during melt transport in the uppermost mantle and in the oceanic crust, i.e. i) microstructures indicative of the corrosion of pre-existing minerals in lower crustal olivine gabbros, ii) mineral compositional trends of evolution indicative of the buffering of the melt composition during dissolution-precipitation reactions, iii) the wide MORB compositional field, not consistent with simple fractional crystallization processes and iv) the composition of melt inclusions in olivine and plagioclase phenocrysts, both indicative of melt-rock interactions between the percolating melt and a pre-existing troctolitic matrix in the lower oceanic crust. These several lines of evidence highlight the importance of melt-rock interaction processes in the chemical evolution of the percolating melts building the oceanic crust.

In this thesis, we aim at constraining the structural and geochemical variations related to melt-rock interaction processes in the pre-existing percolated rock and percolating melt in open and closed systems, both in the upper mantle and gabbroic lenses (see Chapter 3 and Chapter 4) and in the layered lower oceanic crust (see Chapter 5).

1.4 Olivine structural and chemical properties

The structural and geochemical studies presented in this thesis are focused on olivine, therefore, the following section is aimed at describing the main structural and chemical characteristics of olivine in magmatic and melt-rock interaction-bearing settings.

1.4.1. Olivine texture: controlling parameters

Olivine is an orthosilicate solid solution of forsterite (Mg_2SiO_4) and fayalite (Fe_2SiO_4). It is characterized by an orthorhombic symmetry (3 crystallographic axes, a= [100], b= [010], and c= [001]; Fig. 1.29; Welsch *et al.*, 2012), and shows a granular euhedral habitus (Fig. 1.29). However textural variations have been observed both in magmatic and reactive systems (Fig. 1.30), from polyhedral olivines to hopper, skeletal and dendritic morphologies. A detailed study of the magmatic and reactive textures of olivine gives insights on the composition of the percolating melt (therefore its reactivity), and the thermal conditions in which the melts crystallize (degree of undercooling, cooling rate; Figs. 1.30, 1.31)

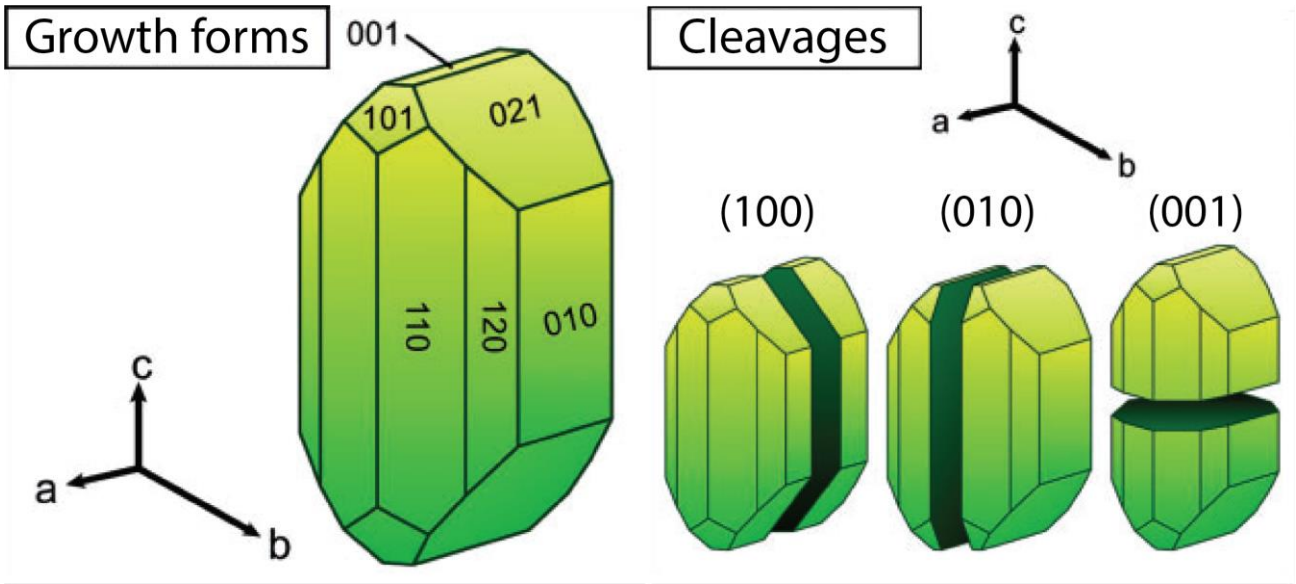

***Figure 1.29**: Habitus and crystallographic characteristics of olivine euhedral crystals, after Welsch et al. (2012).*

Magmatic olivine

High textural variability of olivine has been described in the Rum layered intrusion (Donaldson, 1974, 1976, 1977, 1982; O'Driscoll *et al.*, 2007), and then reproduced during laboratory experiments (Donaldson, 1975, 1976; Donaldson *et al.*, 1975; Faure *et al.*, 2003, 2007). They describe a range of textures from polyhedral granular olivine to hopper, skeletal and branching olivine, defining a layering in the Rum intrusion (Fig. 1.30).

The experimental crystallization studies allowed to constrain the main controlling factors of the olivine texture during crystallization from a melt, that are the ***degree of undercooling*** of the melt and the ***cooling rate*** (Donaldson, 1975, 1976, 1977, 1982; Donaldson *et al.*, 1975; Faure *et al.*, 2003, 2007; O'Driscoll *et al.*, 2007; Welsch *et al.*, 2012, 2014). The degree of undercooling (Faure *et al.*,

2003, 2007; Faure & Schiano, 2005) is defined by the difference between the temperature of the melt and its liquidus temperature (Lofgren, 1975):

$$-\Delta T(°C) = T(melt) - T(liquidus)$$

and thus varies with the melt composition ($T_{liquidus}$ is higher at higher $Mg\#_{melt}$) at a given temperature. The cooling rate is expressed in Degree Celcius per hour (°C/h) (Fig. 1.30).

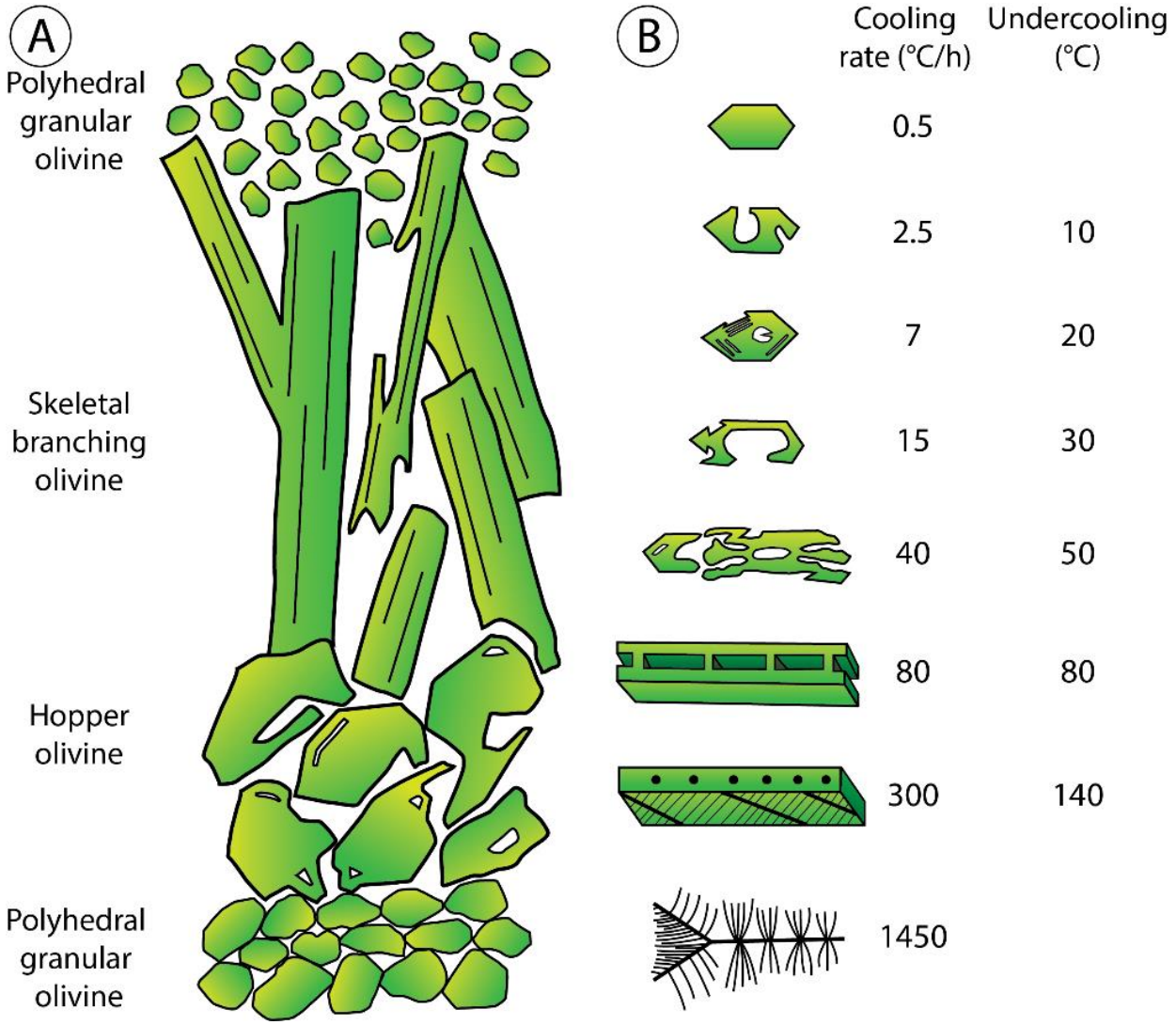

***Figure 1.30**: A: Generalized sketch of textural changes of olivine at the Rum layered intrusion, redrawn after Donaldson (1977). Space between olivines is filled by interstitial plagioclase and clinopyroxene. Not to scale, the skeletal branching olivines can be up to metre-size; B: Olivine morphologies formed during crystallization experiments, redrawn after Donaldson (1976).*

Faure *et al.* (2003) conducted an experimental study of the morphology of olivine crystals at varying degrees of melt undercooling and cooling rates (Fig. 1.31). The development of polyhedral and tabular olivines requires low cooling rates and low degrees of undercooling, whereas a progressive increase in these two parameters will progressively form hopper olivines, and for degrees of undercooling above 70-80°C, baby swallowtail, swalowtail, and chain morphologies of olivine (Fig. 1.31; Donaldson, 1975, 1976, 1977, 1982; Faure *et al.*, 2003, 2007; O'Driscoll *et al.*, 2007). They infer a rapid "disequilibrium" growth of the hopper, skeletal, swallowtail and chain olivine.

The development of an undercooling of the percolating melt has been ascribed to: (1) the melt input into a cooler resident magma or host rock (O'Driscoll *et al.*, 2007; Welsch *et al.*, 2012, 2014); (2) the change of composition of the melt, increasing its liquidus temperature when more primitive; (3) the mixing between a primitive olivine-saturated melt and a gabbroic crystal mush, leading to an enrichment in the melt H_2O and Na_2O, reducing the viscosity of the hybrid melts and delay mineral nucleation, thereby triggering rapid growth crystallization of skeletal and dendritic crystals (Donaldson, 1977; Vernon, 2004; Faure *et al.*, 2007; Renna *et al.*, 2016).

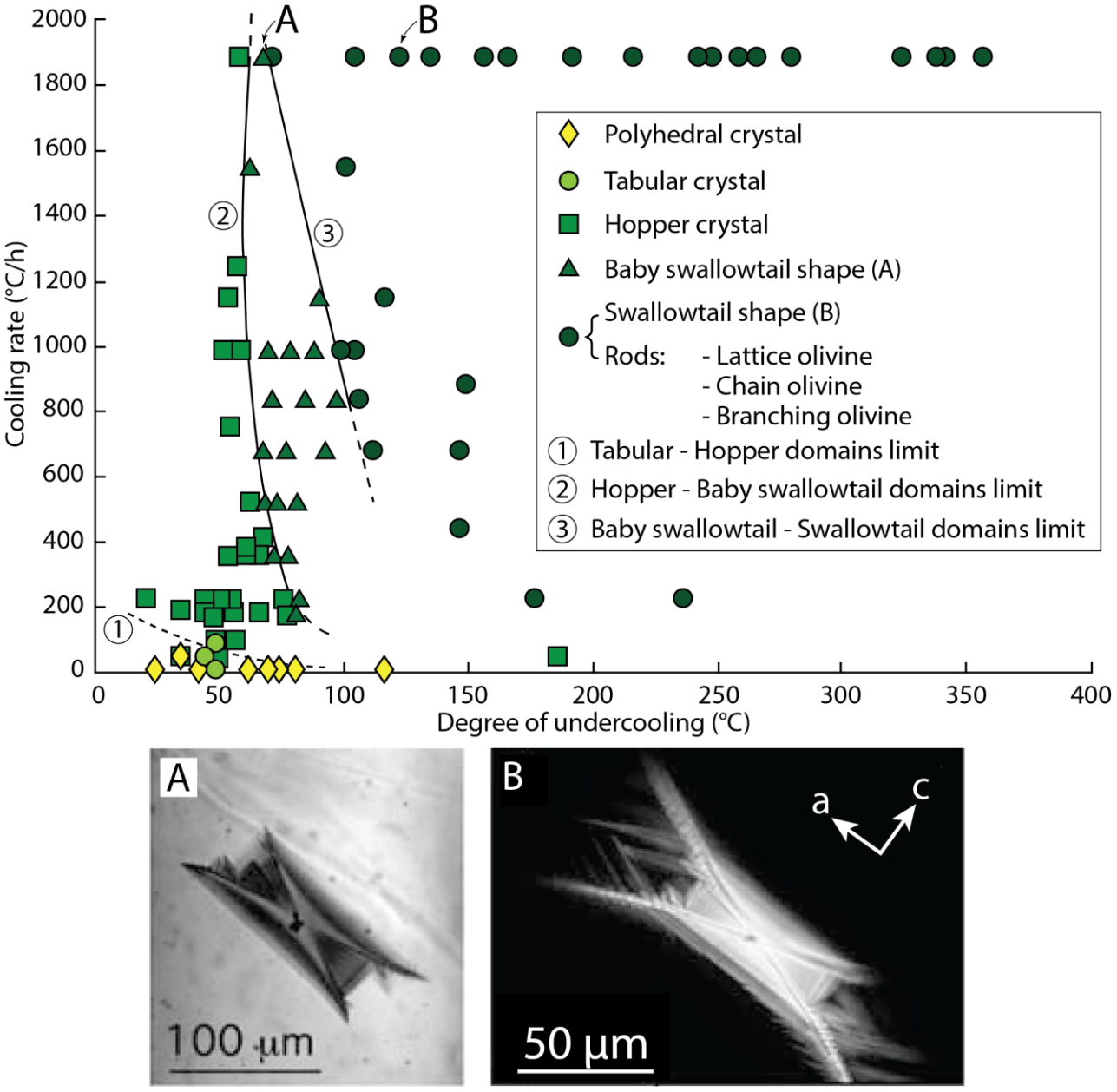

***Figure 1.31**: Degree of undercooling (°C) vs Cooling rate (°C/h) diagram of textural controlling factors, redrawn after Faure et al. (2003). A: Baby swallowtail shapes (-ΔT = 68°C); B: Swallowtail shape (-ΔT = 122°C).*

Recrystallized olivine

Olivine has been extensively described as part of reactive processes leading to the dissolution and/or recrystallization of the olivine. Boudier (1991) showed that during partial melting of peridotites at conditions close to equilibrium, euhedral olivine crystals can be produced by corrosion followed by recrystallization during temperature drop (Fig. 1.32a,b). Magmatic textures can thus develop in restitic olivines and discrimination between restites and newly formed crystals is difficult (Boudier, 1991; Arndt *et al.*, 2010). Similarly, Erdmann *et al.* (2014) studied the textural evolution of olivine crystals during reaction and recrystallization, and reported strikingly similar textures between magmatic primary olivines and secondary recrystallized euhedral olivines (Fig. 1.32a,b).

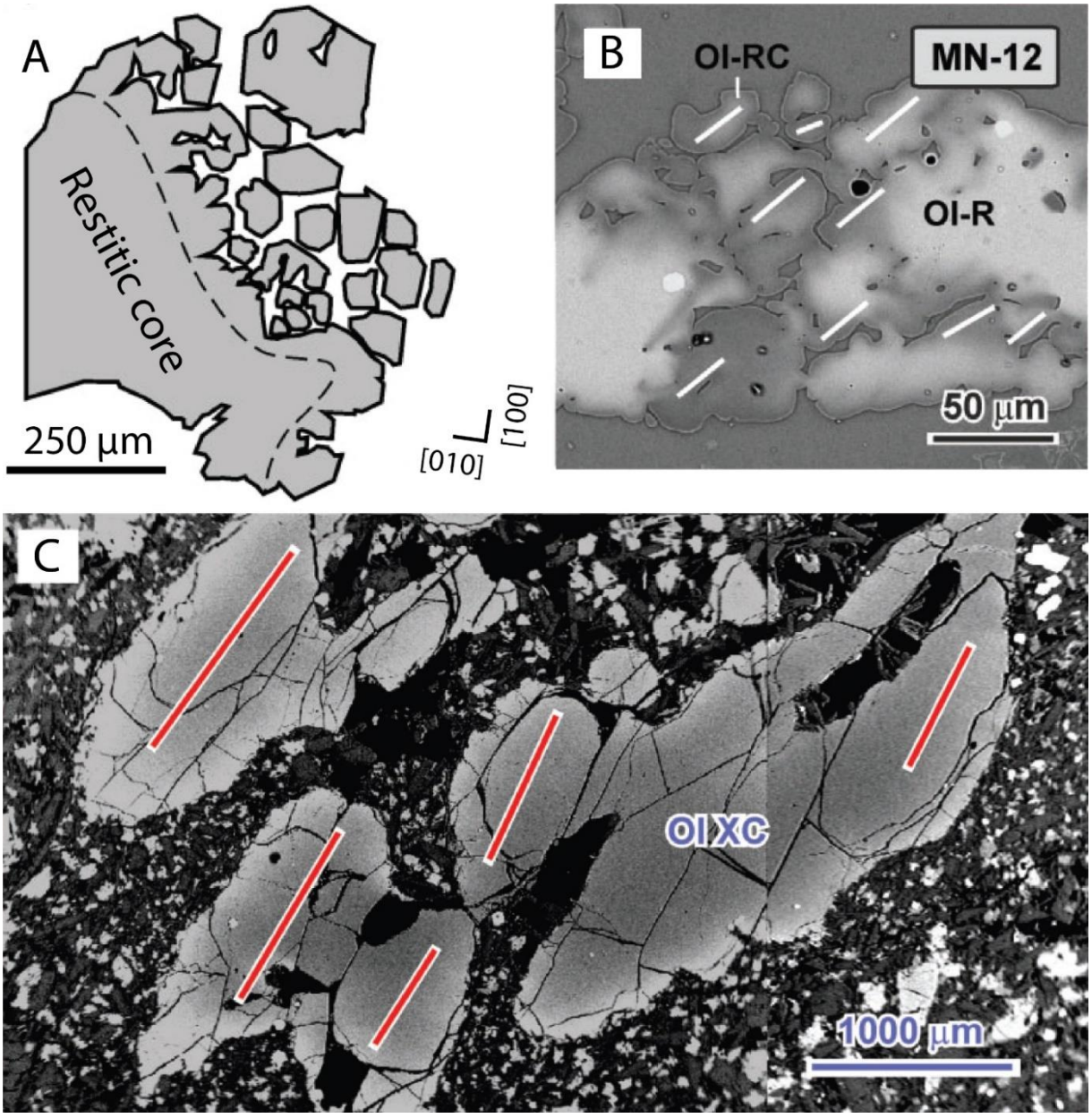

***Figure 1.32**: Textural evolution of olivine during melt-rock interaction and recrystallization, after Erdmann et al. (2014). A: Line drawing of recrystallized "euhedral" olivines from Boudier (1991); B: BSE image of restitic olivines with pervasive dissolution and partial recrystallization along grain margins, Ol-R = restitic olivine, Ol-RC = recrystallized olivine; C: Photomicrograph of dendritic olivine formed after dissolution and partial recrystallization of the olivine, Ol XC = olivine xenocryst.*

Ninomiya & Arai (1998) and Erdmann *et al.* (2014) reported dendritic and branching olivines formed after reaction between large olivine xenocrysts and a basaltic magma. Again, the reactive texture is very similar to the magmatic textures observed at the Rum layered intrusion (Fig. 1.30) and produced by crystallization experiments at high degree of undercooling and cooling rate. It is noteworthy that the branches of the recrystallized dendritic olivine show parallel orientations (Fig. 1.32c), whereas the primary dendritic olivines show an angle between the olivine branches (Fig. 1.30). Texture analyses alone might not be sufficient for a determination of the primary or secondary origin of olivines (Boudier, 1991).

1.4.2. Olivine crystallography, deformation and slip systems

Deformation by dislocation slip can lead to the formation of a Crystallographic Preferred Orientation (CPO) of the rock-forming minerals (Tommasi *et al.*, 2000; Karato *et al.*, 2008). Many slip systems activations are involved in the deformation of a polycrystalline system, but subsidiary mechanisms can contribute to the ease of activation of a single slip system that will therefore dominate the CPO development (Fig. 1.33; Karato *et al.*, 2008; Michibayashi & Oohara, 2013). Therefore, the activation of a specific slip system (lower strain energy) depends on the physical parameters during deformation (Fig. 1.33) (Jung & Karato, 2001; Katamaya *et al.*, 2004, 2005; Mizukami *et al.*, 2004; Jung *et al.*, 2006, 2009; Katamaya & Karato, 2006; Karato *et al.*, 2008; Warren *et al.*, 2008; Michibayashi & Oohara, 2013). Numerous experimental studies of simple shear deformation have been conducted in order to understand the controlling parameters on the ease of activation of specific slip systems, such as temperature, water contents, stress and the presence of melt in the deforming solid assemblage (Figs. 1.34, 1.35, 1.36; Carter & Avé Lallemant, 1970; Ben Ismail & Mainprice, 1998; Tommasi *et al.*, 2000; Jung & Karato, 2001; Katamaya *et al.*, 2004; Karato *et al.*, 2008; Michibayashi & Oohara, 2013).

Temperature

Deformation experiments over a wide range of temperatures (600-1400°C, Fig. 1.34) evidenced a transition in dominant slip system activation in olivine from [001] slip directions at low temperatures (600-1000°C) to [100] slip directions at high temperatures (>1000°C) (Fig. 1.34; Carter & Avé Lallemant, 1970; Karato *et al.*, 2008). This is consistent with the [100] slip directions and resulting A-type CPO typically observed in natural mantle lherzolites and harzburgites (Ben Ismail & Mainprice, 1998; Tommasi *et al.*, 2000; Karato *et al.*, 2008; Le Roux *et al.*, 2008; Soustelle *et al.*, 2009, 2010).

Presence of melt

The presence of melt in a deforming solid assemblage leads to a weakening of the rock, as illustrated in the Fig. 1.35 (Hirth & Kohlstedt, 1996; Bai *et al.*, 1997; De Kloe, 2001) in experiments of deformation at varying melt contents in the matrix. The melt-free assemblage exhibit strength levels intermediate between the olivine [a]- and [c]-slip (Fig. 1.35a), whereas at progressively increasing melt content, the strength level of the assemblage decreases, and strain rates increase at constant stress (Fig. 1.35b,c). It is consistent with natural and experimental studies (Holtzman *et al.*, 2003; Le Roux *et al.*, 2008; Kaczmarek & Tommasi, 2011) that described a change of olivine CPO during melt-bearing deformation towards B-type CPO by activation of dominant (010)[100] together with (010)[001] (Tommasi *et al.*, 2000; Mainprice *et al.*, 2005).

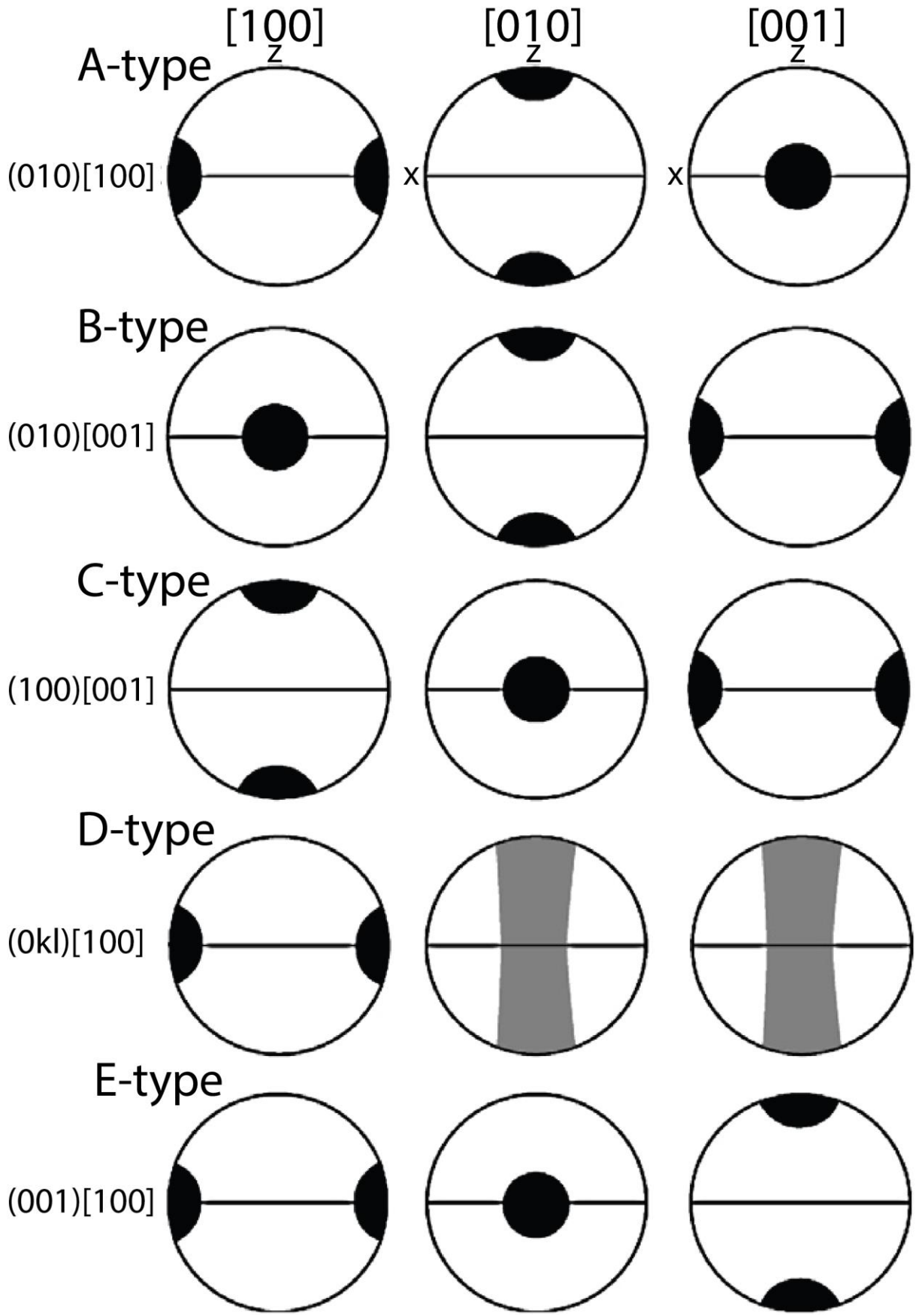

***Figure 1.33**: Typical olivine CPO found in simple shear deformation experiments, after Jung & Karato (2001); Katamaya et al. (2004); and Michibayashi & Oohara (2013).*

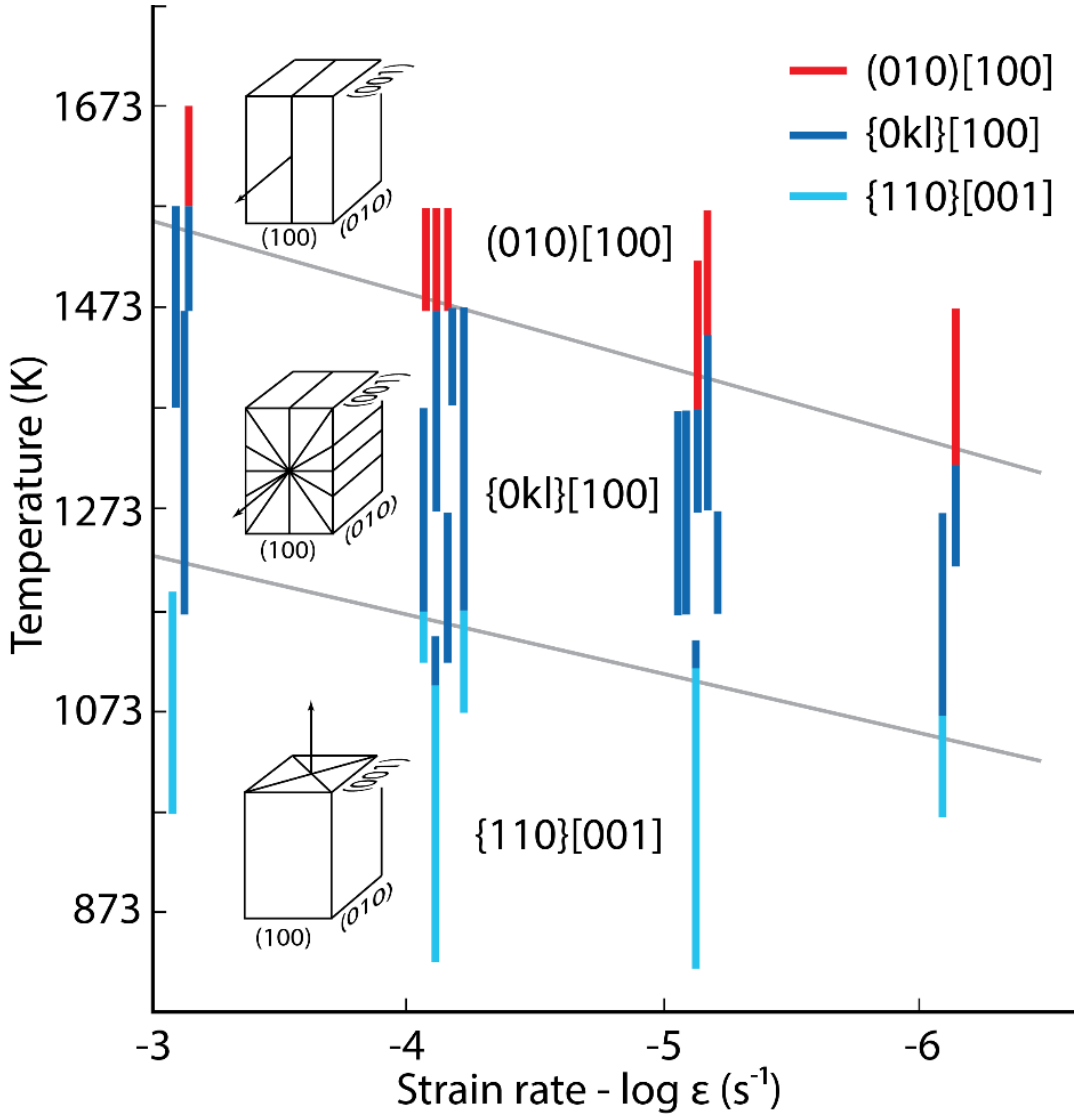

***Figure 1.34**: Dominant slip systems in olivine as a function of strain rate and temperature (at P=1.5 GPa), after Carter & Avé Lallemant (1970), and Karato et al. (2008).*

Water contents / Stress

Figure 1.36 reports changes of high-temperature CPO (1200-1300°C) in olivine induced by an increase in water content and/or stress (Bystricky *et al.*, 2001; Katamaya *et al.*, 2004; Karato *et al.*, 2008). Several slip system transitions have been observed in water-bearing and high-stress deformation experiments (Jung & Karato, 2001; Katamaya *et al.*, 2004; Jung *et al.*, 2006; Katamaya & Karato, 2006; Karato *et al.*, 2008; Michibayashi & Oohara, 2013), from A-type to E-type to C-type CPOs (Fig. 1.33) at increasing water contents (ppm H/Si, Fig. 1.36). These CPO types transitions are related to changes in the dominant slip system from (010)[100] (A-type) to (001)[100] (E-type) to (100)[001] (C-type). At higher stress during deformation (>350 MPa), independently of the water content, another slip system transition is observed, towards B-type CPO (dominant activation of (010)[001], Figs 1.33, 1.36).

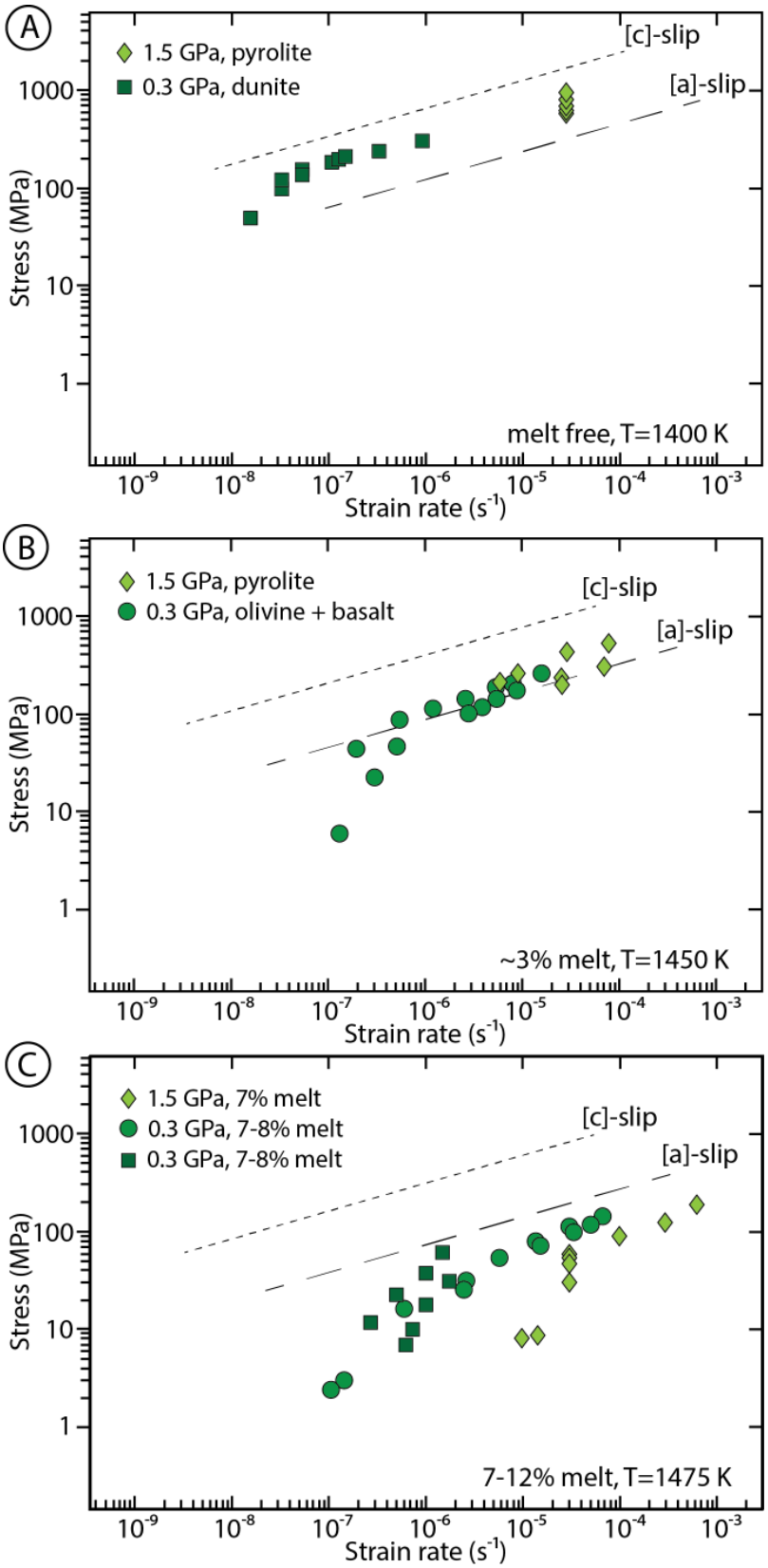

***Figure 1.35**: Stress-Strain rate data of deformation experiments, illustrating the magnitude of melt-related weakening at increasing melt content, after Hirth & Kohlstedt (1996); Bai et al. (1997); De Kloe (2001). A: Melt-free samples exhibit strength levels intermediate to olivine single crystals [a]- and [c]-slip; B: Strength levels of samples containing 3% melt coincide with the strength of olivine single crystal [a]-slip; C: Substantial weakening to levels below the strength of olivine single crystal [a]-slip occurs at melt fractions exceeding 5%.*

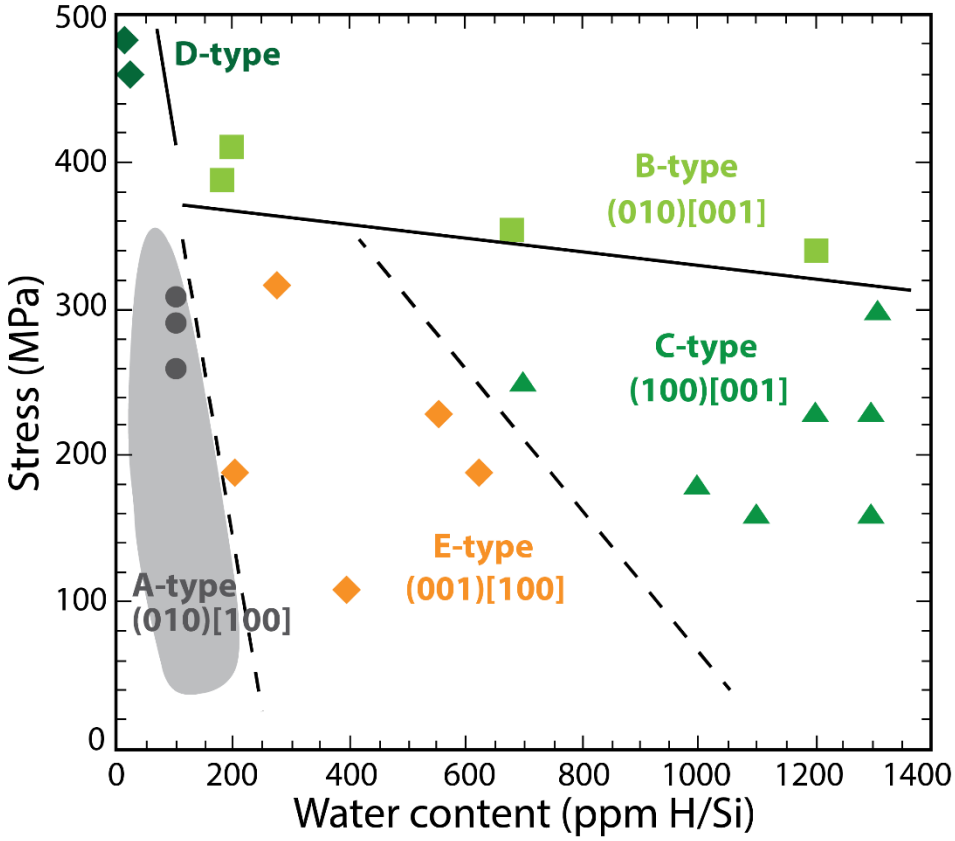

***Figure 1.36**: Deformation fabrics of olivine at high temperatures (T = 1200-1300°C) as a function of water content and stress, after Bystricky et al. (2001); Katamaya et al. (2004) and Karato et al. (2008). Water content was estimated using the Paterson (1982) calibration.*

These CPO transitions (Fig. 1.33) can therefore be used as an indicator of the conditions in which the deformation took place (Karato *et al.*, 2008), and provide insights into the distribution of water associated with plume-asthenosphere interactions, formation of the oceanic lithosphere, and subduction zones (Jung & Karato, 2001; Katamaya *et al.*, 2004; Karato *et al.*, 2008).

In addition to the changes observed in the olivine CPO, related to variations in the dominant slip system activation, the orientation of the subgrain boundaries in olivine crystals is also a direct consequence of the activated slip system during dislocation creep (Fig. 1.37; Tommasi *et al.*, 2000; De Kloe, 2001; Soustelle *et al.*, 2010). It is therefore another indicator of the transitions of slip systems in olivine during deformation. The typically observed orientation of subgrain boundaries in mantle peridotites is linked to the A-type CPO formation (activation of (010)[100] slip system), therefore observed along [001] axis of olivine (Fig. 1.37). Discrepancies between the CPO of olivine and the orientation of its subgrain boundaries can be indicative of the loss of cohesion of the solid matrix after reactive porous flow at high melt/rock ratios (20-40%; Rosenberg & Handy, 2005), as described by Drouin *et al.* (2010) during the replacive formation of olivine-rich troctolites in the lower oceanic crust at the Atlantis Massif. This loss of cohesion allows for a randoming of the olivine matrix CPO during crystal suspension flow, without affecting the internal olivine misorientation (subgrain boundaries preserve their [001] orientation).

The correlation/lack of correlation between the CPO and olivine internal misorientation is a good indicator of the conditions of deformation processes in a solid matrix.

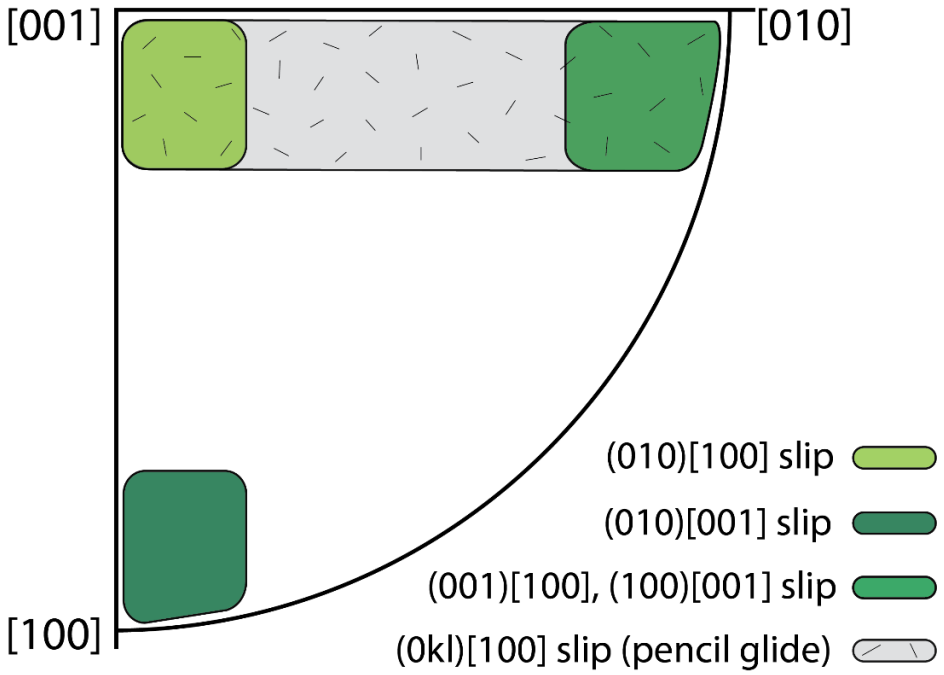

***Figure 1.37**: Inverse pole figures of the expected rotation axes orientations for the most common slip systems in olivine, after De Kloe (2001).*

1.4.3. Olivine composition: Partition coefficients and subsolidus reequilibration

The distribution of an element between a melt and a solid phase is ruled by the partition coefficient, defined as the ratio of concentration:

$$Kd = C_s^i / C_{liq}^i$$

for a given element *i* between the solid phase *s* and the liquid phase *liq*. It expresses the likelihood of an ion, defined by a charge and ionic radius (Fig. 1.38), to integrate the crystalline lattice of the solid phase (Goldschmidt, 1937). The partition coefficient Kd of an element depends on the intrinsic characteristics of the ion (ionic radius and charge, Fig. 1.38), but also on the temperature, pressure, oxygen fugacity of the system, and the chemical composition of the solid phase (Kennedy *et al.*, 1993; Beattie, 1994; Taura *et al.*, 1998; Blundy & Wood, 2003; Wood & Blundy, 2003; Zanetti *et al.*, 2004, Lee *et al.*, 2007; Spandler *et al.*, 2007; Spandler & O'Neill, 2010; Sun & Liang, 2012, 2013a,b, 2014, 2017). These external parameters lead to variations in the elasticity parameters of the lattice sites on which elements are accommodated (Blundy & Wood, 2003), therefore changing the ease for a given element to enter the crystal lattice. Partition coefficients tend to increase at decreasing temperature (most mineral phases have positive enthalpy and entropy of fusion), to decrease at increasing water contents (water dissolves non-ideally in silicate melts, so reduce component activities more than by simple dilution) (Blundy & Wood, 2003), and an increase in pressure decreases the partition coefficients of Rare Earth Elements (REE) (Taura *et al.*, 1998; Zanetti *et al.*, 2004; Lee *et al.*, 2007). Stead *et al.* (2017) recently investigated the effect of olivine composition (Mg#) on the REE partitioning and site elasticity, with a decreasing Ce/Yb fractionation at increasing olivine Mg# (Fig. 1.39). Table 1.1 reports several sets of partition coefficients of olivine major and trace elements adapted for magmatic systems and melt-rock interaction processes.

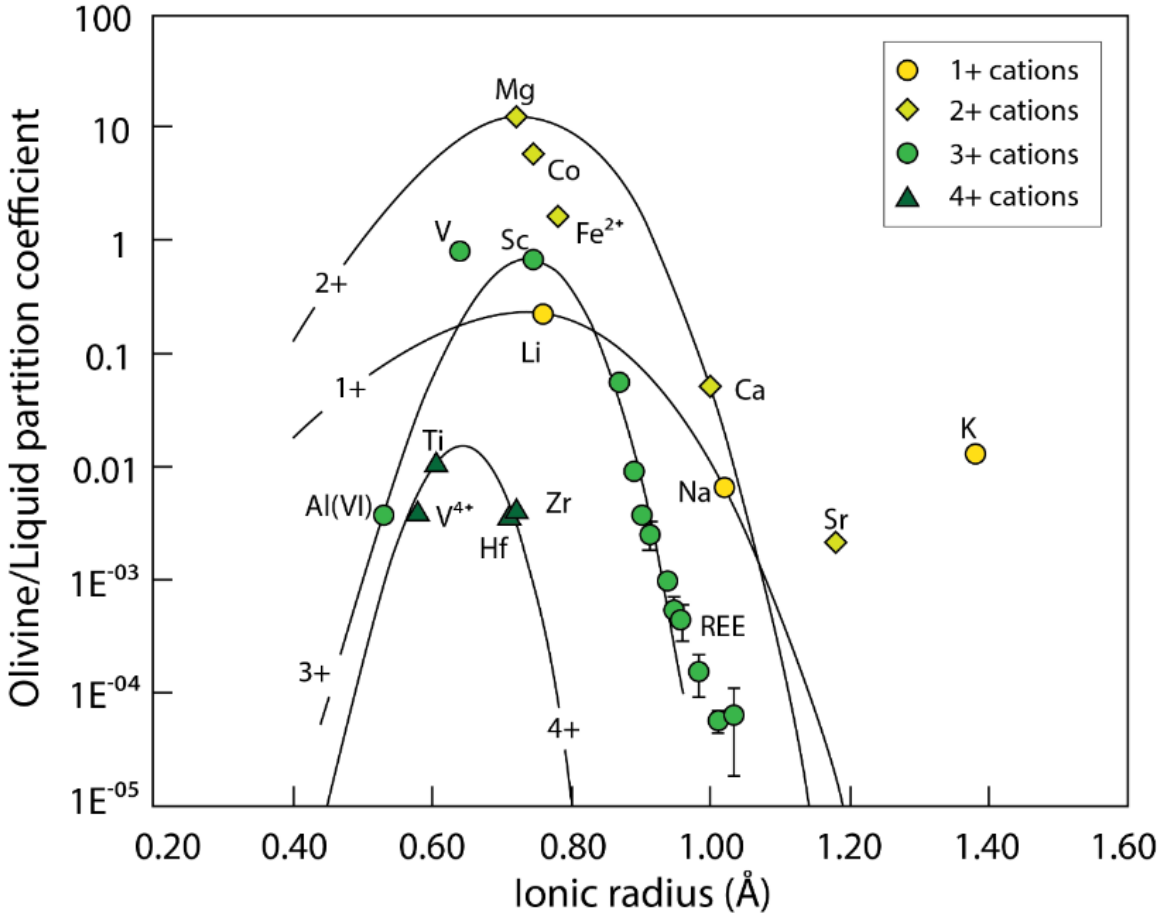

***Figure 1.38**: Olivine/melt partition coefficients of major and trace elements, redrawn after Zanetti et al. (2004).*

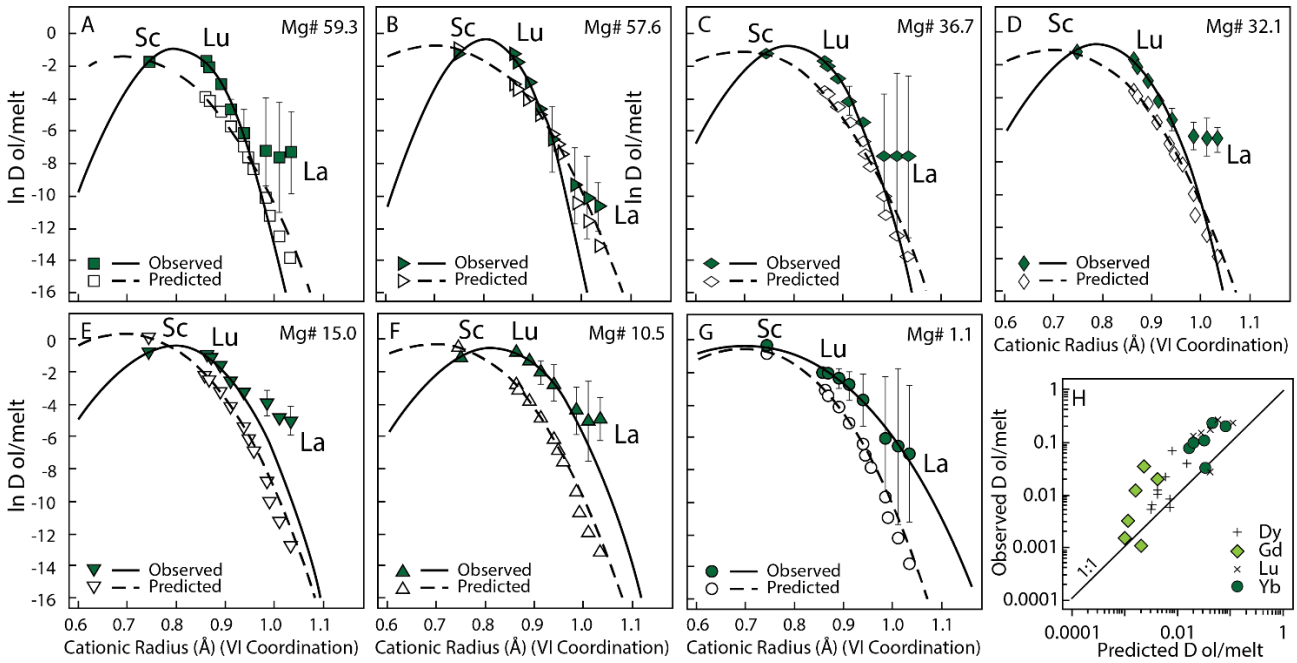

***Figure 1.39**: Apparent and predicted olivine/melt partition coefficients for the REE and Sc plotted as ln D ol/melt vs cationic radius in VI coordination (Shannon et al., 1976), redrawn after Stead et al. (2017); Panels are organized from high Mg# (A) to the lowest (G); H: Predicted vs observed D ol/melt values for Dy, d, Yb and Lu; solid line represents the ideal 1:1 ratio. Predicted values were calculated using the model of Sun and Liang (2013, 2014). Errors are 1σ of measured replicates.*

The variability of mineral/melt partition coefficients with pressure and temperature conditions leads to changes in the mineral/mineral partition coefficients in the solid assemblage at subsolidus conditions (Stead *et al.*, 2017). Sun & Liang (2012, 2013a,b, 2014) and Sun *et al.* (2017) developed a lattice strain model for Rare Earth Elements partitioning among mantle minerals (olivine, orthopyroxene, clinopyroxene) during subsolidus reequilibration (T<1300°C). With decreasing temperature, REEs are preferentially partitioned into clinopyroxene (Fig. 1.40), the extent of the REE redistribution being dependent on the modal composition of clinopyroxene in the peridotite. As a result, the REE concentrations of olivine and orthopyroxene are progressively decreasing ($Ce_{olivine}$ (800°C) = 0.002 x $Ce_{olivine}$ (1300°C), Fig. 1.40) and fractionated with decreasing temperature (Ce/Yb = 0.04 in olivine at 800°C, Fig. 1.40) (Sun & Liang, 2012, 2013a,b, 2014).

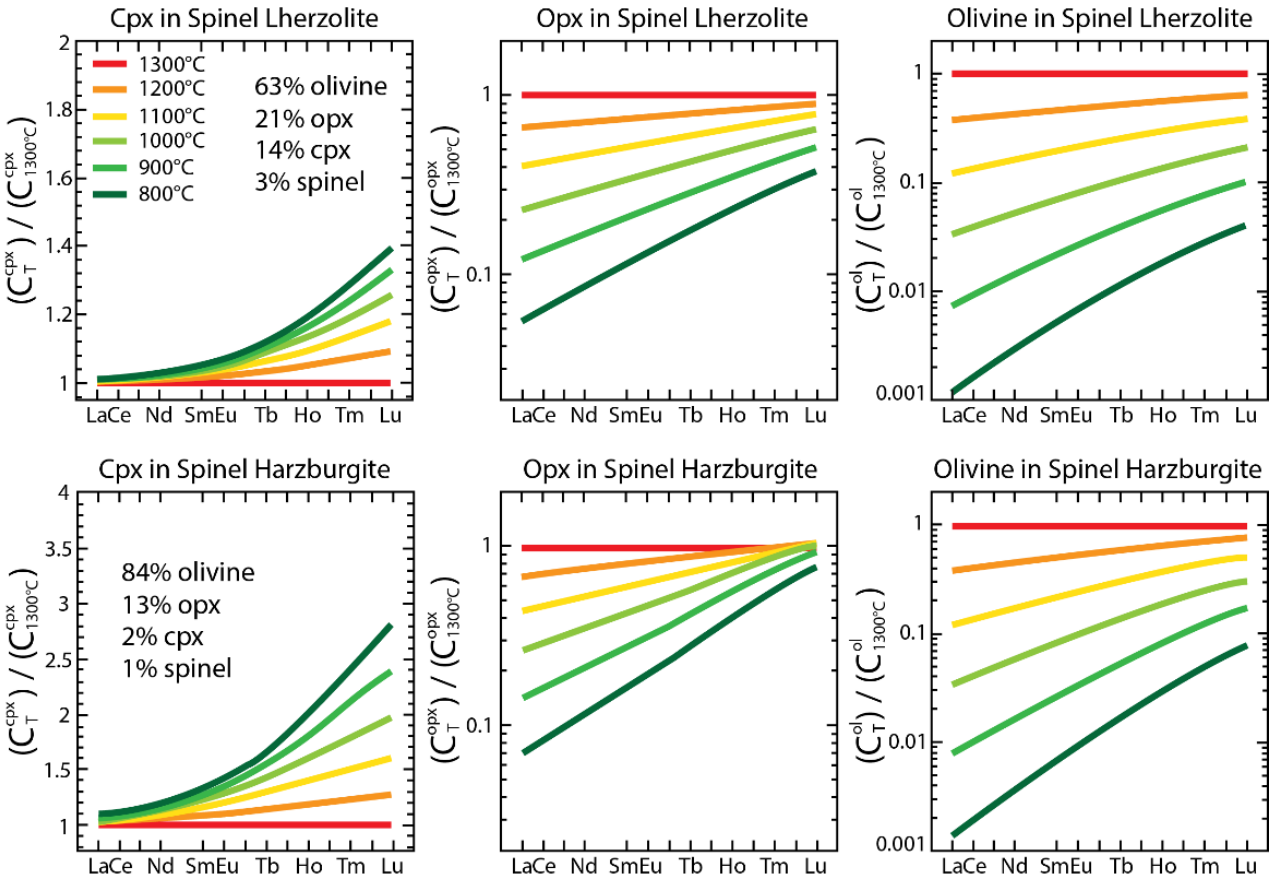

***Figure 1.40**: Subsolidus re-distribution of REEs among clinopyroxene, orthopyroxene and olivine in a spinel lherzolite and a spinel harzburgite at selected temperature and 1GPa, redrawn after Sun & Liang (2014). Mineral REE concentrations are normalized by their respective values at 1300°C.*

Table 1: Compilation of olivine/melt major and trace elements partition coefficients commonly used in mantle, magmatic and melt-rock interaction processes, after Suhr *et al.* (1998); Kelemen *et al.* (2003); Zanetti *et al.* (2004); Lee *et al.* (2007); Spandler & O'Neill (2010); Le Roux *et al.* (2011); Sun & Liang (2014); Warren (2016).

	Spandler & O'Neill, 2010 1 bar - 1300°C	Le Roux et al., 2011 1.5GPa - 1300°C	Kelemen et al., 2003 1300°C	Zanetti et al., 2004 1.4GPa - 1055°C
Ti	0.0019	n.d.	n.d.	0.011
Al	n.d.	n.d.	n.d.	0.0044
Fe	n.d.	1.57	n.d.	n.d.
Mn	0.73	1.15	n.d.	n.d.
Ni	7.21	10.28	10	n.d.
Ca	0.0125	n.d.	n.d.	n.d.
Na	0.02	n.d.	n.d.	0.0065
K	n.d.	n.d.	1.00E-09	0.013

	Spandler & O'Neill, 2010 1 bar - 1300°C	Lee et al., 2007 1.5GPa - 1300°C	Kelemen et al., 2003 1300°C	Sun and Liang, 2014 1 GPa - 1300°C	Suhr et al., 1998
Sc	0.11	n.d.	n.d.	n.d.	n.d.
Ti	0.0019	n.d.	0.015	0.015	n.d.
V	0.094	n.d.	n.d.	n.d.	n.d.
Cr	0.75	n.d.	n.d.	n.d.	n.d.
Co	2.28	n.d.	n.d.	n.d.	n.d.
Rb	n.d.	n.d.	1.00E-09	n.d.	n.d.
Sr	n.d.	n.d.	0.00001	n.d.	n.d.
Y	0.0036	n.d.	0.023	0.0039	n.d.
Zr	0.00038	n.d.	0.004	n.d.	0.004
Nb	n.d.	n.d.	0.001	n.d.	n.d.
Ba	n.d.	n.d.	1.00E-09	n.d.	n.d.
La	n.d.	0.000001	0.000007	0.0000023	0.000007
Ce	n.d.	0.000003	0.00001	0.0000073	0.00001
Pr	0.00017	0.00001	0.00004	0.000021	n.d.
Nd	n.d.	0.000036	0.00007	0.000058	0.00007
Sm	n.d.	0.00026	0.0007	0.00029	0.001
Eu	0.00024	0.00058	0.00095	0.00055	0.001
Gd	0.00067	0.0012	0.0012	0.0010	0.0012
Tb	0.0026	0.0024	0.0026	0.0017	n.d.
Dy	n.d.	0.0046	0.004	0.0029	0.004
Ho	0.007	0.0079	0.007	0.0045	n.d.
Er	n.d.	0.013	0.009	0.0066	0.009
Tm	n.d.	0.019	n.d.	0.0092	n.d.
Yb	n.d.	0.027	0.023	0.0121	0.014
Lu	0.018	0.036	0.03	0.0153	n.d.
Hf	0.0006	n.d.	0.004	n.d.	n.d.
Ta	n.d.	n.d.	0.001	n.d.	n.d.
Pb	n.d.	n.d.	0.00001	n.d.	n.d.
Th	n.d.	n.d.	1.00E-09	n.d.	n.d.
U	n.d.	n.d.	1.00E-09	n.d.	n.d.

n.d. = not determined

Chapter 2 – Field and analytical methods

This chapter aims at describing the general methods used in this study. As described previously in the **1.5 Aim of the Study, studied objects**, this PhD work focuses on three different case studies. More details on specific methods adopted for a single case study will be provided in each following chapter.

2.1 Field work

Detailed field work was performed in the Erro-Tobbio peridotites and associated troctolitic body (Ligurian Alps), in the area previously studied by Borghini et al. (2007), and in the Monte Maggiore peridotitic massif (Alpine Corsica). In the Erro-Tobbio ultramafic unit, we investigated the already described lithological and textural complexity within a troctolitic body primarily associated to mantle peridotites (Borghini et al, 2007), in a series of specific outcrops characterized by the occurrence of variable olivine texture (from skeletal to granular textures), and crosscutting relationships between different generations of troctolites. In the Mt.Maggiore peridotite unit (Corsica), detailed field work and sampling focused on selected outcrops showing the transition from spinel peridotites containing spinel dunite pods, to plagioclase-bearing impregnated peridotites, dunites and troctolites, the latter being previously described as magmatic cumulates (Rampone et al, 2008; Piccardo & Guarnieri, 2010). The work was aimed at investigating the textural evolution of mantle olivines with ongoing impregnation of dunites, and replacive formation of plagioclase-bearing dunites and troctolite of hybrid (mantle olivine matrix plus magmatic interstitial phases) origin.
We mapped the lithological variations observed in the field, as well as the structures relevant to the mantle evolution and melt-rock interaction history (e.g. mantle foliation, pyroxenite layers, mineralogical layering in the Erro-Tobbio troctolites and in Mt.Maggiore plagioclase-rich peridotites, gabbroic intrusions). Measured data have been merged with pre-existing published data (Jackson & Ohnenstetter, 1981; Borghini et al, 2007) in structural maps, panorama, and cross-sections (see section Field occurrences **3.4** and **4.4)**. In both the Erro-Tobbio troctolitic body and the Monte Maggiore peridotitic massif, the samples, representative of the lithological and textural variability, have been oriented relative to the plagioclase-enrichment mineralogical layering. Thin sections were prepared normal to the layering and parallel to the mineralogical lineation when identified (Figure 2.1). When no layering, foliation, or lineation was observed, samples were oriented relative to the general orientation of the layering measured on the field (the mineralogical layering within the Erro Tobbio troctolites and the plagioclase enrichment layering within the Corsica peridotitic body). Hence, all studied samples have a common orientation and context.

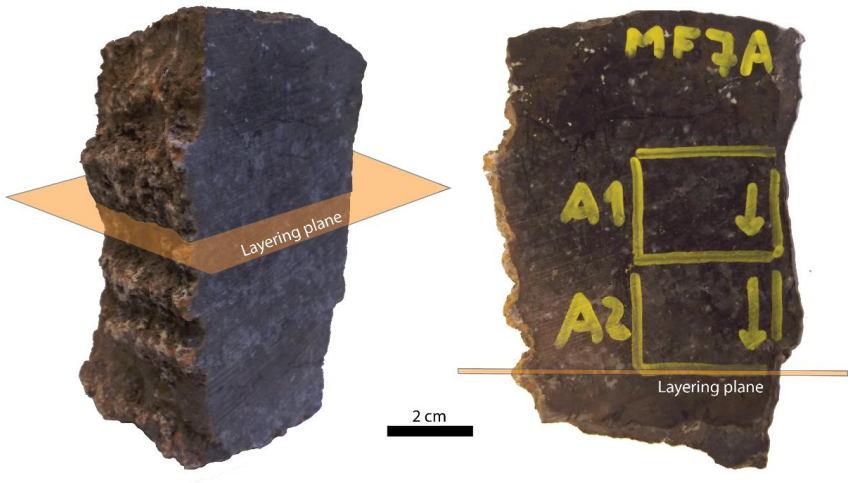

***Figure 2.1**: Orientation of the prepared samples according to observed layering at macroscopic scale. The thin sections are prepared normal to the foliation and parallel to the lineation.*

2.2 Petrography

Sample sections were prepared at DISTAV, University of Genova, both as 30µm- and 100µm- thick polished sections, the latter allowing both structural and chemical analyses on the same thick section. Polishing of all analysed sections was refined at Géosciences Montpellier (University of Montpellier, France), to optimize the quality of the EBSD analyses. Before performing structural and chemical analyses, a detailed microstructural study of all studied samples was used to describe the textural variability, the relationships between the different mineral phases (mostly olivine, spinel, plagioclase, clinopyroxene and orthopyroxene), and the degree of alteration of primary minerals. Serpentinization of olivine and alteration of plagioclase by low-grade mineral aggregates can be significant, and thus the selection of samples is critical for later structural and chemical in-situ analyses. The most preserved and representative samples, in terms of textures and mineral modal compositions, were selected for Electron Back Scattered Diffraction (EBSD – Géosciences Montpellier) analyses and major elements (by Electron Probe Micro Analyses – University of Milano) and trace elements chemical analyses (by Laser Ablation-Inductively Coupled Plasma-Mass Spectrometry – Géosciences Montpellier). The common orientation of all thin sections according to the foliation and the lineation enables direct comparison between the structural and textural EBSD analyses of all samples.

2.3 EBSD structural analyses

Structural maps and crystallographic preferred orientations (CPO) of olivine, plagioclase, clinopyroxene, and orthopyroxene were measured by indexation of electron-backscattered diffraction patterns using the SEM-EBSD facility at Géosciences Montpellier (University of Montpellier, France). The EBSD patterns were generated by interaction of a vertical incident electron beam with a carefully polished thin section tilted at precisely 70° in a scanning electron microscope (JEOL JSM 5600). The diffraction pattern was projected onto a phosphor screen and recorded by a digital CCD camera. The image was then processed and indexed in terms of crystal phase and orientation using the AZtec software from Oxford Instruments.

For each sample, we obtained crystallographic orientation and structural maps covering almost entirely the thin section (usually between 30 and 40mm long and 20mm wide), with sampling steps between 15 and 40µm, depending on the grain size. Indexation rates, mostly dependant on the serpentinization of the samples, range from 40 to 95% in the raw maps.

Post-acquisition data processing, using the Channel 5 software suite, was performed to (1) eliminating isolated pixels, (2) fill the non-indexed pixels that have up to five identical neighbours with this orientation, and (3) searching and correcting for systematic indexation errors caused by the olivine hexagonal pseudo-symmetry, which results in similar diffraction patterns for orientations differing by a rotation of 60° around [100].

2.3.1. EBSD maps

EBSD data were used to generate a set of structural maps of each measured thin section. Grains were identified using the MTEX MatLab toolbox (Hielscher and Schaeben, 2008) with a 10° threshold angle between neighbouring pixels, enabling grain analyses, as a useful complementary dataset to the optical microstructural observations.

Phase maps (Figure 2.2, map 1) are used to describe the sample texture at the scale of the thin section, and quantify the modal composition of the sample.

Misorientation maps (Figure 2.2, map 2) show the difference in orientation between each pixel of a grain and the average orientation of this grain. Deformation can lead to differences in orientation in parts of a crystal. Since the reconstruction of the grain boundaries is based on a misorientation greater than ten degrees between two neighbouring pixels, it is possible to observe and quantify deformation within single grains.

Orientation maps (Figure 2.2, map 3) give the three-dimensional orientation of each analyzed pixel. Orientation data are used to represent a Crystallographic Preferred Orientation of the different crystallographic axes of a specific phase.

Identification of the grains enables to quantify textural characteristics of the measured grains, like the **Aspect Ratio** (Figure 2.2, map 4) and **Shape Factor** (Figure 2.2, map 5). The Aspect Ratio, indicative of the elongation of a grain, is defined as the ratio between long and short axis of the ellipse that best fits the grain shape. The Shape Factor corresponds to the ratio between the Perimeter of the grain and the Equivalent Perimeter (perimeter of a circle of the same area as the considered grain). This parameter quantifies the tortuosity of the grain boundary; it is lower for a euhedral or rounded grain (minimum = 1) than for a tortuous, irregular grain.

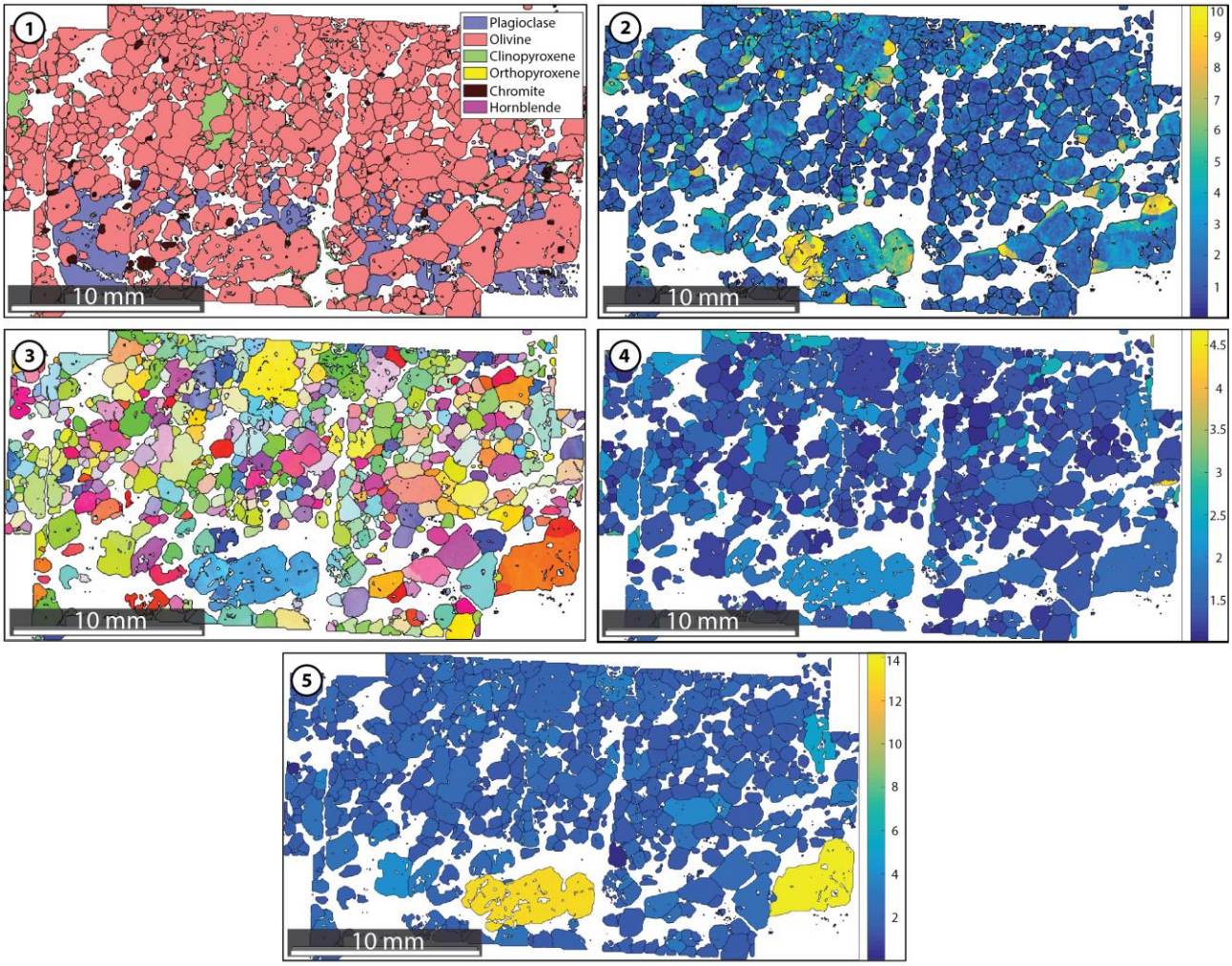

Figure 2.2*: EBSD processed maps of an Olivine-rich Troctolite. The grains boundaries are represented by continuous black lines, 1: Phase map, 2: Olivine misorientation map, the scale bar is in degrees of misorientation according to the mean orientation of the olivine grain, 3: Olivine orientation map, 4: Olivine Aspect Ratio map, 5: Olivine Shape Factor map.*

2.3.2. Single grain analyses

EBSD data processing enables the quantification of textural parameters (Grain area, Shape factor, Aspect ratio) and misorientation (misorientation according to the mean orientation of the olivine grain) in single olivine grains. These parameters are used to monitor textural heterogeneity within and between samples. We investigate the preferred orientation of misorientation (e.g. kinking within a grain, Figure 2.3A), indicative of the deformation process and the possible activation of specific slip systems. This misorientation is represented in an Inverse Pole Figure, according to olivine's crystallographic axes (Figure 2.3B). The activation of a slip system is dependant of the conditions in which deformation takes place, in terms of temperature, pressure, strain and hydration (e.g., Nicolas and Christensen, 1987; Tommasi et al, 2000; Karato et al, 2008; see section **1.4.3 Olivine Crystallography**). The same investigation of misorientation within a grain and its orientation can be applied to a sample and can thus represent the average misorientation over all grains of olivine present in the studied area (Figure 2.3C and D). The Inverse Pole Figure (Figure 2.3D) is then indicative of the misorientations rotation axes and of possibly different activated slip systems in the olivines forming the sample.

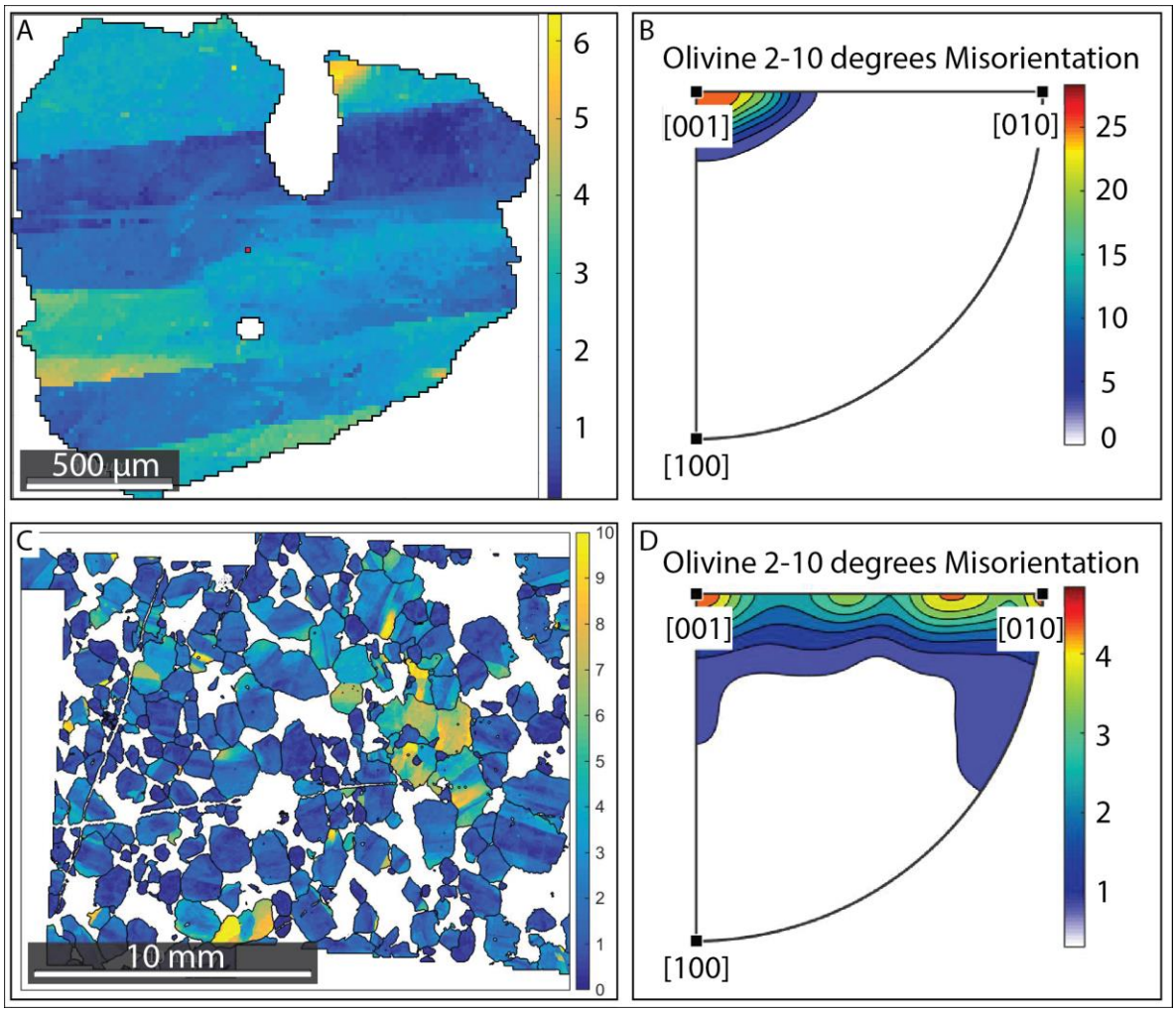

***Figure 2.3**: Misorientation analysis. A: Misorientation map of a single grain of olivine, showing a clear kinking. The scale bar is in degrees of misorientation from the calculated mean orientation of the grain; B: Inverse Pole Figure representing the 2-10° misorientation within the deformed olivine, according to the crystallographic axes of olivine. C: Olivine misorientation map of a sample of troctolite. The different grains of olivine are separated by a continuous black line. The scale bar is in degrees of misorientation from the calculated mean orientation of the grain D: Inverse Pole Figure representing the mean 2-10° misorientation in the sample of troctolite, according to the crystallographic axes of olivine.*

2.3.3. Crystallographic Preferred Orientation

The Crystallographic Preferred Orientation (CPO) pole figures correspond to equal-area, lower hemisphere stereographic projections of the orientation of the three crystallographic axes of all the crystals of a single phase (Figure 2.4). This representation is dependent on the number of grains of a single phase in the analyzed sample. A minimum of 100 grains of a single phase are needed to obtain a good statistical orientation and thus a representative Crystallographic Preferred Orientation (e.g., Ben Ismail and Mainprice, 1998). In samples from both the Erro-Tobbio and the Monte Maggiore peridotitic bodies, interstitial minerals are often coarse-grained poikilitic crystals, and cannot be used to obtain a reliable representation of a fabric. For most samples of the Erro-Tobbio peridotites, troctolites and olivine gabbros, olivine Crystallographic Preferred Orientation is statistically representative, but in the Corsican peridotites and dunites, the centimetre-grain size of

olivine does not allow the samples to be composed of more than 100 grains. The CPO strength is quantified by the J-index, which is the volume-averaged integral of the squared orientation densities, and hence is sensitive to peaks in the orientation distribution function (Bunge, 1982; Mainprice et al, 2014). J is dimensionless; it ranges from 1 for a random distribution to infinity for a single crystal orientation. It usually ranges between 2 to 20 in natural peridotites (Ben Ismail and Mainprice, 1998).

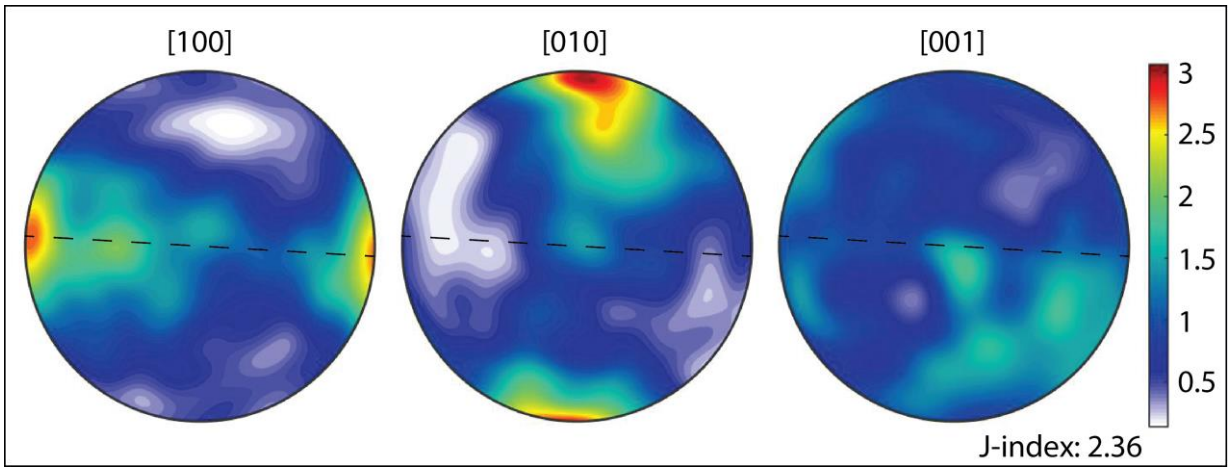

***Figure 2.4**: Pole Figure representing the Crystallographic Preferred Orientation of the olivine grains in a sample of olivine-rich Troctolite. Equal-area lower hemisphere stereographic projection. The foliation is oriented East-West and represented by the dashed black line.*

2.4 Major elements mineral chemistry – EPMA analyses

Major elements chemical analyses of minerals in the most representative samples were obtained for every case study. Chemical analyses were made in all microstructural sites, to cover the range of observed textural variability (from millimetre-size to coarse centimetre-size, euhedral to anhedral, undeformed to deformed olivine grains, from euhedral and poikilitic cores to interstitial vermicular crystals of plagioclase, clinopyroxene and orthopyroxene).

Major element (SiO_2, TiO_2, Al_2O_3, Cr_2O_3, FeO, MgO, MnO, CaO, NiO, Na_2O and K_2O) compositions of Olivine, Plagioclase, Clinopyroxene, Orthopyroxene and Spinel were analysed by JEOL JXA 8200 Superprobe equipped with five wavelength-dispersive (WDS) spectrometers, an energy dispersive (EDS) spectrometer, and a cathodoluminescence detector (accelerating potential 15 kV, beam current 15nA), operating at the Dipartimento di Scienze della Terra, University of Milano. The analyses of all elements were performed with a 30 second counting time. Analyses with total oxide percentage lower than 98%, and higher than 102% were immediately excluded. A second quality check of the analyses has been done based on the atom per formula unit, discarding every analysis that showed more than 0.5% of error from the theoretical expected value.

Chemical profiles (from 10- to 50-points each) have been analysed either within large single crystals (core to rim profiles), or across the contact between distinct mineral phases, with a step size between 20 and 150 µm, depending on the grain size of the analysed crystals. Along the profiles, all major elements were analysed with a 60 second counting time, to decrease the detection limits. Olivine-Plagioclase, Olivine-Clinopyroxene, and Plagioclase-Clinopyroxene contacts were all investigated.

2.5 Trace elements mineral chemistry – LA-ICP-MS analyses

In-situ trace element compositions were determined by Laser Ablation-Inductively Coupled Plasma Mass Spectrometry at Géosciences Montpellier (University of Montpellier, France). As for the major elements analyses, the investigated mineral grains (olivine, plagioclase, clinopyroxene, orthopyroxene) cover the range of textural variability observed within the samples (based on optical petrographic observations and EBSD analyses and maps). Specific care had to be taken regarding the selection of the ablated zone, since olivine serpentinization can be important in some samples, and because of the occurrence of small inclusions in olivine (see section **2.6 Olivine inclusions - SEM – FESEM analyses**).

The analyzed trace elements are: Li, B, Sc, Ti, V, Cr, Mn, Co, Ni, Cu, Zn, Rb, Sr, Y, Zr, Nb, Sb, Ba, rare earth elements (REEs), Hf, Ta, Pb, Th and U. Analyses were performed with a Thermo Scientific Element XR (eXtended Range) high resolution ICP-MS. The ICP-MS was coupled to a laser ablation system consisting of a Geolas (Microlas) automated platform with a 193 nm Excimer Compex 102 laser from LambdaPhysik. Ablation analyses were performed using an in-house modified 30 cm^3 ablation cell with a helium atmosphere to enhance sensitivity and reduce inter-element fractionation (Günther and Heinrich, 1999). Helium gas and ablated sample material were mixed with argon gas before entering the ICP-MS. The laser energy density was set to 12 J cm^{-2} at a frequency of 8 Hz and the beam size was set to 77µm or 102µm for olivine, plagioclase, orthopyroxene and clinopyroxene. Because of the limited interstitial grain size, some thin rims of vermicular clinopyroxenes were analyzed using a 51µm spot size. Data were collected in time resolved acquisition mode, collecting the background signal for two minutes, followed by one minute of sample ablation (480 pulses at 8Hz).

Data were processed with the GLITTER software package (Van Achterberg et al, 2001), using the linear fit to ratio method. Data were filtered for spikes on an element by element basis. After comparing the variability between the internal standardization relative to EMPA data using ^{43}Ca and ^{29}Si, the standardization for all minerals was done using ^{29}Si. Mean detection limits were <7 ppb for Rb, Sr, Y, Zr, Nb, Sb, Ba, REE, Hf, Ta, Pb, Th, U; they were <70 ppb for Zn, Cu, Co, Mn, V, Sc, <170 ppb for Li and B and <1 ppm for Ti, Cr and Ni. Values that were within 1σ of the detection limit were excluded during data reduction. An additional filter was applied to remove any analysis that had more than 50% error in concentration. Oxide interferences on Gd, Tb, Dy, Ho, Er, Tm, Yb, Lu were monitored using reference basalt BIR 1-G (see Appendix 3). Interferences resulted in a bias in the calibration based on NIST 612 measurements (underestimation of abundances), which were adjusted using a correction factor. It was calculated on a day-by-day basis by fitting the mean concentration of analyzed reference basalt BIR 1-G to the GEOREM accepted values of concentration (Jochum et al, 2005; Appendix 3). Instrument sensitivity due to analytical conditions was determined from the average across all days of repeated measurements of the synthetic NIST 612 glass (Pearce et al, 1997; Appendix 3). Sensitivities were >300 cps/ppm for Ni and Ti, >1000 cps/ppm for B and Zn, 1000-5000 cps/ppm for Li, Cr, Cu, Ba, Nd, Sm, Gd, Dy, Er, Yb and Hf and >5000 cps/ppm for all other elements. Reproducibility as constrained by 57 analyses of reference basalt BIR 1-G was better than 5% for all elements except Rb, Y, Zr, Hf and Pb which are better than 12%, and measured values were comparable within analytical uncertainties to GEOREM accepted values (Jochum et al, 2005).

2.6 SEM – FESEM analyses

Within troctolitic samples from the Erro Tobbio ultramafic body, small inclusion rods are found within the olivine grains. The inclusions are found in major proportions in the most deformed and corroded olivine grains. They are less than 50µm-long, all oriented in the same direction (Figure 2.5), and follow the deformation kinks in olivine. Similar rods, constituted by ilmenite, were previously described by Risold et al (2001) and Hermann et al (2005), and interpreted as a consequence of the breakdown of isolated humite layers in olivine. We performed Scanning Electron Microscope (SEM) (equipped with an X-SDD detector) and Field Emission – Scanning Electron Microscope (FE-SEM) analyses in DISTAV, Genova (Italy), to investigate the organization of the inclusions according to the orientation of olivine crystallographic axes. The high-magnification FE-SEM images reveal a varying brightness along the inclusion in QBSD images and thus suggest that a single inclusion rod is heterogeneous and not monocrystalline (Figure 2.5) (see chapter **3.7** Mineral chemical composition).

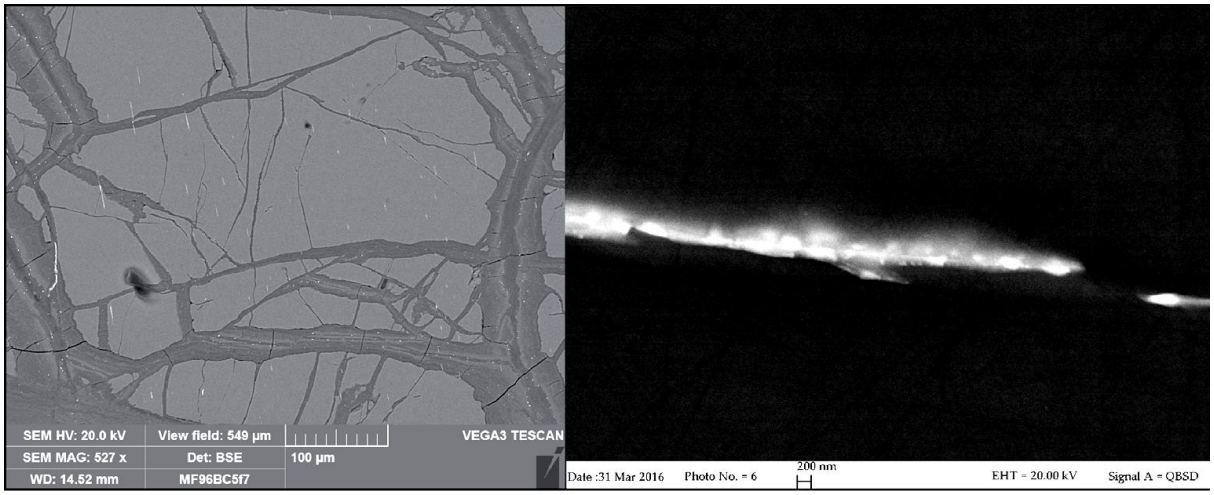

***Figure 2.5**: Left: SEM Back-Scattered Electron image of a deformed olivine bearing inclusion needles. The orientation of the inclusions follows the kinks in olivine. Right: QBSD FE-SEM image of a single inclusion needle. The varying brightness suggests that the inclusion is heterogeneous and not monocrystalline.*

Since the inclusions are too small for a direct quantitative SEM-Energy Dispersive Spectroscopy (EDS) analyses (1 μm^3 analyzed), SEM-EDS qualitative analyses were performed by comparing the compositional difference between the background olivine and the inclusion-bearing olivine point analysis (Figure 2.6).

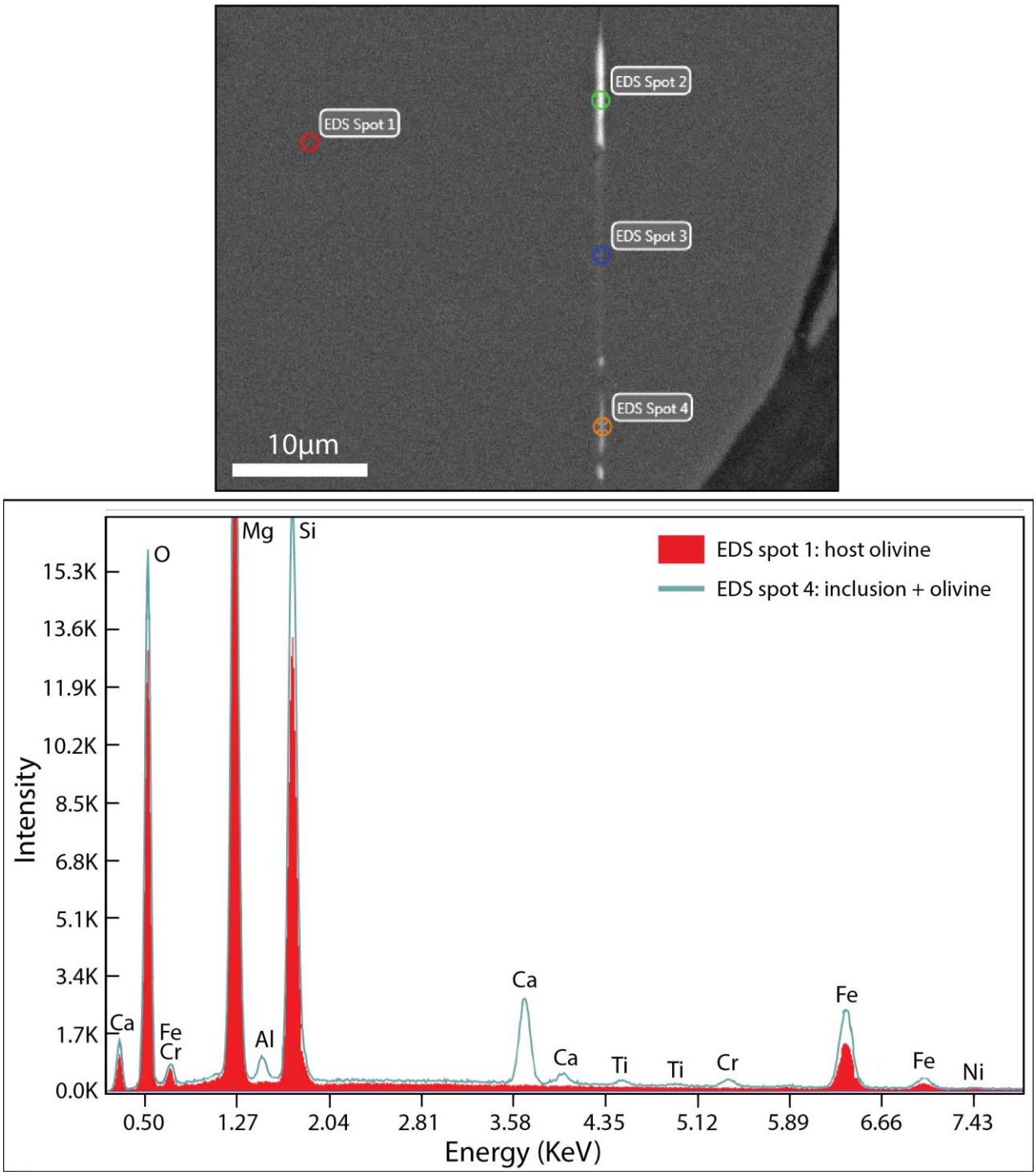

***Figure 2.6**: SEM-EDS qualitative analyses of the host olivine (Spot 1) and different parts of the inclusion rod (Spot 2, 3, 4). Top: localization of the analyzed spots. Bottom: Compositional spectra of the Spot 4 here compared with the host olivine (Spot 1). It reveals a higher Ti, Cr, Fe, Si, Al, Ca in the inclusion-bearing zone.*